

**Microfabrication and characterization of PVDF copolymer
thin films suitable for integrating with optical microsystems**

KIRAN KUMAR CHATRATHI

A Thesis

in

The Department

of

Mechanical and Industrial Engineering

Presented in partial fulfillment of the requirements for the
Degree of Master of Applied Science (Mechanical Engineering) at
Concordia University
Montreal, Quebec, Canada

December, 2006

© Kiran Kumar Chatrathi 2006



Library and
Archives Canada

Bibliothèque et
Archives Canada

Published Heritage
Branch

Direction du
Patrimoine de l'édition

395 Wellington Street
Ottawa ON K1A 0N4
Canada

395, rue Wellington
Ottawa ON K1A 0N4
Canada

Your file *Votre référence*
ISBN: 978-0-494-28936-5
Our file *Notre référence*
ISBN: 978-0-494-28936-5

NOTICE:

The author has granted a non-exclusive license allowing Library and Archives Canada to reproduce, publish, archive, preserve, conserve, communicate to the public by telecommunication or on the Internet, loan, distribute and sell theses worldwide, for commercial or non-commercial purposes, in microform, paper, electronic and/or any other formats.

The author retains copyright ownership and moral rights in this thesis. Neither the thesis nor substantial extracts from it may be printed or otherwise reproduced without the author's permission.

AVIS:

L'auteur a accordé une licence non exclusive permettant à la Bibliothèque et Archives Canada de reproduire, publier, archiver, sauvegarder, conserver, transmettre au public par télécommunication ou par l'Internet, prêter, distribuer et vendre des thèses partout dans le monde, à des fins commerciales ou autres, sur support microforme, papier, électronique et/ou autres formats.

L'auteur conserve la propriété du droit d'auteur et des droits moraux qui protègent cette thèse. Ni la thèse ni des extraits substantiels de celle-ci ne doivent être imprimés ou autrement reproduits sans son autorisation.

In compliance with the Canadian Privacy Act some supporting forms may have been removed from this thesis.

Conformément à la loi canadienne sur la protection de la vie privée, quelques formulaires secondaires ont été enlevés de cette thèse.

While these forms may be included in the document page count, their removal does not represent any loss of content from the thesis.

Bien que ces formulaires aient inclus dans la pagination, il n'y aura aucun contenu manquant.


Canada

ABSTRACT

Microfabrication and characterization of PVDF copolymer thin films suitable for integrating with optical microsystems

Kiran Kumar Chatrathi

In the emerging field of Micro Electro Mechanical Systems (MEMS) silicon continues to be the best material to integrate with mechanical and electrical miniature systems such as microsensors and microactuators that use various schemes of sensing and actuation. The functionality of these systems may be enhanced from extended type of materials with enhanced sensitivity and improved actuation. The integration of piezoelectric materials in MEMS facilitates the functionality of the devices. PVDF (Polyvinylidene fluoride) and its copolymers in the domain of piezoelectric materials have always been upfront to integrate with MEMS, in particular, copolymers of PVDF possess a much enhanced material properties and can eventually deliver better performance than PVDF homopolymer. The application of copolymers extends to all classes of miniaturized systems such as optical microsystems, sensors, actuators etc. In thin film technology, it is very important to have a better understanding of the crystal structure and material properties of thin films.

In the present work microfabrication and characterization of P(VDF-TrFE) copolymer thin films are carried out. Various deposition techniques for PVDF thin films are presented and spin coating technique is finally adopted for microfabrication of PVDF copolymer thin films due to its advantages. Further spinning characterization of PVDF copolymer thin films are presented. An optimized set of spin parameters are found in

order to develop a uniformly deposited PVDF copolymer thin films. In the current work, polarization of the films is performed through step-wise poling method. A simple experimental setup for stepwise poling method is presented. The main aspect of the present work is focused on the material characterization of the microfabricated PVDF copolymer thin films through “Fourier Transform Infrared Spectroscopy” (FTIR). An in-depth FTIR analysis on the effect of annealing PVDF copolymer thin films is presented and the analysis is extended through the study on the variation of the significant optical parameters such as absorbance and transmittance spectra in the infrared region. The study focuses on the variation of the spectra in the piezoelectric phase of the thin films. Further, the effect of polarization (*poling*) of PVDF copolymer thin films on the absorbance and transmittance spectra is also presented, FTIR analysis is further extended through comparison of the spectra of the microfabricated PVDF copolymer thin films with the available commercial PVDF thin films.

In the present work, the mechanical properties of the spin coated PVDF copolymer thin are characterized through the measurement of piezoelectric constant, d_{31} for the considered geometry of PVDF copolymer thin films. The results are compared with the measured piezoelectric constant of commercial PVDF thin film. Finally a novel variable optical attenuator (VOA) through piezoelectric actuation is presented. The design of the VOA using PVDF copolymer thin films is discussed and the optical attenuation properties of the VOA are analyzed.

**This thesis is
dedicated to my parents
and to my brother**

Acknowledgements

The author expresses highest gratitude and is deeply privileged to work under thesis supervisors Dr. Ion Stiharu and Dr. Muthukumaran Packirisamy. The author expresses sincere thanks for their guidance and continuous support through out the studies. The author personally thank Dr. Muthukumaran Packirisamy for his encouragement and significant discussions which were helpful to move forward in the work.

The author expresses his sincere gratitude to the co-supervisor Dr. Ion Stiharu the many discussions with him through out the thesis were really helpful and progressive to complete the work.

A special thanks is reserved for the technical support staff in Mechanical and Industrial Engineering Department, John Elliot, Brian Cooper, Gilles Huard, Brad Luckhart, and my sincere heartfelt thanks to Dan Juras for his continuous support. A special thanks is reserved for Dr.Sergeyi for his helpful discussions through out the work

The author thanks for the many discussions with his colleagues and friends, Saeed, Gino, Raghavendra, Avinash, Ashwin, Rakesh, Arvind, Jian Liang You, Jeetender, Li, Anand, Nagarajan for providing valuable help during different stages of this work. Last, but not the least, the author would like to thank his mother, his brother and his friends for being there always.

TABLE OF CONTENTS

(i)	List of Figures	Xii
(ii)	List of Tables	Xix
(iii)	Nomenclature	Xx
(iv)	List of symbols	Xxii

CHAPTER 1 - Introduction 1

1.1	Motivation for the research	1
1.2	Dielectric Materials	2
1.2.1	Polar forms	3
1.2.2	Piezoelectricity	3
1.2.3	Piezoelectric effects	3
1.3	Piezoelectric Polymers	5
1.3.1	PVDF and comparison with its copolymers	7
1.3.2	Merits and demerits of PVDF copolymers	13
1.4	Microfabrication of PVDF copolymer thin films	14
1.5	Polarization of PVDF copolymer thin films (Poling)	15
1.6	PVDF MEMS	16
1.6.1	Applications of PVDF copolymer as thin films	18
1.7	Literature review on attenuators	18

1.7.1	VOA's design parameters	19
1.7.2	External VOAs	19
1.7.3	Internal (built-in)	20
1.7.4	Actuation mechanism	20
1.8	Methodology	21
1.9	Thesis layout	26
1.10	Summary	27
 CHAPTER 2 Microfabrication techniques of PVDF copolymer thin films		28
2.1	Microfabrication of PVDF/TrFE copolymer thin films	28
2.1.1	Chemical vapor deposition (CVD)	29
2.1.2	Physical vapor deposition(PVD)	30
2.1.2.1	Thermal evaporation	30
2.1.2.2	Sputtering	31
2.1.2.3	Ionized-vapor deposition method	31
2.1.2.4	Electron beam depositon	32
2.1.2.5	Laser ablation (Pulsed laser deposition)	33
2.1.2.6	Electrostatic spray assisted vapor deposition(ESVAD)	34
2.1.2.7	Electrophoretic deposition	35
2.2	Spin coating deposition	35
2.2.1	Spin coating process theory	36

2.2.2.	Spin coating modeling	40
2.2.3	Spin coating parameters	42
2.2.3.1	Angular speed	42
2.2.3.2	Speed rate	43
2.2.3.3	Fume exhaust	44
2.2.4	Process trend charts	46
2.3	Spin coating of PVDF copolymer thin films	47
2.3.1	Film preparation	48
2.3.2	Thickness measurement	49
2.4	Annealing of PVDF copolymer thin films	52
2.5	Polarization of PVDF copolymer thin films	54
2.5.1	Step-wise poling	54
2.6	PVDF thin film patterning	58
2.7	Summary	59
 CHAPTER 3- FTIR characterization of PVDF copolymer thin films		60
3.1	Infrared spectroscopy theory	60
3.1.1	Electromagnetic spectrum	62
3.1.2	Absorbance	64
3.1.3	Transmittance	65
3.2	FTIR of PVDF copolymer thin films	65
3.2.1	Investigation of polarized phase of pvdf copolymer	66

3.2.2	Effect of annealing on PVDF copolymer thin films	67
3.3	IR spectra variation of PVDF copolymer thin films	68
3.3.1	Variation of the spectra with respect to change in annealing temperature	68
3.3.2	Variation of the spectra with respect to number of cycles of annealing.	71
3.3.3	Variation of the spectra with respect to poling.	73
3.3.4	Variation of spectra with respect to number of cycles of poling.	76
3.3.5	Comparison of IR spectra with commercial PVDF thin films	77
3.4	Summary	80
	CHAPTER 4- Characterization of microfabricated PVDF copolymer thin films	81
4.1	Measurement of piezoelectric constant (d_{31}) of commercial PVDF thin film and microfabricated PVDF copolymer thin film.	81
4.1.1	Piezoelectric constants	82
4.1.2	Piezoelectric charge constant	83
4.2	Experimental setup for measurement of piezoelectric constant (d_{31})	85
4.2.1	Estimation of piezoelectric constant (d_{31}) of PVDF thin film	87
4.2.2	Estimation of piezoelectric constant (d_{31}) of microfabricated PVDF copolymer thin film	93

4.3	Results and conclusions	102
4.4	Summary	102
	CHAPTER 5 – Modeling and simulation of PVDF copolymer thin film actuated optical attenuator	103
5.1	Introduction	103
5.2	VOA (Variable optical attenuator)	104
5.3	Modeling and simulation of the VOA	105
5.4	Piezoelectric actuation using commercial PVDF thin film	108
5.5	Piezoelectric actuation using PVDF copolymer thin film	110
5.6	Application of piezoelectric actuator as an optical attenuator using commercial PVDF thin films and PVDF copolymer thin films	113
5.7	Modeling and simulation of the VOA using PVDF thin film deposition.	118
5.8	Results and discussions	122
5.9	Summary	124
	CHAPTER 6 – Conclusions and future work	125
6.1	Conclusions	125
6.2	Future Work	130
	References	131

LIST OF FIGURES

Figure 1.1	A diagram illustrating direct and converse effects of piezoelectricity	4
Figure 1.2	A study of surface charge on PVDF samples at 22-35 years after preparation	7
Figure 1.3	Copolymer polymerized with Trifluoroethylene (TrFE)	8
Figure 1.4	IR transmission spectra of PVDF and P (VDF-TrFE) in the range 4000-500 cm^{-1}	9
Figure 1.5	IR transmission spectra of P(VDF-TrFE) at different irradiation doses in the range 400-4000 cm^{-1}	10
Figure 1.6	Detail of the transmittance FTIR spectra at room temperature for poled and non-poled β -PVDF films in parallel and transversal modes. Some of the modes with more relevant changes upon poling are indicated by arrows.	12
Figure 1.7	Direction of forces affecting the piezoelectric constants	23
Figure 1.8	Experimental setup for the measurement of piezoelectric constants of PVDF copolymer thin film	24
Figure 2.1	Solution being spin coated on the substrate	36
Figure 2.2	Basic stages involved in spin coating process	38
Figure 2.3	Substrate spinning	42
Figure 2.4	Drying of the substrate	44

Figure 2.5	Exhaust valve of the substrate	45
Figure 2.6	Variation of film thickness with various parameters	47
Figure 2.7	WS-400B-Lite series spin processor	47
Figure 2.8	Variation of film thickness at different speeds for different spin durations for concentration of 10% PVDF copolymer solution.	51
Figure 2.9	Spin coated PVDF copolymer thin film sample	52
Figure 2.10	Spin coated PVDF copolymer thin film sample peeling off the silicon wafer	53
Figure 2.11	A schematic of the step-wise poling charge technique	55
Figure 2.12	Block diagram of step-wise poling set up	56
Figure 2.13	Experimental setup for step-wise poling	57
Figure 2.14	PVDF copolymer thin film clamped between two copper plates	57
Figure 3.1	Schematic diagram of FTIR	61
Figure 3.2	Electromagnetic spectrum	62
Figure 3.3	Infrared region in electromagnetic spectrum	63
Figure 3.4	Perkin Elmer Spectrum BX II FT-IR system	66
Figure 3.5	PVDF Copolymer thin film placed in the sample holder of FTIR system	67
Figure 3.6	Absorption spectra of Spin coated PVDF-TrFE thin films in the region 4000-400 cm^{-1}	69
Figure 3.7	Transmission spectra of spin coated PVDF-TrFE thin films in the region 4000- 400 cm^{-1}	70
Figure 3.8	Absorption spectra of spin coated PVDF-TrFE thin films in the	71

	region 1400- 400 cm^{-1}	
Figure 3.9	Split view of absorption spectra of PVDF copolymer thin films in the region 4000-400 cm^{-1} subjected to subsequent annealing	71
Figure 3.10	Overlay view of Absorption spectrum of PVDF Copolymer thin films in the region 4000-400 cm^{-1} subjected to subsequent annealing.	72
Figure 3.11	Comparison of absorption spectrum of poled samples with respect to unpoled sample and commercial GoodFellow PVDF thin film in the region 4000-400 cm^{-1}	73
Figure 3.12	Comparison of transmission spectrum of poled samples with respect to unpoled sample and commercial GoodFellow PVDF thin film in the region 4000-400 cm^{-1}	74
Figure 3.13	Comparison of absorption spectrum of poled samples with respect to unpoled sample and commercial GoodFellow PVDF thin film in the region 4000-400 cm^{-1}	75
Figure 3.14	Comparison of transmission spectrum of poled samples with respect to unpoled sample and commercial Good fellow PVDF thin film in the region 1400-400 cm^{-1}	76
Figure 3.15	Comparison of absorption spectrum of poled sample (poled once) with respect to subsequent poled sample (poled twice).	76
Figure 3.16	Comparison of transmission spectrum of poled sample (poled once) with respect to subsequent poled sample (poled twice).	77
Figure 3.17	Comparison of transmission spectra of microfabricated PVDF	78

	copolymer thin film with commercial thin films.	
Figure 3.18	Comparison of Transmission spectra of PVDF copolymer thin films with commercial in the region $1500-400\text{cm}^{-1}$	79
Figure 4.1	Polarization conventions.	82
Figure 4.2	Geometry of PVDF thin film	84
Figure 4.3	Experimental setup for the measurement of piezoelectric constant, d_{31}	85
Figure 4.4	PVDF thin film clamped for testing	86
Figure 4.5	Variation of $V_{\text{PVDF,C}}$ with respect to applied load for the commercial PVDF thin film at 10 Hz excitation	90
Figure 4.6	Variation of $V_{\text{PVDF,C}}$ with respect to applied load for the commercial PVDF thin film at 15 Hz excitation	91
Figure 4.7	Variation of $V_{\text{PVDF,C}}$ with respect to applied load for the commercial PVDF thin film at 20 Hz excitation	91
Figure 4.8	Variation of $V_{\text{PVDF,C}}$ with respect to applied load for commercial PVDF thin film at different excitation frequencies	92
Figure 4.9	Variation of $Q_{\text{PVDF,C}}$ with respect to applied load for commercial PVDF thin film at different excitation frequencies	92
Figure 4.10	Variation of d_{31} (C/N) with respect to applied load for commercial PVDF thin film at different excitation frequencies	93
Figure 4.11	Microfabricated PVDF copolymer thin film clamped for testing	94
Figure 4.12	Variation of $V_{\text{PVDF/TFE}}$ with respect to applied load for the microfabricated PVDF copolymer thin film at 10 Hz excitation	99

Figure 4.13	Variation of $V_{\text{PVDF/TiFE}}$ with respect to applied load for the microfabricated PVDF copolymer thin film at 15 Hz excitation	99
Figure 4.14	Variation of $V_{\text{PVDF/TiFE}}$ with respect to applied load for the microfabricated PVDF copolymer thin film at 20 Hz excitation	100
Figure 4.15	Variation of $V_{\text{PVDF/TiFE}}$ with respect to applied load for PVDF copolymer thin film at different excitation frequencies	100
Figure 4.16	Variation of $Q_{\text{PVDF/TiFE}}$ with respect to applied load for PVDF copolymer thin film at different excitation frequencies	101
Figure 4.17	Variation of d_{31} with respect to applied load for PVDF copolymer thin film at different excitation frequencies	101
Figure 5.1	Schematic diagram of cylindrical waveguide with PVDF layer	104
Figure 5.2	3-D Model of Variable Optical Attenuator VOA	105
Figure 5.3	Cross sectional view of cylindrical waveguide	106
Figure 5.4	Finite element model of cylindrical waveguide	107
Figure 5.5	Distribution of the static deflection of the optical fiber (length 5mm) at 100V	108
Figure 5.6	Distribution of the static deflection of the optical fiber (length 7.5mm) at 100V	109
Figure 5.7	Distribution of the static deflection of the optical fiber (length 10mm) at 100V	109
Figure 5.8	Deflection of optical attenuator using commercial PVDF thin film for different lengths at different applied voltages voltage at 16V	110

	AC	
Figure 5.9	Distribution of the static deflection of the Optical Fiber (length 5mm) at 100V	111
Figure 5.10	Distribution of the static deflection of the optical fiber (length 7.5mm) at 100V	112
Figure 5.11	Distribution of the static deflection of the Optical Fiber (length 10 mm) at 100V	112
Figure 5.12	Deflection of optical attenuator using PVDF copolymer thin film for different lengths at different applied voltages	113
Figure 5.13	Insertion loss of optical attenuator using commercial PVDF thin film for different lengths at different applied voltages	116
Figure 5.14	Coupling efficiency of optical attenuator using commercial PVDF thin film for different lengths at different applied voltages	116
Figure 5.15	Coupling efficiency of optical attenuator using PVDF copolymer thin film for different lengths at different applied voltages	117
Figure 5.16	Insertion loss of optical attenuator using PVDF copolymer thin film for different lengths at different applied voltages	117
Figure 5.17	Schematic diagram of cylindrical waveguide with PVDF thin film deposition layer	118
Figure 5.18	Cross sectional view of cylindrical waveguide	120
Figure 5.19	Cross section of the quarter model of cylindrical waveguide (model-1)	120

Figure 5.20	Deformation of the cylindrical waveguide (model-2)	121
Figure 5.21	Deformation results of the cylindrical waveguide-model-2	121
Figure 5.22	Variation of deflection for different voltages	122
Figure 5.23	Variation of coupling efficiencies for different voltages	123
Figure 5.24	Insertion loss of optical fibers for different Voltages	123

LIST OF TABLES

Table 2.1	Thickness variation of PVDF copolymer thin film at different spinning parameters for 10% concentration of solution	51
Table 2.2	Thickness variation of PVDF copolymer thin film w.r.t concentration at fixed spin time of 45 seconds and spin speed 3000RPM	52
Table 2.3	Microfabrication process flow for PVDF copolymer thin films	53
Table 4.1	Piezoelectric charge constants	84
Table 4.2	Experimental test results of d_{31} for a commercial film at 10 Hz excitation	89
Table 4.3	Experimental test results of d_{31} for a commercial film at 15 Hz excitation	89
Table 4.4	Experimental test results of d_{31} for a commercial film at 20 Hz excitation	90
Table 4.5	Experimental test results of d_{31} for a PVDF copolymer thin film at 10 Hz excitation	97
Table 4.6	Experimental test results of d_{31} for a PVDF copolymer thin film at 15Hz excitation	98
Table 4.7	Experimental test results of d_{31} for a PVDF copolymer thin film at 20 Hz excitation	98

NOMENCLATURE

AC	Alternating Current
AFM	Atomic Force Microscope
CVD	Chemical Vapor Deposition
CMOS	Complementary Metal Oxide Semiconductor
dB	Decibel
DC	Direct Current
DRIE	Deep Reactive Ion Etching
ESVAD	Electrostatic Spray-Assisted Vapor Deposition
EPD	Electrophoretic Deposition
FTIR	Fourier Transform Infrared Spectroscopy
FEA	Finite Element Analysis
FEM	Finite Element Method
I-PVD	Ionized -Vapor Deposition method
IR	Infrared
LECVD	Laser Assisted Chemical Vapor Deposition
MOS	Metal Oxide Semiconductor
MOSFET	Metal Oxide Semiconductor Field Effect Transistor
MEK	Methyl Ethyl Ketone
MEMS	Micro -Electro-Mechanical Systems
MOEMS	Micro-Opto-Electro-Mechanical Systems
MST	Micro Systems Technology

MUMPs	Multi-User MEMS Process System
PECVD	Plasma Enhanced Chemical Vapor Deposition
PLD	Pulsed Laser Deposition
PVD	Physical Vapor Deposition
PVDF	Poly Vinylidene Fluoride
PVDF-TrFE	Poly Vinylidene fluoride-Tri Fluoro Ethylene
PZT	Piezoelectric Lead zirconium Titanate
RF	Radio Frequency
RPM	Revolutions per minute
RIE	Reactive Ion Etching
SCREAM	Single Crystal Reactive Etching And Metallization
SEM	Scanning Electron Microscopy
Si	Silicon
SiO ₂	Silicon dioxide
SOI	Silicon-on-Insulator
TMAH	Tetra Methyl Ammonium Hydroxide
TFE	Tetrafluoroethylene
VDCN	Vinylidene cyanide
VOA	Variable Optical Attenuator
XeF ₂	Xenon Difluoride

LIST OF SYMBOLS

A	Absorbance
A_q	Cross sectional area across the length of the film.
A_f	Cross sectional area across the thickness of the film.
cm	Centimeters
cm^{-1}	Wavenumber
C	Coloumb
d_{31}	Piezoelectric charge constant
d	Piezoelectric constant
D	Charge density
E	Electric field
E_i	Transmitted electric field
F	Force
Hz	Hertz
I	Transmitted intensity
I_o	Incident intensity
l	Length of the PVDF thin film
N	Newton
t	Thickness of PVDF thin film
ti	Pause time
tp	Poling interval
T	Stress

V	Voltage across the film (peak-peak)
w	Width
X	Strain
z	z is the separation distance between the fibers
p	pico
β	piezoelectric beta phase
δ	Field radius
ν	Frequency
η	Coupling efficiency
θ	Angular misalignment
n_o	Refractive index
ρ	Charge density
ϵ	Permittivity of the material
s	Compliance
γ	Gain of the PVDF thin film
λ	Wavelength

Chapter 1

Introduction

1.1 Motivation for the research

Few decades ago the curiosity and ingenuity of engineers along with the knowledge gathered from physicist's and chemist's previous work led to the creation of microstructures. Such structures were made from silicon given the remarkable mechanical properties in conjunction with the perfect crystalline lattice. Silicon continues to be the material of preference for the micro-electro-mechanical systems (MEMS) which are integrations of mechanical and electrical miniature systems enabled with automated designed software despite the remarkable properties of silicon, there has been a lot of search in the diversification of the palette of materials used in MEMS. Micro-sensors may benefit from extended type of materials through enhanced sensitivity or reduced cross sensitivity. Micro-actuators with improved resolution may be actuated by other means than electrostatic or electro thermal.

Piezoelectric materials are of primary interest due to large electrical density per unit volume they can generate, their low electrical impedance and low power requirements. In piezoelectric microsystems, silicon is still often used as substrate for subsequent growth. The application of piezoelectric materials in MEMS facilitates the manufacturing of micro devices that would be otherwise difficult to achieve with silicon alone. Unfortunately, piezoelectric materials are commercially available under an unusable format for MEMS, a thin film with metal electrodes on either side [1]. Thin Film

Technology is pervasive in many applications including microelectronics, optics, magnetic, hard and corrosion resistant coatings, micro-mechanics, etc. Progress in these areas depends upon the ability to selectively and controllably deposit thin films; thickness ranging from tens of angstroms to micrometers with desired physical properties. A further step is taken with the integration of piezoelectric materials in MOEMS [2]. Piezoelectric materials such as PVDF and its copolymers PVDF/TRFE can be used in optical microsystems such as optical microswitches, sensors and actuators. The motivation for the present work is to establish a technology to enable deposition and patterning of thin films of piezoelectric materials from polymeric precursor on MEMS or miniaturize non-conformal surfaces. Such capability will enable significant progress in fine tuning and alignment of the optical fibers in micro-optical system.

1.2 Dielectric materials

Dielectric materials are a class of materials which do not conduct electricity, but they can support an electrostatic field while dissipating minimal energy in the form of heat. These properties are useful in capacitors and radio frequency transmission lines. All solids consist of positive and negative charges, when an electric field is applied. these charges will separate. This separation of charges is called "Polarization" and can be utilized to store or carry charges over short distances. Glass, porcelain, mica, rubber, plastics dry air, vacuums and some liquids and gases are dielectric and these materials store or carry charges over short distances. Piezoelectric materials are a particular type of dielectric material capable of using this separation of charge to convert energy. Most piezoelectric materials are ceramic in nature; however the present work is focused on fabrication, characterization and simple application of PVDF copolymer thin films.

1.2.1 Polar forms

Piezoelectricity, Pyroelectricity, Ferroelectricity are the primary characteristics observed in certain crystal structures. Piezoelectric materials are electrically polarized when subjected to stress or deformation hence they can convert mechanical energy to electrical energy and vice versa. Pyroelectric materials have a crystal structure that is spontaneously polarizable and is influenced by a change in temperature. In the class of ferroelectricity certain ionic crystals and piezoelectric polymers may exhibit a spontaneous dipole moment, which can be reversed by the application of an electric field.

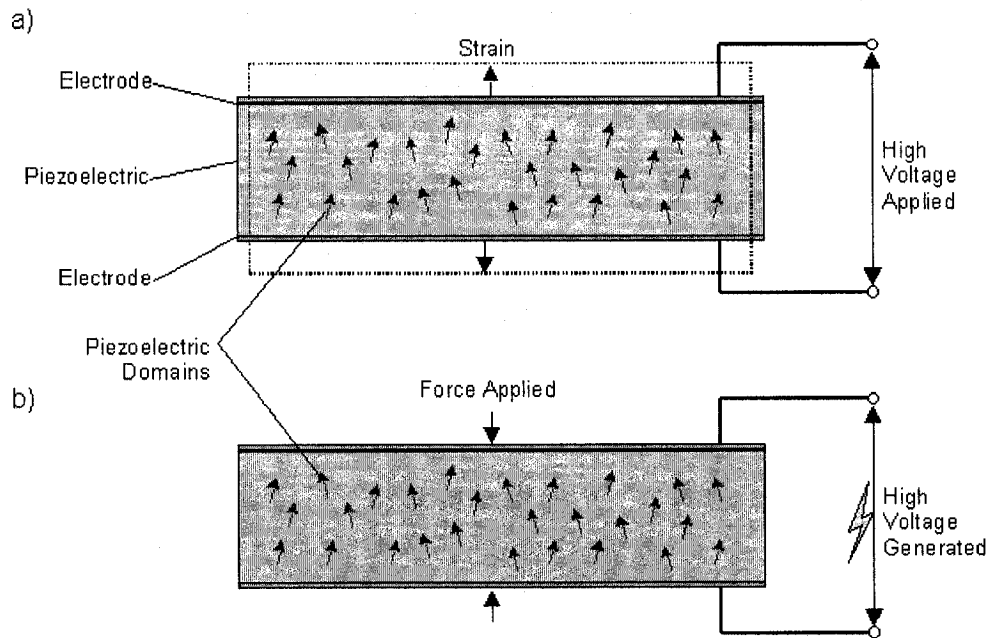
1.2.2 Piezoelectricity

The phenomenon “Pyroelectricity” was first discovered in the early 1700’s. Scientists noticed that when tourmaline crystals were initially placed in hot ashes they would attract and repel the ashes [3]. It was not until 1880 that the phenomenon “Piezoelectricity” was discovered by Pierre and Jacques Curie, they noted that when certain crystals generate a charge on their surfaces when compressed in particular directions. Eventually, both developed the basics of piezoelectric behavior and documented responses of materials such as rochelle salt, quartz, and topaz [4]. In 1946, Walter Guyton wrote one of the first articles to explain the physics of piezoelectricity. His book, *Piezoelectricity*, provided a core understanding of piezoelectric behavior and led the way for current work in the domain of piezoelectricity [5].

1.2.3 Piezoelectric effects

Piezoelectric materials have two responses allowing them to convert between mechanical and electrical energy. The primary effect is called the direct effect. This is when a force

applied to a piezoelectric crystal charge produces on the crystal surface. The secondary effect is known as the converse, or the indirect effect as shown in Figure 1.1. This is when the application of a voltage across a piezoelectric crystal results in a shape change. Both the direct and converse effects are commonly used for various applications.



a) When a voltage is applied across a poled electroded piezoelectric device, the material expands in the direction of the field and contracts perpendicular to the field;
b) When a force is applied to the piezoelectric, an electric field is generated.

Figure 1.1: A diagram illustrating direct and converse effects of piezoelectricity [5]

The equations below are the constitutive equations of piezoelectric materials. They describe the two piezoelectric effects with respect to electrical and elastic properties [5].

Direct Effect

$$D = dT + \epsilon E$$

Converse Effect

$$X = sT + dE$$

Where

$E = \text{Electric field}$

$T = \text{Stress}$

$\varepsilon = \text{Permittivity of the material}$

$X = \text{Strain}$

$s = \text{Compliance}$

$D = \text{Charge density}$

$d = \text{piezoelectric constant}$

D is equal to the surface charge divided by area; d is a piezoelectric coefficient. The above equations are commonly represented in a matrix to form a set of equations that can relate properties of a material along various orientations.

1.3 Piezoelectric polymers

Piezoelectricity originates with its existence in synthetic and biological polymers; examples of natural piezoelectric polymers are wood and tendon tissue. Kawai [6] was one of the pioneers in the area of piezoelectricity. He realized that piezoelectric and pyroelectric activity could be generated in synthetic polymer films after being subjected to a strong DC electric field at higher temperatures [6]. The inherent mechanical properties of piezoelectric materials which can be tailored accordingly for new applications and devices made it an interesting and emerging topic in the arena of science and later on, in the area of Micro Electro Mechanical Systems. The best known polymer

which is being widely used in the area of MEMS is PolyVinylidene Fluoride (PVDF) and its copolymers.

For commercial and technical application, any polymer of high piezoelectric response will be of interest. To have high piezoelectric properties it is necessary to form a remnant polarization; coincidentally, few polymers that do form a remnant polarization are also ferroelectric. The four polymer families are known to have ferroelectric properties are

- PVDF and its copolymers with trifluoroethylene (TrFE) and tetrafluoroethylene (TFE).
- Nylons and various Vinylidene Cyanide (VDCN) copolymers.
- Aromatic and aliphatic polyurea.

Different methods are adopted to stabilize the remnant polarization the VDCN copolymers which may be stabilized by applying a DC electric field (poling) while the material is cooled through the curie temperature. Although the Curie temperature varies for these polymers, PVDF shows the highest piezoelectricity at room temperature [7]

PVDF is of high interest in the area of research in the last 25 years as it shows the highest piezoelectric response at room temperature. In 1969 when Kawai discovered a presence of piezoelectricity in PVDF, it has been found that strong piezoelectricity exist from uniaxially drawn polyvinylidene fluoride after it has been poled in a suitable electrical field [7]. The ferroelectric, and thus piezoelectric, properties of PVDF are an example of the interaction of charges and dipoles, charge injection, charge trapping and detrapping. and the influence of different crystal phases on the physical and electrical properties of polymers. PVDF copolymers, such as, trifluoroethylene (TrFE) have also been in the area

of study for almost 20 years, with most of the copolymers having strong ferroelectric properties of their own. PVDF-TrFE also shows a reversible transition at the curie temperature, from a ferroelectric to a paraelectric phase, with strong dependence of the curie temperature depending on chemical composition [7]

PVDF has also been found to remain ferroelectrically stable after many years of storage. The plot below shows the surface charge on PVDF samples measured after 22, 27, and 35 years of being wrapped in metal foil and stored in a dessicator [8]

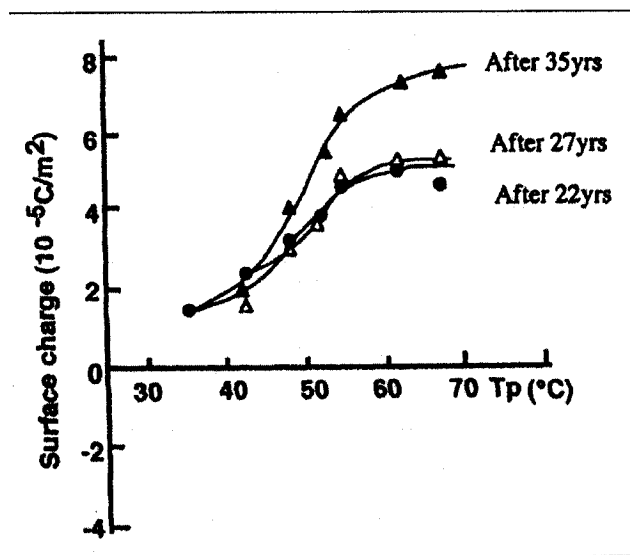


Figure 1.2 Study of surface charge on PVDF samples at 22-35 years after preparation [8].

The magnitude of the surface charge is plotted against the poling temperature with a poling electric field of 4 MV/m.

1.3.1 Polyvinylidene fluoride and comparison with its copolymers.

If PVDF is polymerized with trifluoro ethylene (TrFE), which is commonly known as P(VDF-TrFE) with randomly distributed monomer units shown in Figure 1.3. The extra fluorine atoms in the chain reduce the influence of the head to head and tail to tail

defects. This effect increases the crystallinity of the copolymers to about 80%, after the copolymer films have been annealed at a particular temperature.

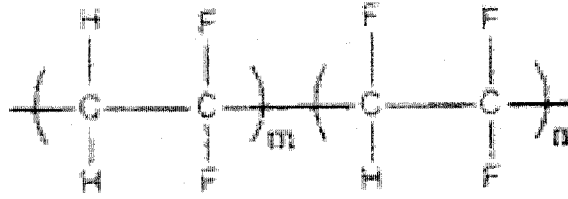


Fig 1.3: PVDF Copolymer polymerized with Trifluoroethylene (TrFE) [9].

It is reported in earlier work that if the TrFE content is higher than 18%, then the PVDF/TrFE copolymer will crystallize with the same chain conformation as the β -PVDF. The β phase of this copolymer can be further improved by annealing and simultaneous stretching and poling, because of the large fluorine atoms, the a and b axis of the unit cell of the copolymer are larger than those of β -PVDF and therefore cause faster dipole alignment than β -PVDF[9-10]. The resulting lattice structure and dipole alignment of the copolymer are the same as PVDF. Even though the TrFE monomer unit has a smaller dipole moment than PVDF, the polarization of the copolymers is usually higher than pure PVDF because of higher crystallinity of the copolymers.

Another way to form highly oriented PVDF copolymer structures is vacuum evaporation of the polymer on suitable substrates. The total thickness, the substrate temperature, the deposition rate, the application of electric field and the substrate type and material strongly influence the alignment of the polymer on the substrate. In such cases the polymer chains are produced by evaporation on glass with an intermediate layer of highly oriented PTFE [11-12]

Unlike PVDF homopolymer, PVDF copolymer exhibits higher electro negativity due to higher abundance of the polar all-trans conformation and also P(VDF-TrFE) copolymer crystallizes directly into β -phase when the molar ratio of VDF(x) and TrFE ($1-x$) is within an adequate range [13]. In these polymers β -phase is of primary interest as it exhibits highest polarization capability of all the phases. Hence, extensive research work has been focused to investigate on β -phase by several techniques such as Fourier Transform Infrared Spectroscopy (FTIR) studies. Several authors reported the IR transmission spectra of PVDF and P(VDF-TrFE) (80/20) films clearly shows many absorbance peaks at 1402, 1286, 1186, 1124, 1077, 883, 844, and 476 cm^{-1} and many weak absorbance peaks at 1430, 943, 678, 505 cm^{-1} , and so on as illustrated in Figure 1.4 [14].

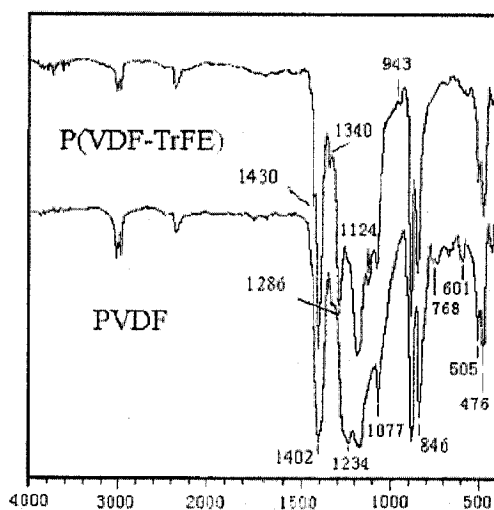


Figure 1.4: IR transmission spectra of PVDF and P (VDF-TrFE) in the range 4000-500 cm^{-1} [14].

Compared with PVDF, the P(VDF-TrFE) exhibits the appearance of a new strong absorbance peak at 1286 cm^{-1} as shown in Figure 1.5, which is characteristic of the ferroelectric β -phase [15]. At the same time, the peaks at 1234 and 768 cm^{-1} disappear

and the peaks at 1077 and 601 cm^{-1} become weaker. All these peaks are attributed to the TG sequence of the paraelectric β -phase. The peak at 812 cm^{-1} is characteristic of the β -phase (T_3G), which is seen in PVDF but not in P(VDF-TrFE) copolymer [16, 17]. It can therefore be concluded that P(VDF-TrFE) (80/20) directly crystallizes into the ferroelectric β -phase from melting temperature.

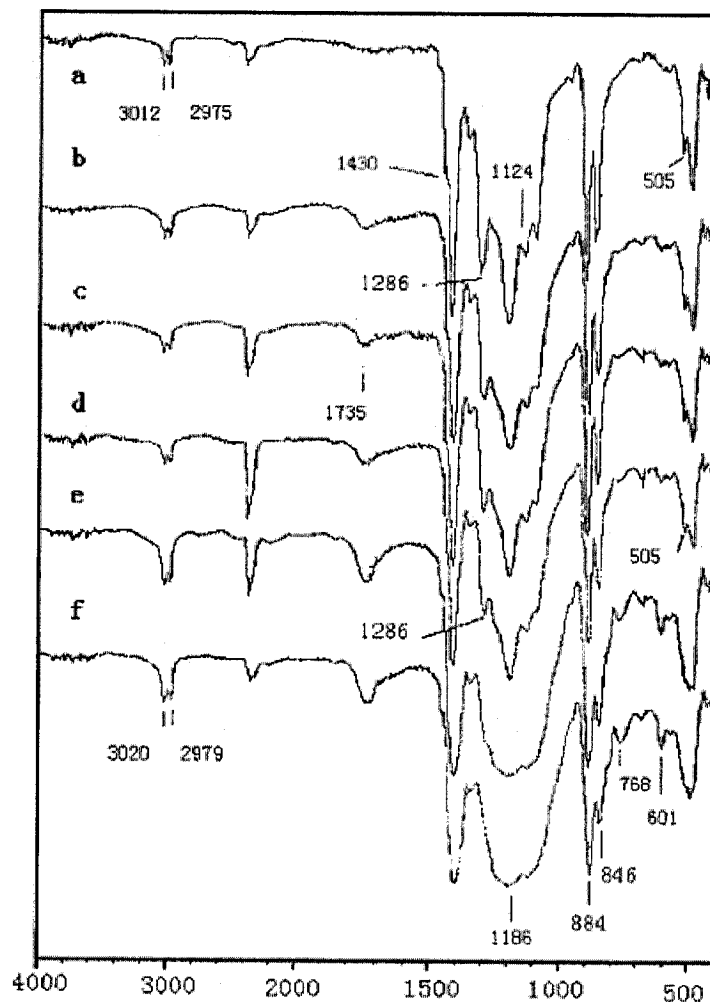


Figure 1.5: IR transmission spectra of P(VDF-TrFE) at different irradiation doses in the range 400-4000 cm^{-1} : (a) 0 Mrad, (b) 60 Mrad (c) 70 Mrad (d) 80 Mrad , (e) 100 Mrad , (f) 110 Mrad[19].

IR transmission spectra of P(VDF-TrFE) at different electron irradiation doses are presented in Figure 1.5. The absorbance at 2360 cm^{-1} is attributed to vibration of CO_2 existing in the sample chamber. For no irradiated film, the spectrum shows a broad and very weak band at the region of 1730 cm^{-1} and two peaks at 3012 and 2975 cm^{-1} , which are the asymmetric stretching vibration of the C-H bond [19]. With increasing irradiation, the bands at 3012 and 2975 cm^{-1} shift slightly to a high wave number region (3020 and 2979 cm^{-1} at 110-Mrad dose), which is attributed to the decreasing concentration of comonomer unit ($-\text{CHF}-\text{CF}_2-$) in the irradiated copolymer structure [19-21].

Several authors carried out structural identification of copolymers of PVDF extending their analysis on polymer matrix such as PVDF/TrFE-PbTiO₃ [22-23]. In the PVDF/TrFE-PbTiO₃ spectrum, the absorption band at 800 cm^{-1} is common to α , β and γ phases, and therefore cannot be used to uniquely characterize a phase. However, the absorption band at 834 cm^{-1} characterizes the β phase and the absorption band at 795 cm^{-1} also characterizes the α phase only [24]. In the range of $700\text{-}1000\text{ cm}^{-1}$, when the 880 cm^{-1} and 834 cm^{-1} bands are compared relatively, it is observed that β phase (834 cm^{-1}) increases, the band at 880 cm^{-1} (common to the α , β and γ phases) decreases. Hence it is reported that the annealing process increases the crystallization of the copolymer in the β form even in the presence of the PbTiO₃. Pyroelectric and dielectric measurements of P(VDF-TrFE) also support these results. Properties of the polymers, in which CF_2 dipoles are connected strongly by covalent bonding to the main chain, are sensitive to conformational changes. The changes can be induced by mechanical orientation, electric poling or heat treatment, and are rather drastic in the temperature range of the ferroelectric-paraelectric phase transition. The conformational structure of the copolymer

is determined by the molar contents of PVDF and film preparation conditions [24-25]. The FTIR technique of PVDF samples is also used to analyze poled and non poled thin films.

The poling process induces a slight increase of the dielectric constant of the material [26] and this increase is attributed both to the preferred alignment of the dipoles of the β phase material and to the α to β transformation due to the application of the electric field. The effect of poling on the relaxation mechanism of the polymer is not significant, i.e., poling does not significantly influence the amorphous part of the semicrystalline material.

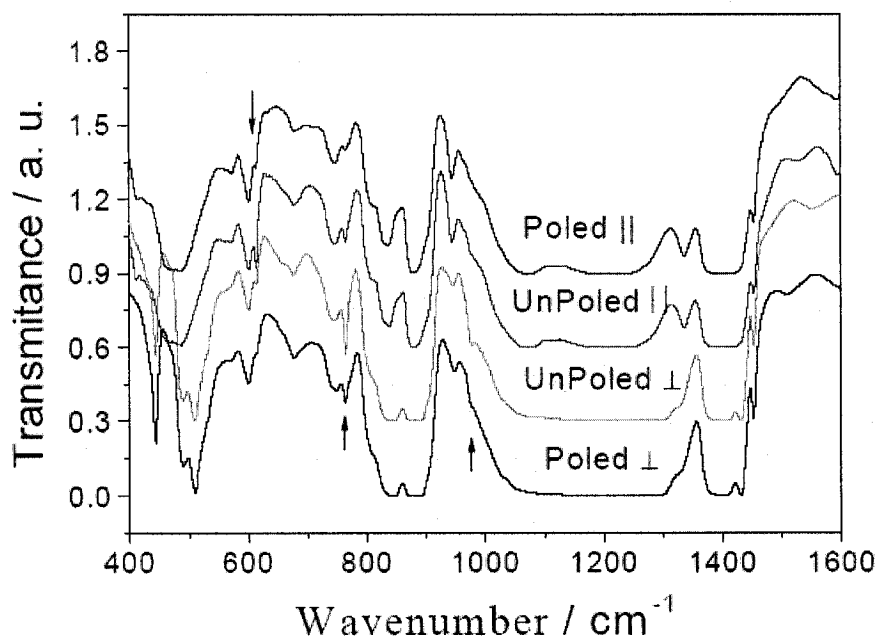


Figure 1.6. Detail of the transmittance FTIR spectra at room temperature for poled and non-poled β -PVDF films in parallel and transversal modes. Some of the modes with more relevant changes upon poling are indicated by arrows [26].

Although the general kinetics of the segmental mobility process is not affected (here quantified by the fragility) the non-poled material shows a higher T_g , which points out at more restrictions to the cooperative mobility in the amorphous phase for this film. Poling induces a general increase of the conductivity of the material, i.e., charge injection must exist during the poling of the material. On the other hand the mechanism responsible for the ionic conductivity does not seem to be affected by poling.

From the FTIR spectra shown in Figure 1.6, partial rotation of the molecular chains (alignment of the dipoles with the applied field) and conversion of α into β phase are the main effects of the poling field. The α to β transformation that occurs by mechanical stretching of the polymer is optimized by the poling field [26].

1.3.2 Merits and demerits of PVDF copolymers.

Compared to PVDF homopolymer, the application of PVDF copolymer with Trifluoroethylene proves to be a very promising application in thin film technology. It has been reported in previous studies that PVDF copolymer crystallizes directly into highly polar crystalline (β phase) upon cooling from the melt to below the curie (paraelectric-ferroelectric) unlike in PVDF homopolymer [27]. It is estimated that P(VDF-TrFE) parameters confirms better properties of copolymer for application in the area of transducers then those of homopolymer. The main advantage being that they have an electromechanical coupling factor by about 50% larger and also wider usable annealing temperature range. Moreover the copolymer film does not require mechanical stretching to be made piezoelectric, unlike the pure polymer film and these copolymers can be operated in air at ambient temperature and have a consistent response over a large

bandwidth [28]. In the present study, microfabrication and characterization of PVDF copolymers using thin film technology is presented.

It is the PVDF family that appears to have found most widespread applications, the advantages of these polymers are as follows.

- Excellent mechanical properties and chemical resistance.[29]
- High temperature capabilities (continuous use at temperature up to 150° C and excellent chemical ageing resistance)
- Easy processing by extrusion, injection, compression, blow moulding, solution process and high purity resin
- Suitable for microfabrication in the domain of thin film technology [30]

1.4 Microfabrication of PVDF copolymer thin films

In the area of thin film technology there have been several methods adopted for deposition of thin films. However, as all methods have their specific limitations and involve compromises with respect to process specifics, substrate material limitations, expected film properties, and cost, which makes it difficult to select the best technique for any specific application. In deposition of films, if the thickness of film is greater than 2 microns it is generally referred as thick film. However in the present study, the obtained films are termed as thin films irrespective of the film thickness. In the present study of various available methods such as Physical vapor deposition, Chemical vapor deposition, etc. The *Spin-coating* method is adopted for microfabrication of PVDF copolymer thin films. Detailed description of various microfabrication techniques are further discussed in Chapter 2 of the thesis.

Preparation of proper polymer solution to cast thin films is a very important factor to achieve a proper and uniform thin films on the substrates moreover the selection of suitable solvent for the copolymer is again an important factor for preparing thin films. In spin-coating technique film thickness can be controlled mainly by the concentration of solution prepared and spin parameters such as spin time, spinning speed etc [31]. The film on the substrate is sandwiched between two metal electrodes such as aluminium or gold. In the present work an in-depth analysis on spin-coating technique of thin PVDF copolymer films is presented in the subsequent chapters.

1.5 Polarization of PVDF copolymer thin films (*poling*).

The significant phase of piezoelectric thin film processing is the polarization of PVDF thin films commonly referred as “poling”. There are various methods of poling of piezoelectric polymers adopted in the process according to the feasibility of the desired piezoelectric device. Polarization of these polymers is generally based on the application of a high electric field across the thickness of the copolymer which result in piezoelectric property of the film. Polarization methods For P(VDF-TrFE) copolymers is generally made through the application of a high electric field across the thickness of the copolymer film The resulting pyroelectric coefficient of the copolymers depends on the degree of polarization and thus on the applied field strength. Two basic methods of poling have been systematically used in polarization of piezoelectric copolymers, thermal and corona poling. Electrode poling (thermal poling) method uses the direct application of a potential difference across electrodes mounted on the two sides of the film at room temperature or elevated temperatures [32]. In corona poling, one deposits charge of opposite polarities on the film surfaces by exposing at least one surface to a corona

discharge [33-34]. With electron-beam poling, the front surface of the polymer is irradiated, while the rear surface is connected to the ground [35]. The polarization profiles achieved with the corona poling and electron-beam poling are less uniform than with electrode (thermal) poling. Furthermore, these two methods are not proficient for on-chip poling of P(VDF-TrFE) copolymers deposited on an integrated silicon substrate due to the risk of damage of the readout electronics. The application of a high electric field involves the risk of electrical and thermal breakdowns, particularly if the film thickness is not constant or if the film contains imperfections, voids or impurities. Breakdown occurs then at a lower field than the electric breakdown strength of the copolymer. In the present work “step-wise” poling is adopted in this work. It is performed by a series of five consecutive pulses of several minutes, and with successively increasing the voltage amplitude [36]. The methodology of step-wise poling is presented in Chapter 2.

1.6 PVDF MEMS

Usually, for device applications, the oxide ferroelectric is superior on the non oxide material since the PZT material permits low actuation voltages due to its intrinsic electrical properties with the drawback of much complex manufacturing means. The PVDF material deposition is much simpler than other piezoelectric materials. In the emerging area of piezoelectric thin film technology it is observed that some of the copolymers of PVDF with Trifluoroethylene (TrFE) have been found to possess significant piezoelectric properties

PVDF MEMS is having an edge over other piezoelectric materials with respect to applications in MEMS. PVDF is of use in sensor applications due to its piezo and

pyroelectric materials. It can be built into panel switches for alarm and control applications or pyroelectric detectors for rugged infrared sensors [37]

Several authors proposed and fabricated piezoelectric devices in MEMS technologies. Lee et al proposed and batch fabricated using standard IC technologies a piezoelectric sensor using PVDF copolymers in which a 70/30 molar ratio vinylidene/trifluoroethylene copolymer is used for a N-channel enhancement type MOS transistors with extended metal gates. A thin (2.5 μm) copolymer film was spin coated on the wafers, electroded, poled and selectively etched [37]. Similarly, Philip et al developed a 64 element array of pyroelectric elements fully integrated on silicon wafers with MOS read out devices [28]. The application of PVDF MEMS is further extended in the application of imaging sensors by D Setiadi et al in which a novel two dimensional vinylidene/trifluoroethylene copolymer pyroelectric sensor is fabricated, in this work to improve the performance of integrated pyroelectric sensors, the silicon wafers that contains the read out electronics is coated with a VDF/TrFE copolymer thin film using a spin coating technique [38-39].

Application of PVDF films found a place in the area of vibration sensors made from PVDF film attached to resonant structures which are used in acoustic and fluid flow detectors. Thus "singing" sensors in which the piezoelectric properties of PVDF film enabled to excite a structure resonate and detect changes in its resonant frequency, are used as tactile sensors, contact sensors and fluid level meters [40]. In the area of robotics applications of force sensors are beginning to require the construction of arrays of miniature sensing elements to replicate the tactile cells of human fingertips. Currently these are built as two-dimensional arrays of MOSFET' on a silicon wafer, on top of which

a PVDF thin film is placed or by the deformation of mechanical beams etched on the surface [28].

1.6.1 Applications of PVDF copolymer as thin films

PVDF copolymers are known to exhibit higher electro negativity than that of PVDF homopolymer due to higher abundance of the polar all-trans conformation. Hence PVDF copolymers are chosen in this work since they promise to yield excellent piezoelectric properties. In the present work, a novel application of PVDF copolymers in the area of MEMS has been proposed, integrating with optical microsystems. A simple application of PVDF thin films as Variable Optical Attenuator (VOA) is presented as a potential application.

1.7 Literature review on attenuators.

Optical attenuators play an important role in optical systems and networks. An optical path can be attenuated by introducing some type of mechanism affecting the losses of the path. This can be regarded as a transfer function incorporated between the coupling and the load reducing the amplitude of the input signal detected at the output. The attenuation can be a fixed value, but ideally, for improved performance of a system, variable attenuation for flexibility and practicability is preferred [41]. The conventional approaches to manufacture optical attenuators are quite large compared to other optoelectronic components such as detectors, amplifiers and other components. The need for smaller, better performance and simple attenuators created a motivation to the MEMS application and technology communities to invest more energy in research and development to achieve the market demand. For an existing optical bench, the

introduction of some attenuation in a certain path requires the addition of an extrinsic component to satisfy the attenuation characteristics. The Variable Optical Attenuator (VOA) can be categorized as external and internal components. The external VOAs are attenuators that are added to an existing system without altering the existing design. The internal VOAs are considered as components already present in the system, like fiber optic sections modified originally during the manufacturing in order to present normal fiber operation when no actuation mechanism applied, and present attenuation when some actuation means is performed. Hybrid type components (external and internal) can also be used where the complementary of external and internal components improve the efficiency and flexibility of the complete system and the optical architecture. The proposed work uses a PVDF (Poly Vinylethane Fluoride) actuation approach in the design and implementation of these variable attenuators. The restrictions and design parameters of the project dictate the technology that would be implemented during the fabrication cycle and the necessary processes to meet the specified requirements.

1.7.1 VOAs design parameters

The most significant design parameters for VOAs are given by [42-43]:

- Insertion loss
- Return loss
- Attenuation range
- Polarization dependant loss
- Temperature dependant loss
- Wavelength range and wavelength dependant loss
- Maximum optical power and response time

- Environmental conditions (stability with temperature, humidity and water immersion)
- Packaging solutions and reliability.

Practical attenuation ranges would be between 40 to 50 dB, with typical insertion and return losses of 0.8 dB and 45 dB respectively. Usually polarization losses are less than 0.2 dB.

1.7.2 External VOAs

Commercial external VOAs are very common and can be inserted between two fibers. When the attenuation value is fixed, then the usual VOAs are air gap type attenuators. They are less expensive, less accurate, with wavelength dependant attenuation and usually with poor back reflection performances. Variable attenuators are very common but are more expensive than the fixed ones. Most of these attenuators are in-line type attenuators.

1.7.3 Internal (built-in) VOAs

These attenuators are usually factory installed or factory processed on fibers. Variable attenuation can be obtained by using some electronic means to apply electrostatic voltages on actuation structure. In order to attenuate an optical signal, the simplest way is to create some type of perturbation by adding a material and/or displacing a component in the optical path. In microsystems the controlled displacement of a piece or structure is considered as an actuation.

1.7.4 Actuation mechanism.

The attenuation of an optical signal based on actuation mechanism can be ensured with different type of forces. The major types of actuation means are the following:

- Piezoelectric (ferroelectric)

- Metal bimorph thermal effect
- Electrostatic
- Thermal
- Magnetic.

Each of these types of actuations has its own advantages and disadvantages. The advantages of piezoelectric actuation over the other actuation mechanisms are the high sensitivity and good linearity. The disadvantages are the complexity of the design and the limitation of strain.

In this work modeling, simulation of the proposed piezoelectric variable optical attenuator are discussed in detail in Chapter 5.

1.8 Methodology

Piezoelectric thin film is a heart of the piezoelectric MEMS sensor and actuators, hence it is very important to have a detailed understanding of the development of crystal structure, micro structure and properties of these films are very much necessary for the MEMS structural design and process integration

The objectives of the work are to primarily discuss on novel applications of piezoelectric materials in MEMS. The work mainly emphasis on thin film technology. Piezoelectric crystal can be obtained by various deposition techniques such as PVD, CVD, etc. Spin coating deposition technique appeared to be the most simple, reliable and low cost technique. PVDF copolymer thin films are achieved by spin coating the PVDF copolymer solution onto the silicon wafers/substrates.

The spin coated P(VDF-TrFE) thin films are annealed. Annealing of the samples is performed so as to improve the crystallinity of the thin films; the samples were heated at

temperatures in a range from 100 to 180°C with interval of 10 °C. In previous work Mi Akcan et al reported about the effect of annealing of PVDF copolymer with composition ratio of 70/30 mol% VDF/TrFE the effect of annealing was analyzed through Infrared spectroscopy studies [24]. In the present work the effect of annealing of PVDF copolymer with composition ratio of 65/35 mol% is systematically studied in the temperature range of 100-180 °C within intervals of 10 °C. Further investigation in the “annealing” aspect of the samples was carried out by consecutive annealing of P(VDF-TrFE) thin films so as to monitor the polarized crystalline phase of PVDF-TrFE thin films.

The main aspect of the piezoelectric thin films is polarization. The method of applying high voltages to the PVDF films is referred as “Poling”. As mentioned above, there are several methods proposed for poling of piezoelectric thin films such as ferroelectric poling, electron beam poling, corona poling at room temperature, step-wise poling [36].one of the primary objective of the work is to pole the film, “step wise poling method” is adopted for polarization of thin films as this method is considered to be simple and the most reliable method. Transmission and absorption spectra were analyzed through FTIR technique to investigate the significant polarized phase of PVDF-TrFE thin films subjected to poling FTIR results are analyzed through the interpretation of absorption and transmission spectra of poled PVDF copolymer thin films. Further the spectra of fabricated copolymer thin films are compared with that of commercially available films and analyzed.

The piezoelectric properties of PVDF films are visualized through the piezoelectric constants which attribute to the output of PVDF copolymer thin films.

The piezoelectric constants relating the mechanical strain produced by an applied electric field are termed the strain constants, or the "d" coefficients. The units may then be expressed as meters per meter, per volts per meter (meters per volt).

$$d = \frac{\text{strain development}}{\text{applied electric field}}$$

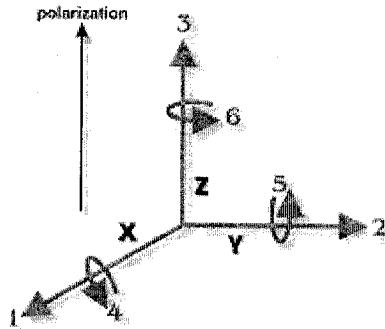


Figure 1.7: Direction of forces affecting the piezoelectric constants.

It is useful to remember that large d_{ij} constants relate to large mechanical displacements which are usually sought in rotational transducer devices. Conversely, the coefficient may be viewed as relating the charge collected on the electrodes, to the applied mechanical stress. d_{33} applies when the force is in the 3 direction (along the polarization axis, as shown in Figure 1.7) and is impressed on the same surface on which the charge is collected. d_{31} applies when the charge is collected on the same surface as before, but the force is applied at right angles to the polarization axis. The subscripts in d_{15} indicate that the charge is collected on electrodes which are at right angles to the original poling electrodes and that the applied mechanical stress is shear.

The units for the d_{ij} coefficients are commonly expressed as coulombs/square meter per newton/square meter.

$$d = \frac{\text{short circuit charge density}}{\text{applied mechanical stress}}$$

When the force that is applied is distributed over an area which is fully covered by electrodes (even if that is only a portion of the total electrode) the units of the area cancel from the equation and the coefficient may be expressed in terms of change per unit force, coulombs per newton. To view the d_{ij} coefficients in this manner is useful when charge generators are contemplated, e.g., accelerometers [40]. The poled PVDF copolymer thin film sample was subjected to strain along its surface. This was applied by a lever mechanism and measured by a load cell at the point of application of force as shown in the schematic Figure 1.8

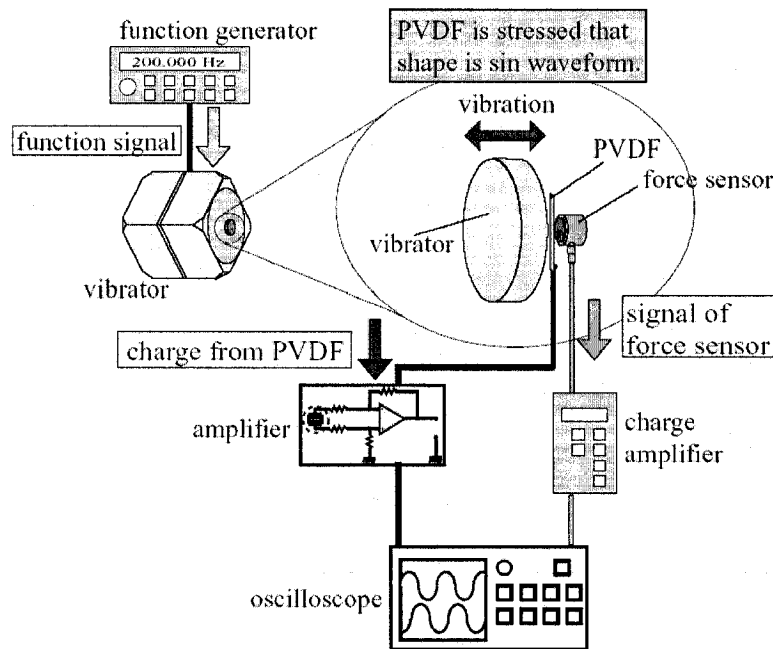


Figure 1.8 Experimental setup for the measurement of piezoelectric constants of PVDF copolymer thin film

The load cell measurements were monitored by charge amplifier which is connected to oscilloscope to monitor the varied applied force. The charge output generated across the sample was measured with another charge amplifier simultaneously with the load cell measurements and a relationship of charge output vs. applied force was obtained and hence the piezoelectric constant d_{31} is evaluated for the specific geometry of the specimen considered.

In the present work the necessary output characteristics of microfabricated PVDF copolymer thin films are visualized by measurement of piezoelectric constants, The piezoelectric d_{31} constant for the best annealed and poled film is presented. The measured piezoelectric d_{31} constant of the microfabricated thin films are compared to that of measured values of the available commercial PVDF thin films from Measurement Specialties Inc.

The other objectives of this work are to propose a design and simulate a specific Variable Optical Attenuator for optical applications using the technology of Micro Optical Electro Mechanical Systems (MOEMS). The first part of the design consists of modeling and simulation of the proposed cylindrical optical waveguide by finite Element Analysis (FEA) using ANSYS. The second part is the evaluation of the attenuator characteristics for different geometrical parameter of the cylindrical waveguides through simulations and also by using the piezoelectric coefficients for the P(VDF-TrFE) copolymer. This will permit to assess the influence of the length variation on the overall performances of the VOA under different applied voltages in comparison with similar attenuator that uses as PVDF.

1.9 Thesis layout

Chapter 1 introduces the research topic and presents the rationale of the work. A brief literature review and survey on the work previously done related to Piezoelectric MEMS and it also discusses extensively about the material characteristics of PVDF and its copolymers. The overview of the thesis is also discussed in brief.

Chapter 2 Literature on various deposition techniques of PVDF thin films is presented, further microfabrication of PVDF copolymer thin films using spin-coating is presented, spinning characterizations of microfabricated PVDF copolymer thin films are presented by varying various spin parameters. Poling of PVDF copolymer thin film through step wise poling technique is presented.

Chapter 3 Characterization of the obtained PVDF copolymer thin films is carried out by FTIR techniques for material characteristics of PVDF copolymer thin films

Chapter 4 Measurement of piezoelectric constants is carried out for characterizing the piezoelectric properties of the obtained PVDF copolymer thin films and are compared with that of commercially available PVDF thin films

Chapter 5 Application of PVDF thin films in MEMS.

A novel model of PVDF based optical attenuator using available commercial thin films and PVDF copolymer thin films are presented. The model is simulated in ANSYS and results are discussed.

Chapter 6 Conclusions and recommendations for future work is presented

1.10 Summary

An introduction to the piezoelectric materials and a brief discussion on thin film technology in PVDF MEMS is discussed, also this chapter discusses about the advantages of PVDF copolymer films over PVDF homopolymer films , further literature review on the FTIR spectra of spin coated PVDF copolymer thin films is discussed, a brief literature review on the commercially available optical attenuators is also presented A short description of the experimental setup on the measurement of piezoelectric constant(d_{31}) is also presented. At the end of the chapter the primary objectives of this work and the thesis layout are presented.

Chapter 2

Microfabrication of PVDF copolymer thin films for MOEMS applications

2.1 Microfabrication of PVDF/TrFE copolymer thin films

Thin film technology is pervasive in many applications, including microelectronics, optics, magnetism, hard and corrosion resistant coatings, micro-mechanics, etc. Progress in each of these areas depends upon the ability to selectively and controllably deposit thin films with thickness ranging from tens of angstroms to micrometers with specified physical properties. This in turn requires control often at the atomic level of film microstructure and microchemistry. There are a vast number of available deposition methods in use today. However, as all methods have their specific limitations and involve compromises with respect to process specifics, substrate material limitations, expected film properties, and cost, which makes difficult to recommend the best technique for a specific application. There are various deposition methods in the domain of thin film technology being implemented, The classification of the deposition techniques can be broadly categorized as

- Chemical vapor deposition
- Physical vapor deposition

2.1.1 Chemical vapor deposition (CVD)

CVD is capable of producing *thick, dense, ductile, and good adhesive coatings* on metals and non-metals such as glass and plastic. Contrasting to the PVD coating in the "line of sight", the CVD can coat all surfaces of the substrate. [41]

Conventional CVD process requires a metal compound that will volatilize at a fairly low temperature and decompose to a metal when it is in contact with the substrate at higher temperature. The thermal energy is the sole driving force in high temperature CVD reactors; for lower temperature deposition an additional energy source is needed. Radio frequency (RF), photo radiation, or laser radiation can be used to enhance the process, known as plasma enhanced CVD (PECVD), photon assisted CVD [42] or laser assisted CVD (LCVD), respectively [42].

In laser assisted and photon CVD systems part of the energy needed for deposition is provided by photons. This method provides the need for an extremely low temperature deposition process, with a laser source capability to write a pattern on the surface directly by scanning the micron-size light beam over the substrate in the presence of the suitable reactive gases, further with adjustment of the focal point of laser continuously, it is even possible to grow three dimensional microstructures such as fibers and springs in a wide variety of materials such as boron, carbon, tungsten, silicon, SiC, Si₃N₄, etc

In Plasma enhanced CVD (PECVD) plasma activation provides the radicals that result in the deposited films, and ion bombardment of the substrate provides the energy required to arrive at the stable desired end products. The operational temperatures are lower, as part of the activation energy needed for the deposition comes from the plasma [43].

Diamond CVD process is introduced to increase the surface hardness of cutting tools. However, the process is done at the temperatures higher than 700 °C (1300 °F), which will soften most tool steel. Thus, the application of diamond CVD is limited to materials which will not soften at this temperature [42]

2.1.2 Physical vapor deposition (PVD)

Physical vapor deposition technique involves atom by atom, molecule by molecule or ion deposition of various materials on solid substrates, various types of thin films in IC and micromachining are deposited by *evaporation* and *sputtering* which are examples of physical vapor deposition (PVD). In the literature review it has been proved that in the case of the physical vapor deposition the substrate temperature is a significant parameter to obtain a uniformly deposited thin film. If the temperature of the heat source is more than 300 °F, the quality of the PVDF homopolymer thin film is not uniform and moreover the deposition rate is also faster. If the temperature is below 300 °F, the quality of the film obtained is not uniform and the deposition rate is low, to obtain a uniform PVDF thin film the substrate temperature is fixed at 285 °F, In previous work it is concluded that to obtain a uniform PVDF thin film the substrate temperature is fixed at 285 °F [43]. Various methods described below can be grouped in physical vapor deposition technique.

2.1.2.1 Thermal evaporation

Thermal evaporation is one of the oldest deposition technique in practice in domain of thin films; thermal evaporation uses the atomic cloud formed by the evaporation of the coating metal in a vacuum environment to coat all the surfaces in the line of sight between the substrate and the target (source). Thermal evaporation is often used in

producing upto 5 μm thick film and *decorative* shiny coatings on plastic parts. The thin coating, however, is fragile and not good for wear applications [44].

2.1.2.2 Sputtering

High-technology coatings such as ceramics, metal alloys, organic and inorganic compounds by connecting the work piece and the substance to a high-voltage DC power supply in an argon vacuum system (10^{-2} - 10^{-3} mm Hg). The plasma is established between the substrate (work piece) and the target (donor) and transposes the sputtered off target atoms to the surface of the substrate. When the substrate is non-conductive, e.g., polymer, a radio -frequency (RF) sputtering is used instead. Sputtering can produce *thin*, less than 3 μm (120 μin), *hard* thin-film coatings [42].

2.1.2.3 Ionized – vapor deposition method (I-PVD)

PVDF film deposition is achieved by ionized vapor deposition technique in which the vapor of the decomposition products of PVDF ejected through the nozzle was ionized by electron bombardment. These ions were accelerated by an acceleration voltage, which is applied to a substrate onto which the PVDF film was deposited. The deposition was carried out at a very high temperature and ionization was done at a high energy, enough for bond cleavage, decomposition of PVDF (such as elimination of HF and formation of unsaturated bonds), is liable to occur. When a high acceleration voltage or a high ionization current was employed, the PVDF films contained significant amounts of oxygen. It is found that deposition under the drastic conditions (a high acceleration voltage and high ionization current) results in bond cleavage. The film prepared under mild conditions (a low acceleration voltage and low ionization current) contained small amounts of oxygen. From these, it was found that elimination of fluorine atoms and

generation of radicals hardly occurred. The molecular weight of the PVDF film was decreased to about a tenth of that of the initial PVDF. Vaporization which takes place during the heating of PVDF is thought to result from cracking of the polymer. Both the acceleration voltage and ionization current affect the formation of the form I crystal. When the acceleration voltage and ionization current were changed, the amounts of ions reaching the substrate varied. Therefore, it is expected that one factor determining the crystal forms in PVDF film prepared by this method is the ion current.

Utilization of the ions in deposition process is effective in controlling crystal forms and their orientation [43].

2.1.2.4 Electron beam deposition

In laboratory settings a metal is usually evaporated by passing a high current through a highly refractory metal containment structure (e.g., a tungsten boat or filament). This method is called resistive heating. However, in industrial applications resistive heating has been replaced by electron-beam (e-beam), in e-beam mode of operation a high intensity electron beam gun (3 to 20keV) is focused on the target material that is placed in a recess in a water-cooled copper hearth. The electron beam is magnetically directed on to the evaporant which melts locally. In this way the metal forms its own crucible and the contact with the hearth is cool for chemical reactions which have fewer source contamination problems that in the case of resistive heating, one disadvantage of e-beam evaporation is that the process might induce X-ray damage and possibly even some ion damage on the substrate. The X-ray damage may be avoided by using a focused, high power laser beam instead of an electron beam[30]. In previous work reported by A. Lee, heating of granulated PVDF in vacuum produces the vapor by electron beam gun, and

then the films were charged in a negative corona by the constant charging current method. PVDF film was recharged in a positive corona to obtain a dielectric hysteresis loop. Pyroelectric activity of evaporated and charged PVDF films measured by a dynamic method and compared with that of extruded and stretched PVDF films and is found to be two times lower than that of extruded films. Not only irradiation affected the surface potential stability of PVDF thin films, in this approach, the substrate temperature is found to be the most important parameter in vacuum deposition of thin films [44]

2.1.2.5 Laser ablation (Pulsed laser deposition) [45]

In laser ablation, high-power laser pulses are used to evaporate matter from a target surface such that the stoichiometry of the material is preserved in the interaction. As a result, a supersonic jet of particles (plume) is ejected normal to the target surface. The plume, similar to the rocket exhaust, expands away from the target with a strong forward-directed velocity distribution of different particles. The ablated species condense on the substrate placed opposite to the target. PLD represents a dry process for the fabrication of thin film of polymeric materials and may be particularly applicable in cases where the polymer is intractable and hence cannot be processed by conventional thermal or solution techniques. In the work done by A. Lee et al [11] PVDF film deposition was achieved through this technique in which films deposited at a higher temperature are significantly smoother. The appearance of several of the small particulates on the surface of the film deposited at 93 degrees suggests that they may have formed as a result of the ejection of molten material from the target. Further improvements in film quality may be obtained by working at lower laser fluence. The use of shorter wavelength radiation may also lead to improvements in film quality because of the stronger absorption of the laser energy [53].

2.1.2.6 Electrostatic spray-assisted vapor deposition (ESVAD) [46]

The ESAVD process involves spraying atomized precursor droplets across an electric field where the droplets undergo heterogeneous chemical reaction in the vapor phase near the vicinity of the heated substrate. This produces a stable solid film with excellent adhesion onto a substrate in a single production run. Optimizing the process conditions can control the structure, stoichiometry, crystallinity, texture and film thickness.

Tailoring the homogeneous gas phase reaction to occur during the deposition can produce powder. For the deposition of oxide materials, the ESAVD process can occur in an open atmosphere without the need of sophisticated and expensive reactor and/or vacuum chamber like in the chemical vapor deposition and physical vapor deposition techniques.

The ESAVD deposition process can occur in an open atmosphere without the need for a sophisticated reactor and/or a vacuum chamber. This technique is a rapid, flexible and cost-effective materials coating method. In the work done by Gregario et al [14], the PVDF solution is corona sprayed onto a heated substrate, the vaporization of the solvent occurs near the vicinity or on the substrate. The corona field was present during deposition and in cooling down after deposition, the corona field is very important to form the oriented polarized PVDF film and it transports the charged droplets of PVDF solution onto the substrate to form the PVDF thin film, and forces the polar group in PVDF thin film to align along the corona field. The utilization of corona field during the deposition process and cooling it down is effective in controlling the crystal forms and their orientation [14].

2.1.2.7 Electrophoretic deposition (EPD)

EPD is an electrodeposition technique in which films are formed by charged particles migrating under the effect of high electric fields. The charged particles may be generated in one of two ways: the “suspension approach”, where polymer particles are dispersed in a nonsolvent (for thick films) or the “solution approach”, where polymer is dissolved in a solvent (for thin films). This is a new technique for depositing piezoelectric polymer films. EPD has been used to electrodeposit films of PVDF copolymer in a conformal manner. Spin coating the typical technique used to deposit PVDF copolymer, is not capable of depositing conformally over severe variations in topography (such as the high-aspect-ratio features often found in MEMS). Hence using EPD, high aspect ratio of PVDF thin films can be obtained which can be applied in micro actuators that utilize sidewall piezoelectric thin films. In solution approach for thin films, solution deposited films are more conformal, due to their higher unannealed density and consequently higher resistivity. The conformal nature of PVDF copolymer electrophoretic deposition makes it suitable for depositing films for high-aspect-ratio piezoelectric microsystems. Additionally, EPD is more versatile than spin coating because it can produce thick and porous films [47].

2.2 Spin coating deposition

With several deposition techniques implemented in thin film technology described above, “*Spin Coating*” technique is chosen for the fabrication of thin PVDF copolymer films in the present study. Spin coating has been used for several decades for the application of thin films and it is the preferred method for application of thin and uniform films to flat substrates. An excess amount of polymer solution is placed on the substrate. The

substrate is then rotated at high speed in order to spread the fluid by centrifugal force. Rotation is continued for some time, with fluid being spun off the edges of the substrate, until the desired film thickness is achieved. The solvent is usually volatile, providing for its simultaneous evaporation. In thin film technology of piezoelectric materials, uniform and consistent PVDF copolymer thin films can be achieved through this technique. In the literature review it has been proved that PVDF copolymer thin films can be coated directly onto silicon transistor, then the film can be optimally heat treated to improve crystallinity, dielectric strength and piezoelectric response. Furthermore, the films can be electrically oriented (poled) right on the silicon wafer. The poled films become piezo and pyroelectrically active [15]. A potential problem during the poling of these thin films is that the large voltage required to activate the films may cause breakdown. For this reason usually corona discharge in air at elevated temperature is preferred to polarize the PVDF copolymer silicon-backed sample [33].

2.2.1 Spin coating process theory

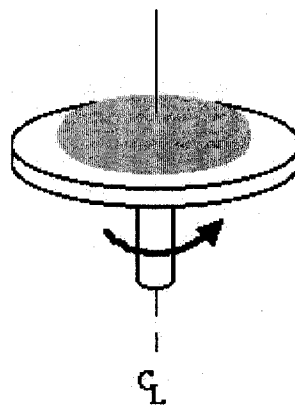


Figure 2.1: Solution being spin coated on the substrate

As explained in the earlier section spin coating involves the acceleration of a fluid resin onto the center of a substrate as shown in schematic Figure 2.1, generally the coating material can be deposited in the center of the substrate manually or through some automated accessories such as robotic arm. The basic theory behind the spin coating technique is governed by the balance between centrifugal forces controlled by the spin speed and viscous forces which arise due to the solvent viscosity.

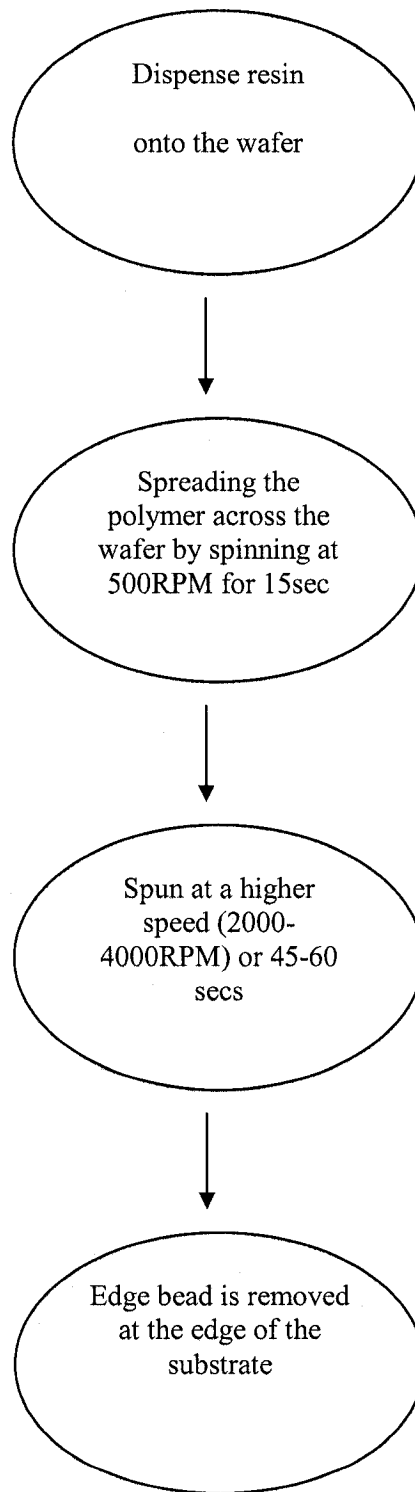


Figure 2.2: Basic stages involved in spin coating process

A typical spin coating process involves four basic stages as shown in Figure 2.2 , initially the polymer is dispensed onto the wafer , the solution is spread across the substrate by spinning at lower speeds around 500 RPM , the substrate is then spun at higher speeds to achieve desired thickness of the deposited resin . It is usually observed that an edge bead is formed due to the surface tension at the edge of the wafer which is removed using a backside wash cycle which causes solvent to curl back over the lip of the wafer and wash off the bead [15].

The spin coating process involves a large number of variables that tend to cancel and average out during the spin process and it is best to allow sufficient time for this to occur. A separate drying step is sometimes added after the high speed spin step, to further dry the film without substantially thinning it. This can be advantageous for thick films since longer drying times may be necessary to increase the physical stability of the film before handling. Without the drying step, problems can occur during handling, such as pouring off the side of the substrate when removing it from the spin bowl. In such a case a moderate spin speed of about 25% of the high speed spin will generally suffice to aid in drying the film without significantly changing the film thickness [38].

Centrifugal acceleration will cause the resin to spread to, and eventually off, the edge of the substrate leaving a thin film of resin on the surface. Final film thickness and other properties will depend on the nature of the resin (viscosity, drying rate, percent solids, surface tension, etc.) and the parameters chosen for the spin process. Factors such as final rotational speed, acceleration, and fume exhaust contribute to how the properties of coated films are defined. One of the most important factors in spin coating is

repeatability. Subtle variations in the parameters that define the spin process can result in drastic variations in the coated film.

2.2.2 Spin coating modeling

An extensive research to develop the mathematical modeling for spin coating was done by Emslie et al [48]; their model was based on the assumption that flow reaches a stable condition where the centrifugal and viscous forces are just in balance, when these forces are in balance they satisfy the following condition represented by the equation (2.1)

$$-\eta \frac{\partial^2 v}{\partial Z^2} = \rho \omega^2 \mathfrak{R} \quad (2.1)$$

Where Z and \mathfrak{R} define a cylindrical coordinate system aligned with the axis of substrate rotation, v is the fluid velocity in the radial direction, ρ is the fluid density, ω is the rotation rate in radians per second, and η is the viscosity in poise.

In a typical appropriate flow of resin and velocity boundary conditions for a film which is uniform initially. The film thickness as a function of time (t), was found to be

$$h = \frac{h_0}{\sqrt{1 + 4Kh_0^2 t}} \quad (2.2)$$

Where h_0 is the film thickness at $t = 0$ and K is a system constant defined as:

$$K = \frac{\rho \omega^2}{3\eta} \quad (2.3)$$

Equation (2.1) and (2.2) are valid only when K is constant, but in the case of complex solutions the system constant need not be constant as both viscosity and density are expected to increase as evaporation progresses. It was also reported by Emslie et al in

their work that for the initial stages of fluid thinning, that is when before evaporation becomes important the thinning rate is given by

$$\frac{dh}{dt} = -2Kh^3 \quad (2.4)$$

While casting films at longer spin times the solvent evaporation becomes an important factor, to estimate the effect of solvent evaporation on final thickness Meyerhofer [49] presented the formulation in which a quite reasonable approximation is that evaporation is a constant throughout spinning, as long as the rotation rate is kept constant, hence a constant evaporation term is added to the equation (2.4) so the governing differential equation 2.4 is modified as

$$\frac{dh}{dt} = -2Kh^3 - e \quad (2.5)$$

Where e is evaporation rate which accounts to the interface velocity that is driven by the evaporation process alone. In this formulation it was assumed that early stages were dominated by the flow and the later stages by evaporation, a transition point is set at the condition where the evaporation rate and the viscous flow rate become equal and this point can be correlated as “fluid-dynamical “set point of the coating process, with these assumptions the final coating thickness h_f is predicted given by the equation (2.6)

$$h_f = c_o \left(\frac{e}{2(1-c_o)K} \right)^{\frac{1}{3}} \quad (2.6)$$

Where c_o is the solid concentration in the solution. In the research of Meyerhofer it is shown that the evaporation rate should be constant over the entire substrate and depends on the rotation rate according to:

$$e = C\sqrt{\omega} \quad (2.7)$$

Where C is proportionality constant, which is determined for a particular experimental conditions.

2.2.3 Spin coating parameters

Some of the significant parameters involved in a typical spin coating process are

- Angular speed
- Speed rate
- Fume exhaust

However, the film forming process is primarily governed by two independent parameters, viscosity and spin speed, generally film thickness in the range of 1-200 μm can be easily achieved. To obtain a relatively thicker films high material viscosity, low spin speed, and a short spin time are necessary. However these parameters can affect the uniformity of the coat and hence multiple coatings are preferred for a film thickness greater than 15 μm [19].

2.2.3.1 Angular speed

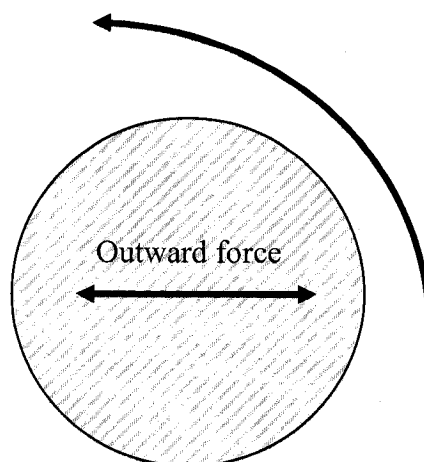


Figure 2.3 Substrate spinning

Spin speed is one of the most important factors in spin coating. The speed of the substrate (RPM) affects the degree of radial (centrifugal) force (as shown in the schematic Figure 2.3) applied to the liquid resin as well as the velocity and characteristic turbulence of the air immediately above it. In particular, the high speed spin step generally defines the final film thickness. In a general spin coating technique relatively minor variations of ± 50 rpm at this stage can cause a resulting thickness change of 10%, film thickness is largely a balance between the force applied to shear the fluid resin towards the edge of the substrate and the drying rate which affects the viscosity of the resin. In the literature review it was explained that as the resin dries, the viscosity increases until the radial force of the spin process can no longer appreciably move the resin over the surface [1]. At this point, the film thickness will not decrease significantly with increased spin time. In the present work spin coating of P(VDF-TrFE) solution is performed the variation of thickness of PVDF copolymer thin films with respect to spin parameters are presented in the later sections of this chapter.

2.2.3.2 Speed rate

The speed rate of the substrate towards the final spin speed can also affect the coated film properties. Since the resin begins to dry during the first part of the spin cycle, it is important to accurately control the speed rate. In some processes, 50% of the solvents in the resin will be lost due to evaporation in the first few seconds of the process [48]. Speed rate also plays a large role in the coat properties of patterned substrates. In many cases the substrate will retain topographical features from previous processes; it is therefore important to uniformly coat the resin over and through these features. While the spin process in general provides a radial (outward) force to the resin, it is the acceleration that

provides a twisting force to the resin. This twisting aids in the dispersal of the resin around topography that might otherwise shadow portions of the substrate from the fluid. In the present work the spin coating of PVDF copolymer thin films are performed with a constant speed rate of 1350m/sec².

2.2.3.3 Fume exhaust

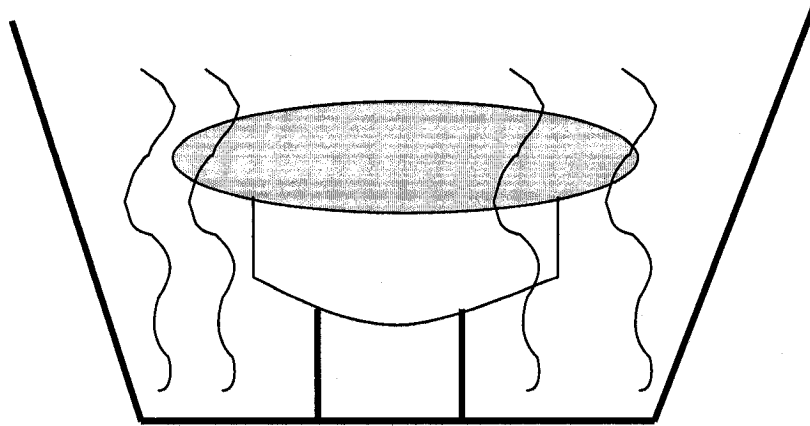


Figure 2.4: Drying of the substrate

The drying rate of the resin fluid during the spin process is defined by the nature of the fluid itself (volatility of the solvent systems used) as well as by the air surrounding the substrate during the spin process. Just as a damp cloth will dry faster on a breezy dry day than during damp weather, the resin will dry depending on the ambient conditions around it. Figures 2.4 & 2.5 schematically illustrates drying of the substrate. It is well known that factors such as air temperature and humidity play a large role in determining coated film properties. It is also very important that the airflow and associated turbulence above the substrate itself be minimized, or at least held constant, during the spin process. All Cee spin coaters employ a “closed bowl” design while not actually an airtight environment, the exhaust lid allows only minimal exhaust during the spin process. Combined with the bottom exhaust port located beneath the spin chuck, the exhaust lid becomes part of a

system to minimize unwanted random turbulence. There are two distinct advantages to this system: slowed drying of the fluid resin and minimized susceptibility to ambient humidity variations. The slower rate of drying offers the advantage of increased film thickness uniformity across the substrates. The fluid dries out as it moves towards the edge of the substrate during the spin process. This can lead to radial thickness nonuniformities since the fluid viscosity changes with distance from the center of the substrate. By slowing the rate of drying, it is possible for the viscosity to remain more constant across the substrate [49].

Drying rate and hence final film thickness is also affected by ambient humidity. Variations of only a few percent relative humidity can result in large changes in film thickness. By spinning in a closed bowl the vapors of the solvents in the resin itself are retained in the bowl environment and tend to overshadow the effects of minor humidity variations. At the end of the spin process, when the lid is lifted to remove the substrate, full exhaust is maintained to contain and remove solvent vapors.

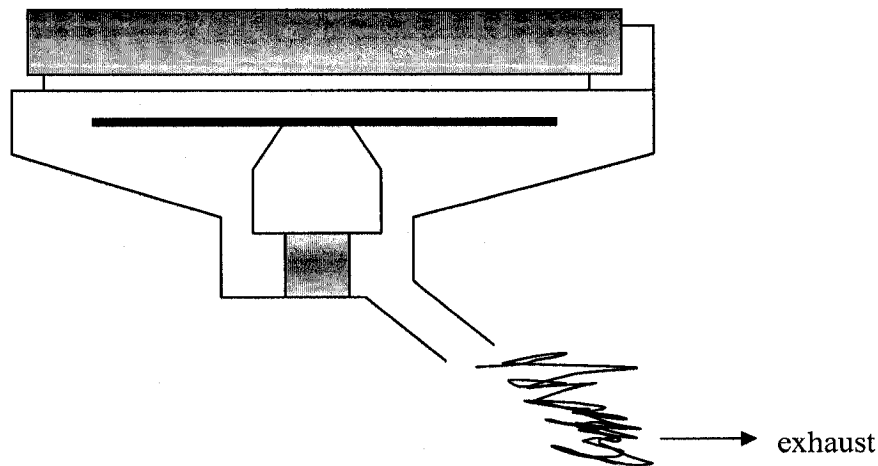


Figure 2.5: Exhaust valve of the substrate

Another advantage to this “closed bowl” design is the reduced susceptibility to variations in air flow around the spinning substrate. In a typical clean room, for instance, there is a

constant downward flow of air at about 100 feet per minute (30m/min). Various factors affect the local properties of this air flow. Turbulence and Eddy currents are common results of this high degree of air flow. Minor changes in the nature of the environment can create drastic alteration in the downward flow of air. It is recommended by the spin coating equipment manufacturers that by closing the bowl with a smooth lid surface, variations and turbulence caused by the presence of operators and other equipment are eliminated from the spin process [49].

2.2.4 Process trend charts

The spin coating process requires good understanding of the role of each variable in the process to enable uniform and controlled films. The figures below (as shown in Figure 2.6) depict the variation of the thickness with respect to the spin coating parameters and these variations are observed in typical spin coating process and are provided by the spin coating manufacturers for bench mark fluids[50].

These charts represent general trends for the various process parameters. For most resin materials the final film thickness will be inversely proportional to the spin speed and spin time. Final thickness will also be somewhat increasing with the exhaust volume although uniformity will suffer if the exhaust flow is too high since turbulence will cause non uniform drying of the film during the spin process.

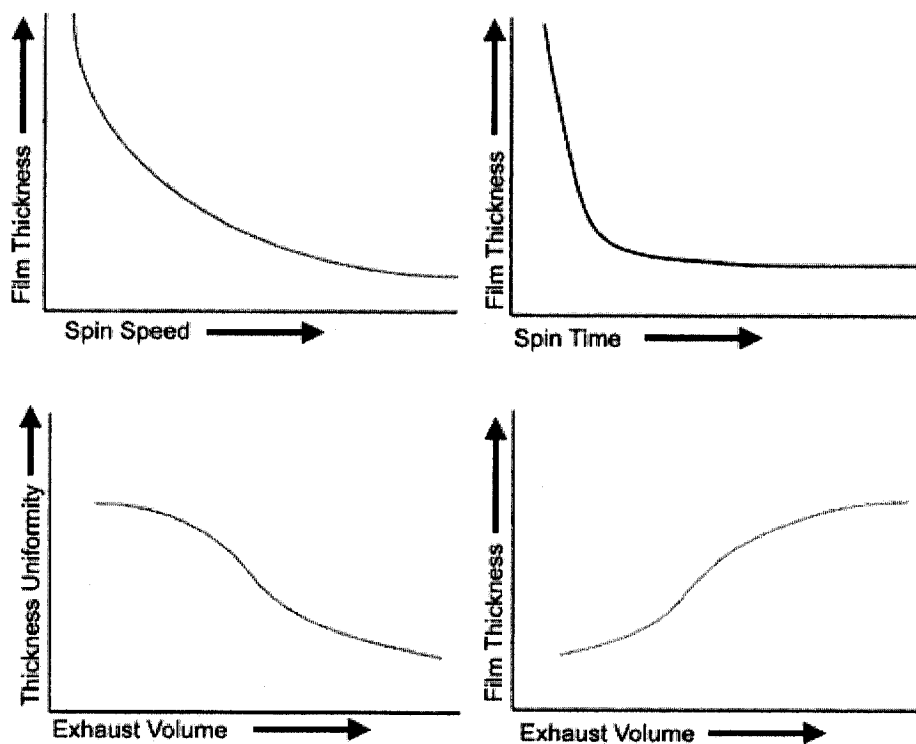


Figure 2.6: Variation of film thickness with various parameters [50].

2.3 Spin coating of PVDF copolymer thin films.

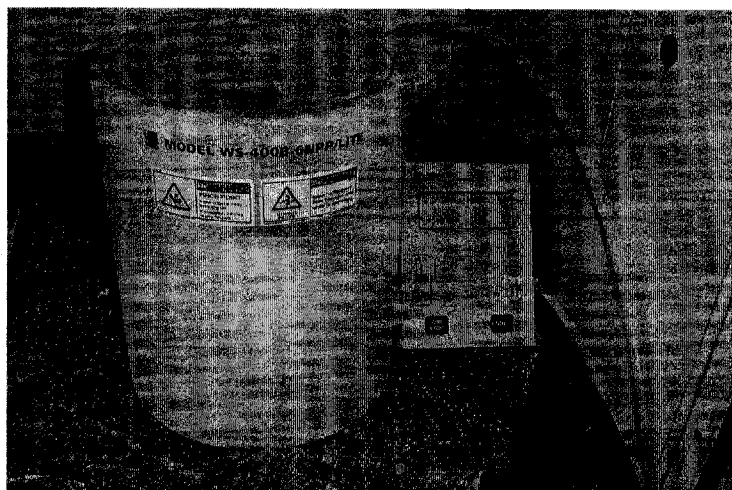


Figure 2.7 WS-400B-Lite series spin processor

Thin films were prepared by using copolymers of PVDF (Poly Vinylidene Fluoride) in powder form using MEK (Methyl Ethyl Ketone) as a solvent using WS-400B-Lite series

spin processor from Laurell Technologies. Spin coating of the PVDF/TrFE solution is performed onto the silicon wafers at room temperature. As discussed previously in this chapter the thickness of P(VDF-TrFE) film can be varied by several parameters of spin coating such as spinning speed, spin time; the thickness can also be controlled by varying the concentration of P(VDF-TrFE) solution.

2.3.1 Film preparation.

Before spin coating PVDF copolymer solution onto the silicon wafer an adhesion reducer teflon is used. Following are the standard steps involved to coat teflon AF solution. The surfaces to be coated are cleaned by boiling in isopropanol for 15 minutes followed by drying. Subsequently the dried silicon wafer is coated with a 2% solution of the fluorosilane in 93% ethanol and 5% water; the wafers are then baked at 100 degrees for 10 minutes. The wafer is then spin coated with the teflon solution, the silicon wafers are then baked at 110 degrees for 30 minutes, the silicon wafers are baked again for an additional 30 minutes at 225 °C degrees. The teflon coated silicon wafer samples are now spin coated with the PVDF copolymer solution. The main purpose of using teflon solution onto the wafers is to remove or peel off the spin coated PVDF copolymer thin films from the wafer which are then used for FTIR characterization in this work.

The PVDF copolymer is obtained in powder form of 65% VDF and 35% TrFE from Solvay & Cie. This copolymer is chosen for its high values of crystallinity and remnant polarization and the small value of dielectric constant and the dielectric loss, respectively. The film solution is prepared by using solvent MEK (Methyl Ethyl Ketone), As discussed in the previous sections of this chapter, selection of a proper solvent to prepare the solution is a very critical factor in spin coating process. For each set of samples; solution

of 10% concentration by weight is prepared, the solution is mixed for 30 minutes at room temperature, proper dissolution of copolymer in the solvents Methyl Ethyl Ketone is achieved after 2 hours approximately. The substrates used for spin coating are silicon wafers.

Spin coating is performed by dispensing the prepared solution drop wise onto the silicon substrates at different set speeds and spin duration. The primary interest of this work is to predict the optimum parameters of spin coating such as spinning speed, spin time in order to obtain a proper uniform coating of PVDF copolymer thin film onto the silicon wafer. The presented results in this chapter depict the variation of film thickness for various parameters of spin coating. The study is further extended by varying the concentration of the prepared solution for considered optimum parameters. Several factors account to obtain a proper uniform PVDF copolymer thin film. The spin coated samples were kept at 80-90 degrees for 10 minutes initially, and then heated up to 100 degrees to allow MEK to evaporate; the samples were slowly cooled back to the room temperature.

2.3.2 Thickness measurement of PVDF copolymer thin films.

The thickness of PVDF copolymer thin films deposited on substrates can be measured by using several techniques such as “surface profilers” and using microscopy including Scanning Electron Microscopy (SEM). In this work thickness is measured using a very high zoom optical microscope that focuses under high magnification within a field that is fraction of a micrometer. By focusing on the substrate and on the deposited layer one could measure the displacement of the microscopic table that will represent the thickness of the deposited layer. For each specimen of PVDF copolymer thin film four

measurements on the microscope are taken, the average of the four measurements of thickness for each specimen is taken as the sample thickness.

For a 10% concentration of PVDF copolymer solution, 3g of P(VDF-TrFE) powder is mixed in 10 ml of Methyl Ethyl Ketone (MEK). PVDF copolymer thin films of different thicknesses are obtained by varying the spin coating parameters. The film thickness obtained at different speeds from 2000RPM to 5000RPM and spin duration from 30 to 90 seconds are given in the table 2.1. and the variation of thickness is shown in Figure 2.8

The thickness of the PVDF copolymer thin film could be also varied by varying the concentration of the prepared solution, concentrations of 5%, 10%, 15%, 20% and 25% PVDF copolymer solution by weight are prepared and spun onto the silicon wafers at fixed spin time of 45 seconds and 3000 RPM the results are given in table 2.2

It is observed that specimens spun at 3000 RPM for 45 seconds for concentration of 25% PVDF copolymer solution appears to be the most consistent and possess good uniformity. A comparatively thicker film of thickness 28-30 μ m is obtained for two spin coats of 25% concentration of solution by weight on the silicon wafer these specimens are considered for the later part of the work for Polarization of PVDF copolymer thin films and for Infrared spectroscopy characterization. The obtained PVDF copolymer thin film is consistent and possesses good viscosity.

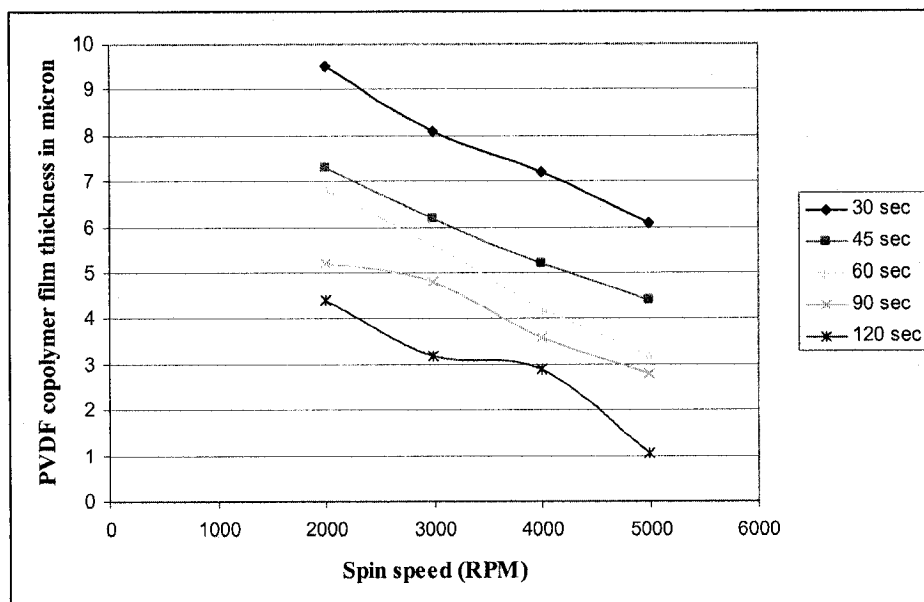


Figure 2.8: Variation of film thickness at different speeds for different spin durations for concentration of 10% PVDF copolymer solution.

Table 2.1: Thickness (μm) variation of PVDF copolymer thin film at different spinning parameters for 10% concentration of solution

Spin speed RPM-1 RPM-2 (15 Sec)	Spin time (seconds)				
	30	45	60	90	120
500 2000	9.5	7.3	6.8	5.2	4.4
500 3000	8.1	6.2	5.6	4.8	3.2
500 4000	7.2	5.2	4.2	3.6	2.9
500 5000	6.15	4.5	3.2	2.85	1.05

Table 2.2: Thickness variation of PVDF copolymer thin film w.r.t concentration at fixed spin time of 45 seconds and spin speed 3000RPM

Solution Concentration(%) by weight	PVDF copolymer thickness (μm)
5	3.6
10	6.2
15	7.8
20	11.3
25	14.1

2.4 Annealing of PVDF copolymer thin films.

Initial heating of the spin coated PVDF copolymer thin films is performed to evaporate MEK. Annealing of the samples is performed so as to improve the crystallinity of the thin films and also to recover the local stresses and to evaporate the remaining MEK the samples are heated at different temperatures of 100, 110, 120, 130, 140, 150, 160 degrees for 10 minutes. After annealing, the samples are left to cool slowly to room temperature.

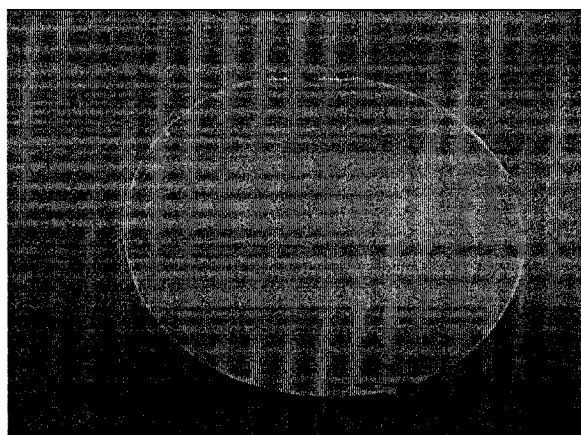


Figure 2.9: Spin coated PVDF copolymer thin film sample.

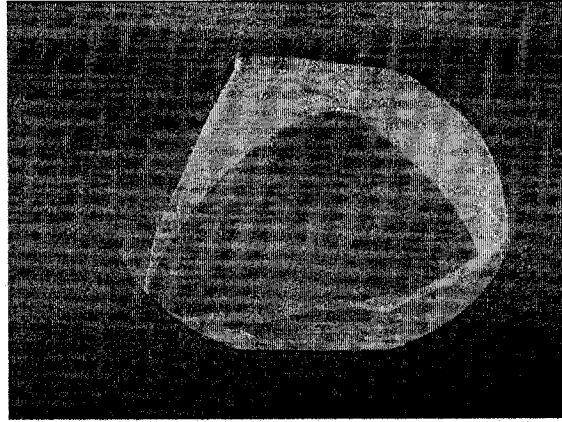
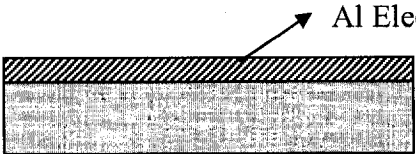

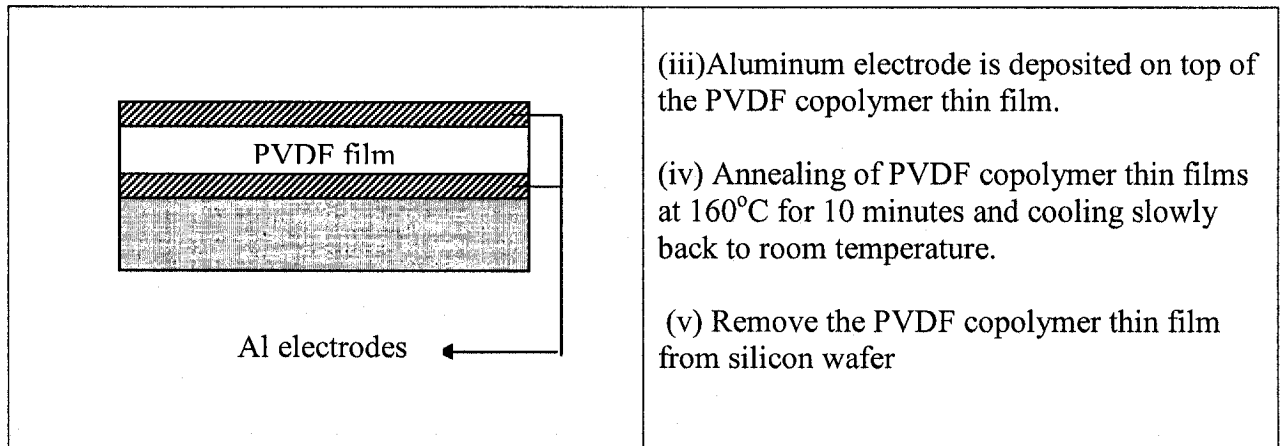


Figure 2.10: Spin coated PVDF copolymer thin film sample peeling off the silicon wafer

Spin coated samples are shown in Figure 2.9, after annealing is performed, samples are left at room temperature for one hour, PVDF copolymer thin film is then carefully peeled off from the silicon wafer as shown in Figure 2.10. The microfabrication process flow is illustrated in Table 2.3.

Table 2.3 Microfabrication process flow for PVDF copolymer thin films

	<p>(i) Aluminum electrode is deposited onto the 4 inch silicon wafer</p>
	<p>(ii) Multiple coatings of PVDF copolymer solution of 25% concentration by weight is spin coated for 45seconds at 3000RPM</p>



2.5 Polarization of PVDF copolymer thin films

The main aspect of piezoelectric materials is “Polarization”, which is performed through the application of high electric field across the thickness of the PVDF copolymer thin film specimen; it is commonly referred as “poling”. A concise introduction about various techniques of poling has been given in Chapter 1. Among various techniques of Poling of PVDF copolymer thin films, “Step-wise Poling” technique is adopted in this work [36]. The main advantages of this poling method are a low failure rate due to electric and thermal breakdowns and a sufficient high pyroelectric coefficient.

2.5.1 Step-wise poling

Step-wise Poling is performed by a series of six consecutive pulses of several minutes and with successively increasing amplitude. In this work the applied DC voltage is varied from 500 Volts to 3000Volts the time width where the voltage is applied between the two copper electrodes is the poling interval (t_p). In this case the poling interval is for 10 minutes, between two poling intervals the applied DC voltage is zero for a period of 2

minutes (t_i), the poling is conducted at room temperature. A schematic diagram of this technique is shown in Figure 2.17 [36]. The main advantage of the step-wise poling is that the probability for both electrical and thermal breakdown also decreases due to limited current through the film. A disadvantage of the step-wise poling is longer polarization time. With step-wise poling, upto 70 minutes is needed to polarize the copolymer.

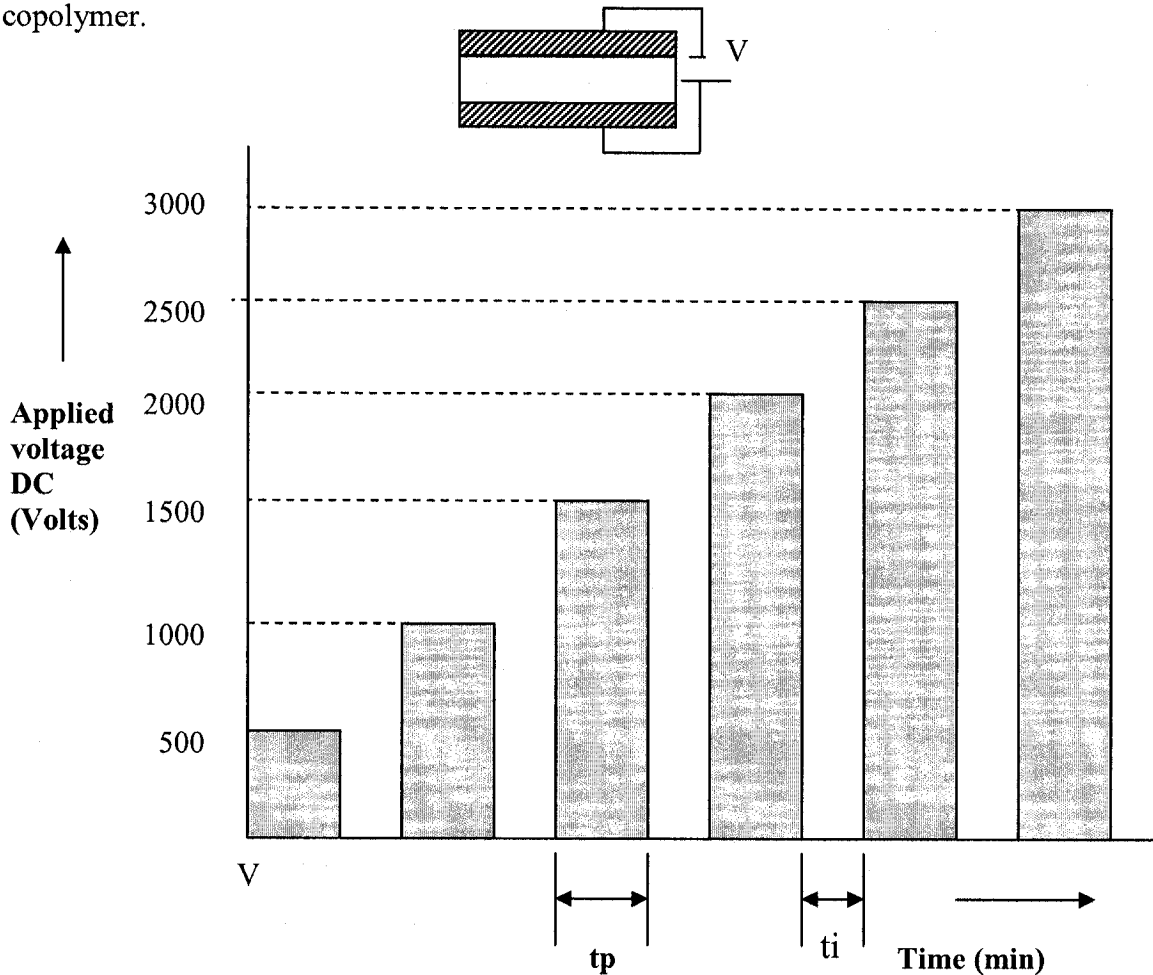


Figure 2.11: A schematic of the step-wise poling charge technique.

A block diagram of the technique adopted is shown in Figure 2.12, for applying high DC voltages across the thickness of the PVDF copolymer thin films, two square copper plates of side 50 mm and thickness 0.1mm is considered. The spin coated PVDF copolymer thin film of dimensions 1 inch x 1 inch and thickness of 28 microns (approximately) is taken

of from the silicon wafer carefully and is clamped between the copper plates as illustrated in the Figure 2.12. The PVDF copolymer thin film is placed in such a way that there is no short between the two copper plates.

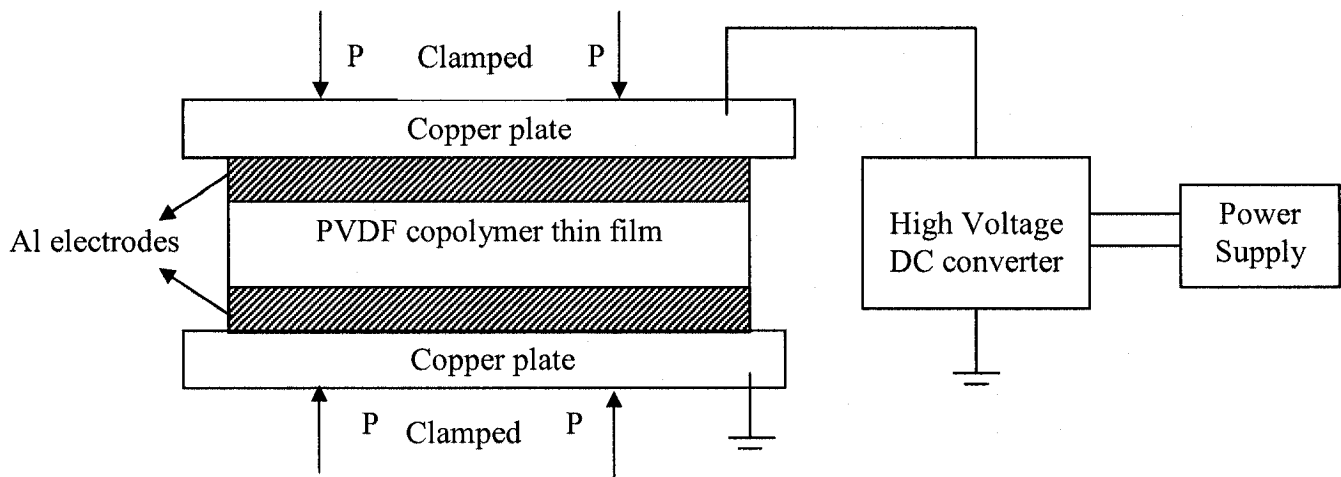


Figure 2.12: Block diagram of step-wise poling set up.

The experimental set up of the step-wise poling is shown in figure, A variable DC power supply is used to connect to a high voltage converter, A high voltage D.C probe is used as voltage divider to sense the high voltage output from the high voltage DC converter.

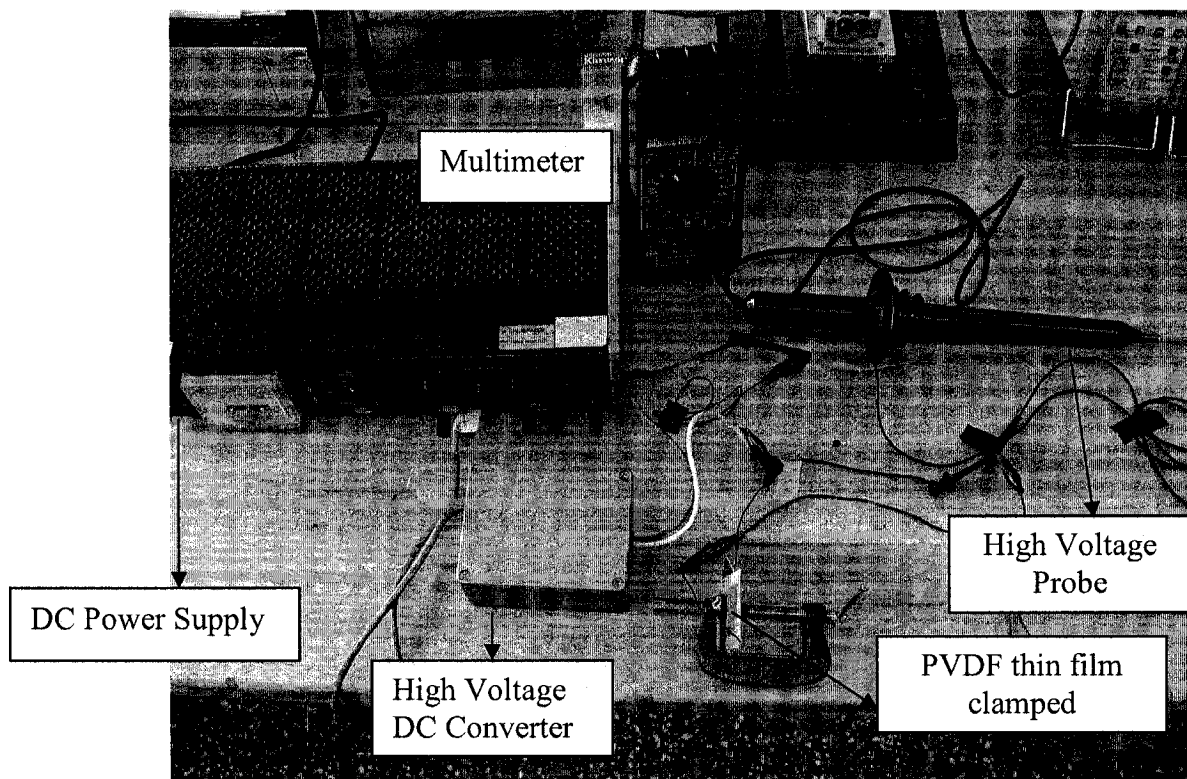


Fig 2.13: Experimental setup for step-wise poling

A close up view of the PVDF copolymer thin film clamped between the copper plates is shown in figure 2.14. A high voltage DC is applied across the copper plates with an initial value of 500Volts, The applied DC voltage is increased in steps of 500 Volts a series of six consecutive pulses of high voltage is applied

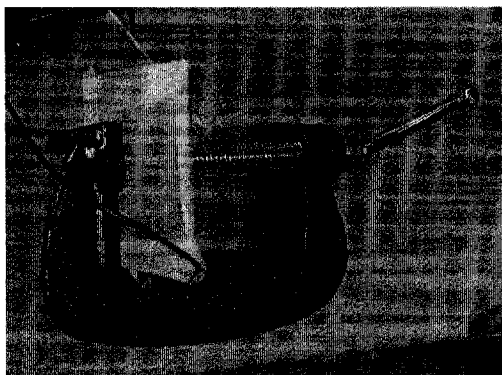


Fig 2.14: PVDF copolymer thin film clamped between two copper plates

Hence PVDF copolymer samples are annealed at different temperatures and then poled, the characterization of samples annealed at different temperatures and that of poled PVDF copolymer thin film samples are investigated through infrared spectroscopy studies which is presented Chapter 3.

2.6 PVDF thin film patterning

Patterning of the PVDF copolymer thin film did not constitute an objective of this work, However a brief presentation of the work as described in the literature by D.Setiadi is presented in this chapter, patterning of the PVDF thin films in general is a very critical step to obtain the desired structures on the deposited PVDF thin film, hence a suitable etchant should be applied so as to obtain the desired structures. As reported by D.Setiadi et al [37], 2-butanone at temperatures between 30 °C and 70°C is used as an etchant. The etch rate of the copolymer film appeared to be about 1µm/ min at 30 °C and increases with an increasing temperature. An etching temperature of 30 °C is chosen, since higher temperatures result in a too much fast etch rate and fast evaporation of the solvent. In the work done by Setiadi, the spin coated samples of PVDF copolymer thin films are patterned to manufacture a matrix array of pyroelectric sensors; the copolymer film has to be patterned. In the first process step; a thick silicon dioxide film (1µm) is grown onto the silicon substrate. This oxide layer reduces the parasitic capacitance and the heat conduction of the sensor element The second process step is the evaporation of the aluminium bottom electrode (600 nm). A 1 µm thick copolymer film is deposited by spin coating the third process step is the annealing of the film for 10 minutes at 160 °C. Patterning of the copolymer is the next step. First, a 600 nm aluminium top electrode is evaporated this aluminium electrode is also used as a mask for etching of the copolymer

film. The deposited aluminium has to be patterned by using a photoresist layer and a photomask. First, the photoresist is exposed to ultraviolet light. The photoresist is then developed to remove it from areas where it is not hardened. An acid resistant protective coating over the selected regions of the electrode is obtained. Unprotected regions of aluminium electrode are chemically etched. Finally, the sample is rinsed and deionized in water for 5 minutes.

2.7 Summary

In this chapter literature on various available deposition techniques in thin film technology is reviewed, basic stages involved in the spin coating process and basic mathematical model of spin coating method are discussed, further microfabrication of PVDF copolymer thin films using spin-coating is presented, spinning characterizations of microfabricated PVDF copolymer thin films are presented by varying various spin parameters. The optimum spin parameters for consistent and uniformly coated PVDF thin films are figured out; a brief description of the stepwise poling method adopted for the obtained PVDF copolymer thin films is discussed, at the end of the chapter a short literature review on PVDF thin film patterning is presented.

Chapter 3

FTIR characterization of PVDF copolymer thin films

3.1 Infrared spectroscopy theory

Infrared spectroscopy is a technique based on the vibrations of atoms in a molecule. An infrared spectrum is generally obtained by passing infrared radiation through a sample and determining what fraction of the incident radiation is absorbed at a particular energy. The energy at which any peak in an absorption spectrum appears corresponds to the vibration of a part of the specimen molecule. The technique is one of the most significant analytical techniques in practice, one of the main advantages of infrared spectroscopy is that virtually any sample in any state can be studied [51].

IR spectra are acquired on a special instrument, called an IR spectrometer. IR is used both to gather information about the structure of a compound and as an analytical tool to assess the purity of a compound. IR spectra are quick and easy to run, In infrared spectroscopy the most significant advance was achieved with the introduction of “*Fourier transform spectrometers*“ these spectrometers employ an interferometer and utilize the well established mathematical process of Fourier Transformation (FTIR). Fourier-transform infrared spectroscopy has dramatically improved the quality of infrared spectra and minimized the time required to obtain the data.

FTIR is based on the idea of the interference of radiation between two beams to yield an interferogram. The latter is a signal produced as a function of the change of path length between the two beams. The two domains of distance and frequency are interconvertible by the mathematical method of Fourier transformation

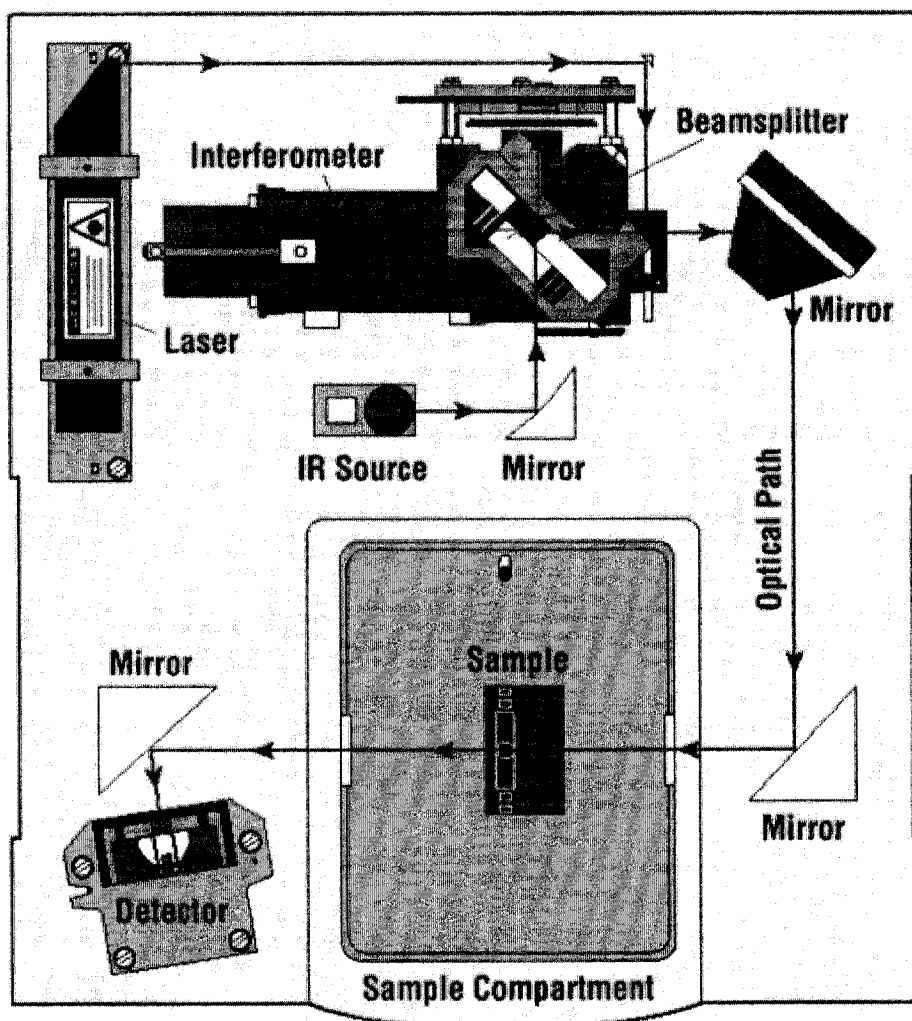


Figure 3.1: Schematic diagram of FTIR [52]

The basic components of an FTIR spectrometer are shown schematically in Figure 3.1. The radiation emerging from the source is passed through an interferometer to the sample before reaching a detector. Upon amplification of the signal in which high frequency

contributions have been eliminated by a filter, the data are converted to digital form by an analog-to-digital converter and transferred to the computer for Fourier transformation [52].

3.1.1 Electromagnetic spectrum

Infrared refers to that part of the electromagnetic spectrum between the visible and microwave regions. Electromagnetic spectrum refers to the seemingly diverse collection of radiant energy, from cosmic rays to X-rays to visible light to microwaves, each of which can be considered as a wave or particle traveling at the speed of light. These waves differ from each other in the length and frequency, as illustrated in fig 3.2

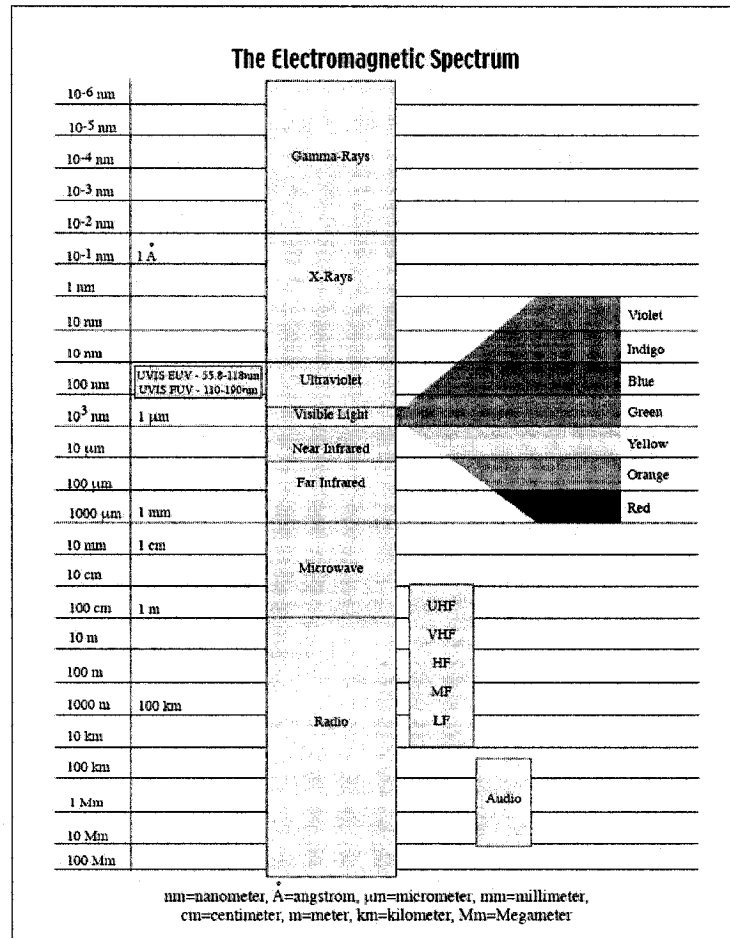


Figure 3.2 Electromagnetic spectrum[52]


Frequency (ν) is the number of wave cycles that pass through a point in one second. It is measured in Hz, where 1 Hz = 1 cycle/sec. Wavelength (λ) is the length of one complete wave cycle. It is often measured in cm (centimeters). Wavelength and frequency is inversely related: and *where* C is the speed of light, 3×10^{10} cm/sec.

Energy is related to wavelength and frequency by the following formulas:

$$E = \frac{hc}{\lambda} \quad (3.1)$$

Where

h = Planck's constant, 6.6×10^{-34} joules-sec



λ (cm) (wavelength)	λ (μm) (wavelength)	ν (wave number) cm^{-1}	Energy (E) Kcal/mo l
7.8×10^{-5} to 3×10^{-4}	0.78 to 3	12820 to 4000	10-37 Kcal/mo l
3×10^{-4} to 3×10^{-3}	3 to 30	4000 to 400	1-10 Kcal/mo l
3×10^{-3} to 3×10^{-2}	30 to 300	400 to 33	0.1-1 Kcal/mo l

Figure: 3.3 Infrared region in electromagnetic spectrum

Note that energy is directly proportional to frequency and inversely proportional to wavelength. The IR region is divided into three regions: the near, mid, and far IR as

shown in Fig 3.3. The mid IR region is of greatest practical use to the organic chemistry. This is the region of wavelengths between 3×10^{-4} and 3×10^{-3} cm [52].

In wave numbers, the mid IR range is 4000-400 cm^{-1} . An increase in wave number corresponds to an increase in energy; this is a convenient relationship for the analysis. Infrared radiation is absorbed by organic molecules and converted into energy of molecular vibration. In IR spectroscopy, an organic molecule is exposed to infrared radiation. When the radiant energy matches the energy of a specific molecular vibration, absorption at that particular frequency occurs. In a typical IR spectrum, the wave number is plotted on the X-axis, is proportional to energy; therefore, the highest energy vibrations are on the left. The percent transmittance (%T) is plotted on the Y-axis. Absorption of radiant energy is therefore represented by a “trough” in the curve: zero transmittance corresponds to 100% absorption of light at that wavelength.

3.1.2 Absorbance

Band intensities can also be expressed as absorbance (A). Mathematically, absorbance is the logarithm, to the base 10, of the reciprocal of the transmittance:

$$A = \log_{10} \left(\frac{1}{T} \right) \quad (3.2)$$

The Infrared spectroscopic analysis can be interpreted in the form of transmittance spectrum as well as in absorbance spectrum. Even simple organic molecules give rise to complex IR spectra. Both the complexity and the wave numbers of the peaks in the spectra give information about the molecule. The complexity is useful to match an experimental spectrum with that of a known compound with a peak-by peak correlation. To facilitate this analysis, compilations of IR spectra are available, most well-known of which are those by Sadtler and Aldrich. While in the past these compilations were

available only in printed form, they are now available in CD ROM format for computer analysis. The wave numbers (sometimes referred to as *frequencies*) at which an organic molecule absorbs radiation give information on functional groups present in the molecule. Certain groups of atoms absorb energy and therefore, give rise to bands at approximately the same frequencies. The chemist analyzes a spectrum with the help of tables which correlate frequencies with functional groups [52]

3.1.3 Transmittance

Transmission spectroscopy is the oldest and most straightforward infrared method; this technique is based upon the absorption of infrared radiation at specific wavelengths as it passes through a sample. It is possible to analyze samples in the liquid, solid or gaseous forms when using this approach

The transmittance of an electromagnetic wave incident on a dielectric is defined by

$$T = \left| \frac{E_t}{E_i} \right|^2 = \frac{I_t}{I_i} \quad (3.3)$$

Where E_t and E_i are the transmitted and incident electric fields.

Transmittance of light through an absorbing medium is similarly defined by

$$T = \frac{I}{I_o} \quad (3.4)$$

where I is the transmitted intensity and I_o is the incident intensity. This is sometimes

explicitly written as a percentage, $T = \frac{I}{I_o} \times 100$ (3.5)

3.2 FTIR of PVDF copolymer thin films

In the present work Infrared spectroscopy technique is used to analyze the structural and phase changes of PVDF-TrFE samples spin coated on silicon wafers. Infrared spectroscopy studies of piezoelectric polymers applied in the area of MEMS is always been an interesting and challenging area of research, a more detailed literature review on FTIR of copolymers has been presented in Chapter 1.

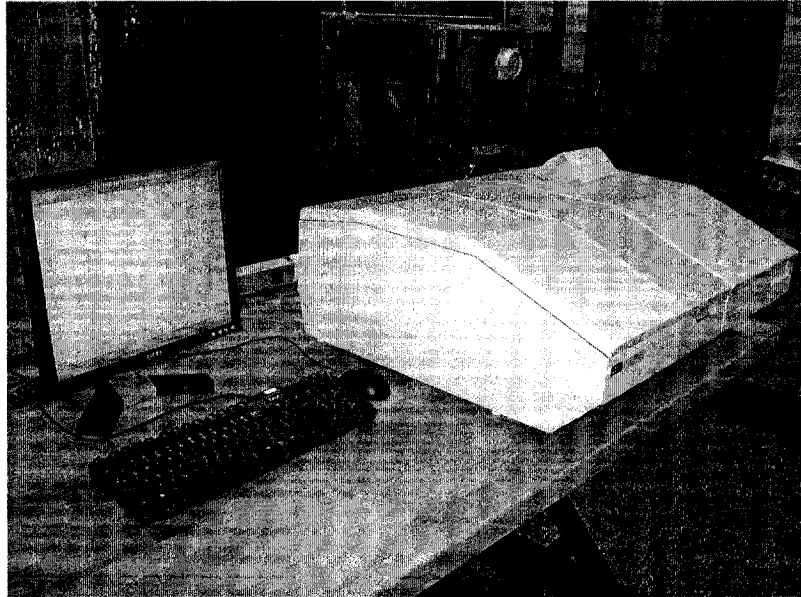


Figure 3.4 Perkin Elmer Spectrum BX II FT-IR system

In the present work the infra red spectra of the samples were obtained on “Perkin Elmer Spectrum BX II FT-IR system” shown in Figure 3.4 the obtained FTIR plots were interpreted with reference to the literature review on FTIR plots of PVDF copolymers.

3.2.1 Investigation of polarized phase of PVDF copolymer.

The main aspect of using FTIR technique is to investigate piezoelectric beta (β) phase in PVDF/TrFE (65/35%) copolymer thin films. In the earlier studies, A.Salimi et al [53] presented the FTIR studies of β -phase crystal formation in stretched PVDF films and Weiping et al reported the ferroelectric β -phase of PVDF-TrFE (80/20%) copolymer

through FTIR studies [19]. This work investigates the variation of absorbance and transmittance of PVDF-copolymer (65/35%) in the region of ferroelectric β -phase,

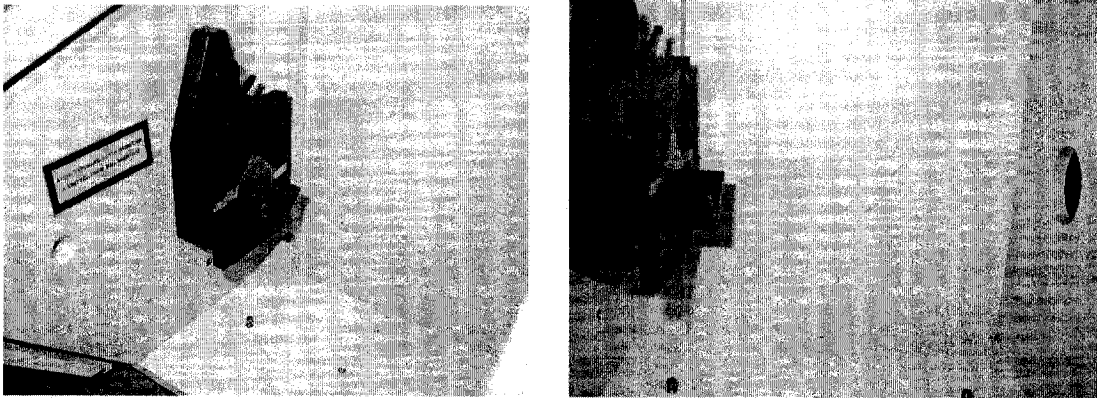


Figure 3.5: PVDF Copolymer thin film placed in the sample holder of FTIR system

The work also investigates the spectra of PVDF-copolymer thin films fabricated by spin coating by comparing with the commercially available PVDF thin films. The work also emphasizes on variation of spectra with respect to annealing of samples at various temperatures and also the variation of spectra with respect to poling. For FTIR analysis, PVDF-TrFE copolymer thin films of thickness 28 microns spin coated on silicon wafers are considered. The spin coated sample is peeled off from the silicon wafer; a film of size approximately 1 inch x 1 inch is cut from the peeled PVDF copolymer thin film and carefully placed in the sample holder of the Perkin Elmer spectrum analyzer BX II FT-IR system shown in Figure 3.5. As mentioned in literature review of Chapter1, PVDF copolymer has many advantages over PVDF homopolymer including that the copolymer crystallizes directly to polarized phase at room temperature [1].

3.2.2 Effect of annealing on PVDF copolymer thin films.

An important aspect of the present work is to investigate on the effect of annealing PVDF copolymer thin films, In the earlier work Mi Akcan et al studied on the effect of

annealing of 70/30% PVDF TrFE thin films. Annealing is performed to enhance the crystallization of deposited PVDF copolymer thin films. The annealing process for polymers is mainly performed to recover the local stresses [9]. After the PVDF copolymer deposition, samples are kept at 100°C on hot plate to evaporate the solvent Methyl Ethyl Ketone (MEK). Subsequently annealing is performed onto the samples for 10 minutes. PVDF-TrFE spin coated on silicon wafers are annealed at various temperatures ranging from 100 °C to 160 °C with an interval of 10°C. After annealing all the samples are left to cool to the ambient (room) temperature. The effect of annealing on the spin coated P(VDF-TrFE) samples can be observed by examining the differences between the IR spectra of the sample before and after the annealing process. The infrared spectra of the samples, coated on silicon wafers, were recorded on a Perkin Elmer BX II Spectrum in the region 4000 cm⁻¹ to 400cm⁻¹ region, which is calibrated by Polystyrene.

3.3 IR spectra variation of PVDF copolymer thin films

Infrared spectroscopic studies of PVDF copolymer thin films subjected to annealing at different temperatures is investigated. Annealing temperatures considered are between 100 °C and 160 °C close to melting temperature (165 °C) of PVDF-TrFE copolymer thin films. The thickness of the spin coated PVDF copolymer thin film samples is 28 μm(±7%).

3.3.1 Variation of spectra with respect to change in annealing temperature.

The following spectrum represents the absorption and transmission spectra of PVDF-TrFE spin coated samples subjected to different annealing temperatures. the absorption

spectrum of PVDF-TrFE thin film samples in the region $4000-400\text{ cm}^{-1}$ is illustrated in the Figure 3.6. The spectrum also shows spectra of the sample at room temperature (23 °C).

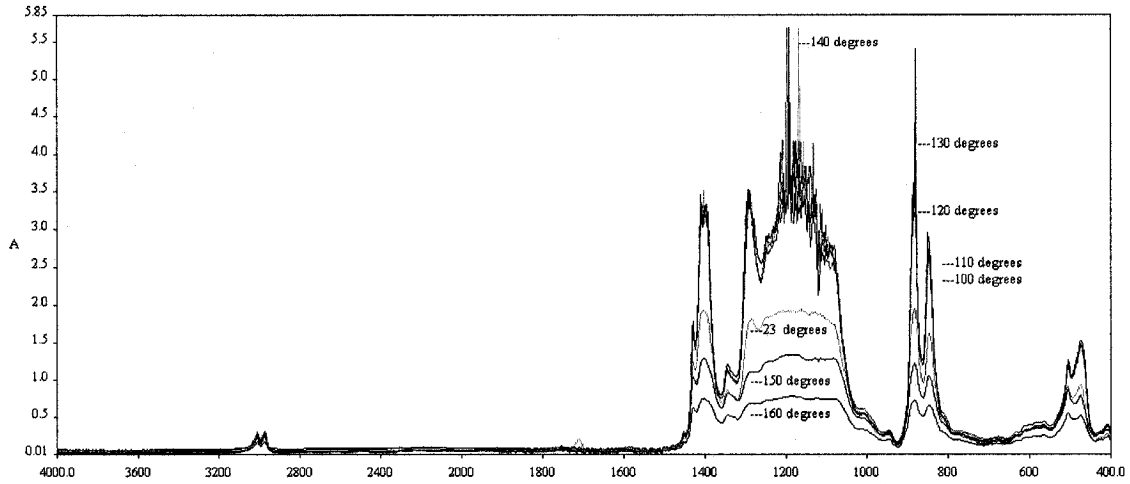


Figure 3.6: Absorption spectra of Spin coated PVDF-TrFE thin films in the region $4000-400\text{ cm}^{-1}$

As reported earlier by Xu [10] the peak at 1286 cm^{-1} signifies the piezoelectric phase, the peaks at 1285.47 cm^{-1} in the region of piezoelectric phase are shown in Figure 3.7. It can be observed that as the annealing temperature increases, the absorbance values in the region of piezoelectric phase (β -phase) increases considerably. In the presented Figure many strong absorbance peaks at $1400, 1285.47, 1150, 884.38, 849.78, 472.57\text{ cm}^{-1}$ are also present. However, the peak at 1285.47 cm^{-1} characterizes the ferroelectric β -phase.

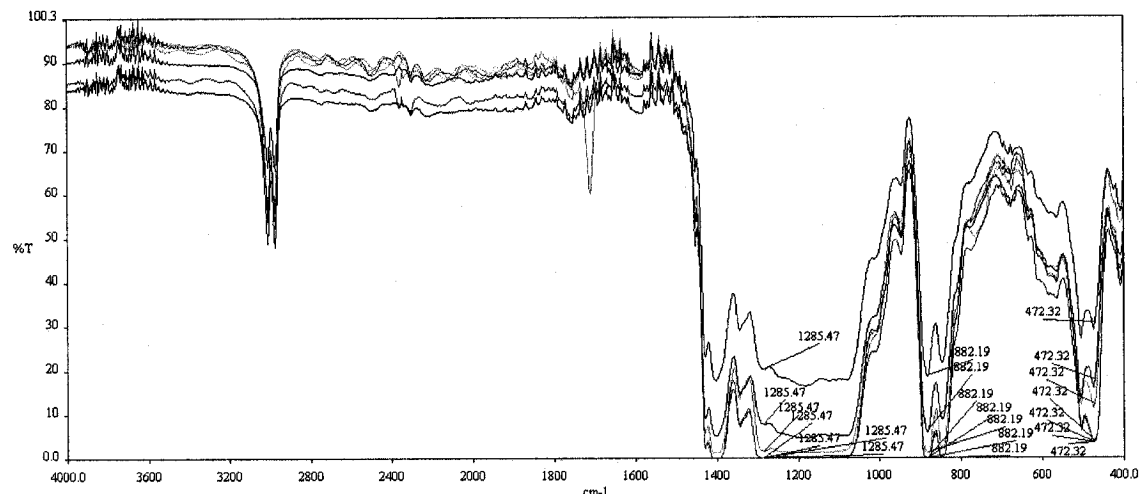


Figure 3.7: Transmission spectra of spin coated PVDF-TrFE thin films in the region 4000- 400 cm^{-1}

It can be observed that as the annealing temperature increases from room temperature (23°C) to 140°C the absorbance increases, when the samples are annealed in the vicinity of melting point (165°C) of P(VDF-TrFE) the absorbance value decreases, which might be due to the sample being almost in molten state which would modify the structure of the material to the extent that absorbance decreases considerably. It can be observed that the absorbance is highest for the annealed sample at 140°C which is close to glass transition temperature (135°C). Hence it can be concluded that spin coated sample annealed at 140 degrees shows strong absorbance peaks in the region of piezoelectric phase which attributes to a better piezoelectric properties than samples annealed at other temperatures. These specimens are further considered to analyze the variation of FTIR plots with respect to subsequent annealing.

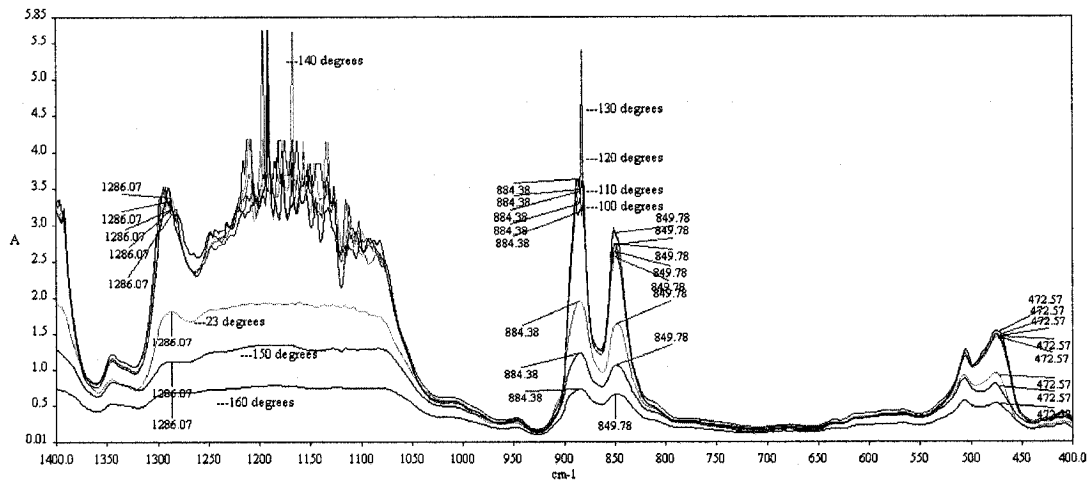


Figure 3.8: Absorption spectra of spin coated PVDF-TrFE thin films in the region 1400-400 cm^{-1}

3.3.2 Variation of the spectra with respect to number of cycles of annealing.

In this work the aspect of analysis with respect to annealing is further extended by performing subsequent annealing on samples, i.e., subsequent annealing is performed on a “Pre-Annealed” sample for 10 minutes.

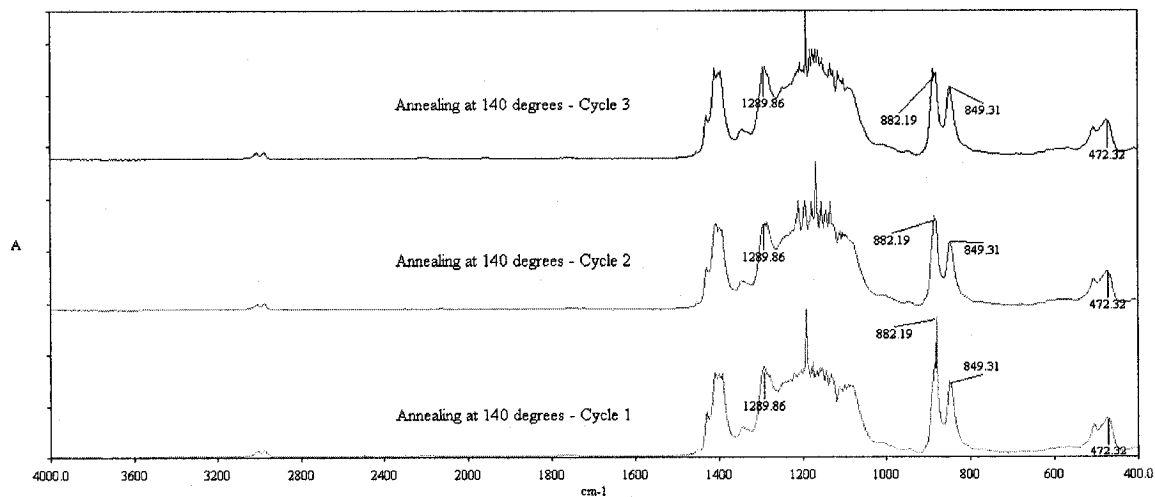


Figure 3.9 Split view of absorption spectra of PVDF copolymer thin films in the region 4000-400 cm^{-1} subjected to subsequent annealing.

For the analysis, samples annealed at 140 °C showing strong absorbance peaks are considered for subsequent annealing. The cycle-1 plot presents the annealed sample initially; subsequent annealing is referred as cycle-2 and cycle -3 samples. The presented Figures show the absorbance spectrum of the annealed samples at 140 ° C. Figure 3.9 presents the split view of the absorbance spectrum of samples in the region 4000- 400 cm-1 and figure 3.10 presents the same graph with an overlay view of all the three specimens.

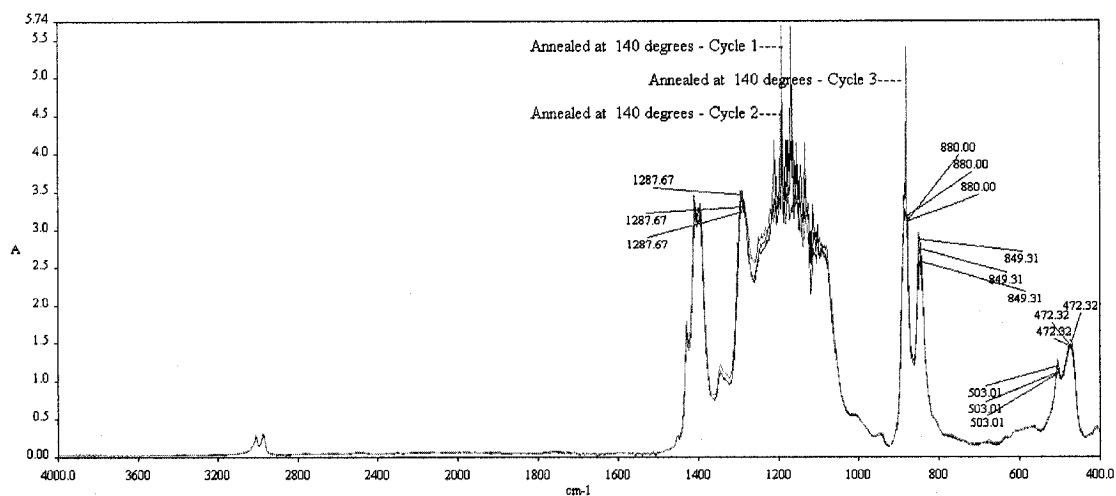


Figure 3.10 Overlay view of Absorption spectrum of PVDF Copolymer thin films in the region 4000-400 cm⁻¹ subjected to subsequent annealing.

It can be observed from the FTIR plots that the absorbance spectrum of the samples subjected to annealing for different cycles is considerably similar. In the piezoelectric phase region which is around 1286 cm⁻¹ there is no significant change in the absorbance. Hence it can be concluded that subsequent annealing of the spin coated samples does not increase the absorbance and hence there is no significant change in the piezoelectric properties of PVDF copolymer thin films. This finding is very important in applications which require cyclic exposure to temperatures in the vicinity of 140 °C of the PVDF

copolymer films. The above finding indicates that three such cycles would not alter the piezoelectric properties of the PVDF copolymer.

3.3.3 Variation of spectra with respect to poling.

As discussed earlier in chapter 2, PVDF copolymer thin films of thickness 28-30 microns which are annealed at 140 degrees are considered for poling. Step wise poling method is adopted to polarize the annealed PVDF thin films for the analysis. The following Figures present the absorption spectrum of poled samples; the plots are compared with respect to spectra of annealed un-poled sample and spectra of commercial 28 μm PVDF thin film.

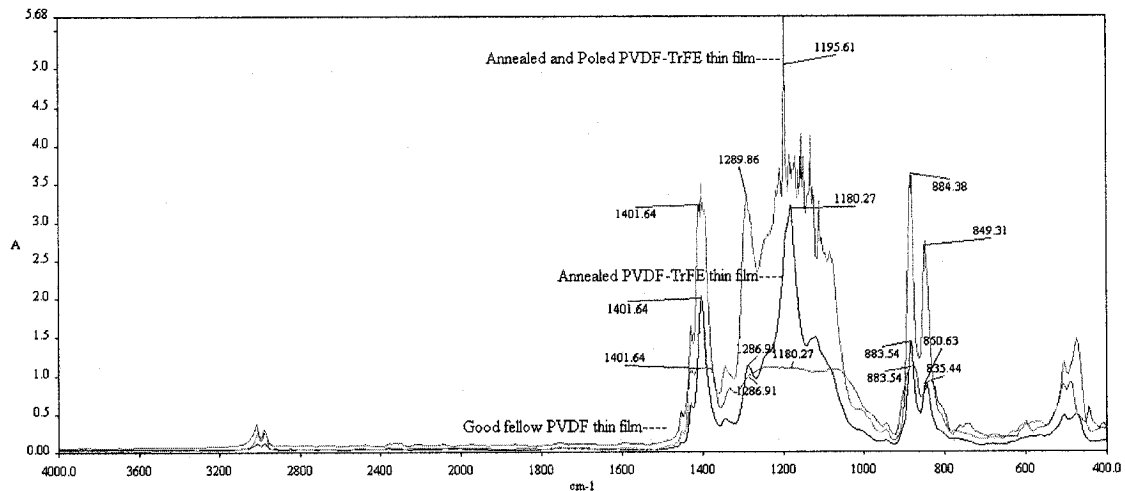


Figure 3.11: Comparison of absorption spectrum of poled samples with respect to unpoled sample and commercial Good Fellow PVDF thin film in the region 4000-400 cm^{-1}

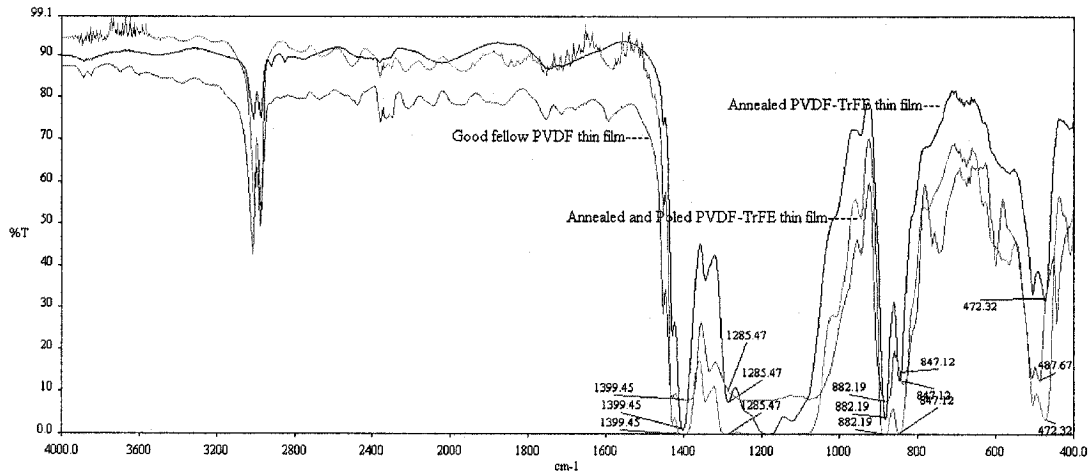


Figure 3.12: Comparison of transmission spectrum of poled samples with respect to unpoled sample and commercial GoodFellow PVDF thin film in the region $4000\text{-}400\text{cm}^{-1}$

Figures 3.11 and 3.12 illustrate the absorption and transmission spectra respectively of poled and unpoled samples, compared with commercial pvdf thin film. In Figure 3.11 it can be observed that many strong absorbance peaks are observed in the plot. The peak at 1285.47 signifies the piezoelectric phase of the copolymer. The absorbance of the sample increases considerably in the piezoelectric phase after poling; which indicates that the polarization of spin coated sample is well accomplished.

The spectrum of polarized sample is compared with respect to commercial PVDF thin film. The comparison clearly shows much higher absorbance values than with commercial PVDF thin film. Hence a much better PVDF copolymer thin film is achieved through spin coating and step-wise poling method

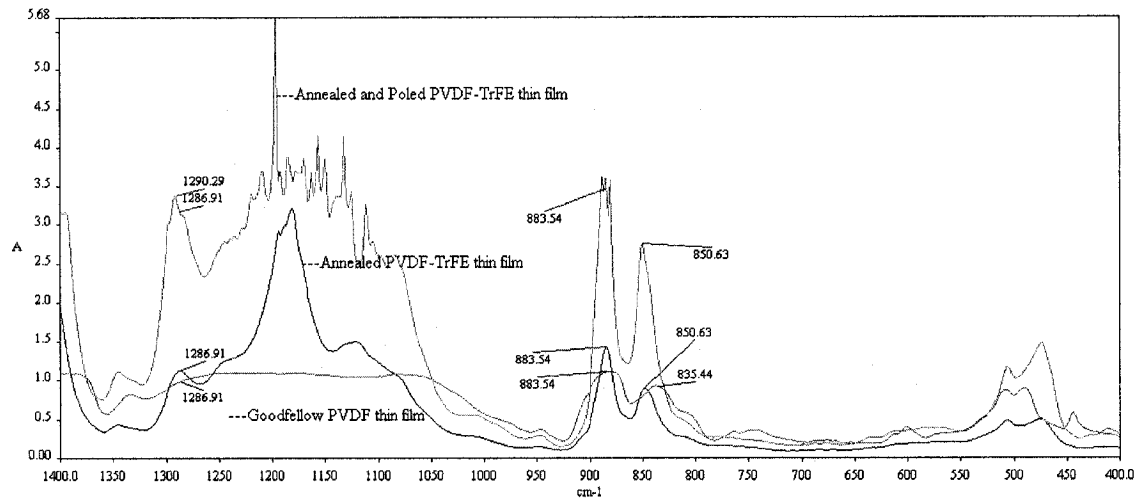


Figure 3.13: Comparison of absorption spectrum of poled samples with respect to unpoled sample and commercial GoodFellow PVDF thin film in the region 1400-400 cm^{-1}

In the Figure 3.11 the transmission spectrum of Poled samples with respect to unpoled sample and commercial PVDF thin film is presented. It can be observed that there is a significant dip in the transmission spectrum of poled PVDF-TrFE sample than in the unpoled sample and the commercial PVDF thin film. The dip signifies that a higher absorbance is found in PVDF-TrFE sample than in the unpoled sample and the commercial PVDF thin film. Figures 3.13 and 3.14 present the absorbance and transmittance plots respectively in the range 1400 – 400 cm^{-1} .

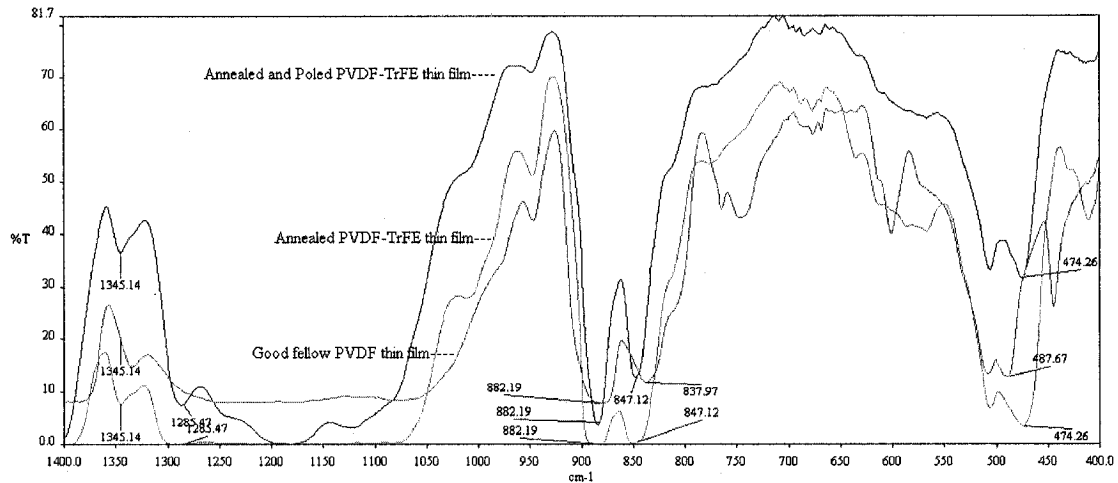


Figure 3.14: Comparison of transmission spectrum of poled samples with respect to unpoled sample and commercial Good fellow PVDF thin film in the region $1400\text{-}400\text{cm}^{-1}$

3.4 Variation of spectra with respect to number of cycles of poling.

The investigation of variation of absorption spectra with respect to poling is further studied by considering subsequent poling of samples and comparing them. Figure 3.15 and Figure 3.16 present the absorption and transmission spectrum of poled samples subjected to subsequent poling. Cycle 1 plot presents the FTIR plot of sample poled once and cycle 2 plot presents the sample poled twice

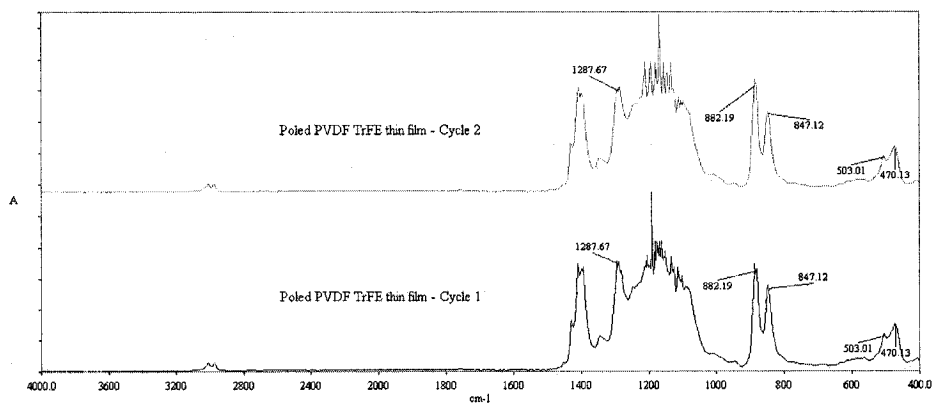


Figure 3.15: Comparison of absorption spectrum of poled sample (poled once) with respect to subsequent poled sample (poled twice).

It can be observed that there is not much significant change in the spectrum of subsequent poled sample, in the region of ferroelectric β phase. There is not a considerable increase in absorbance value in the region of $1286\text{-}1287\text{ cm}^{-1}$ which attributes to an increase in content of β phase. Hence through FTIR spectroscopy studies subsequent step wise poling of the sample does not enhance or reduce the piezoelectric phase of the PVDF copolymer. This finding is also useful when designing applications in which PVDF copolymer films operate in high electric fields. Such type of operation would not alter the piezoelectric properties of the film as obtained from the fabrication steps.

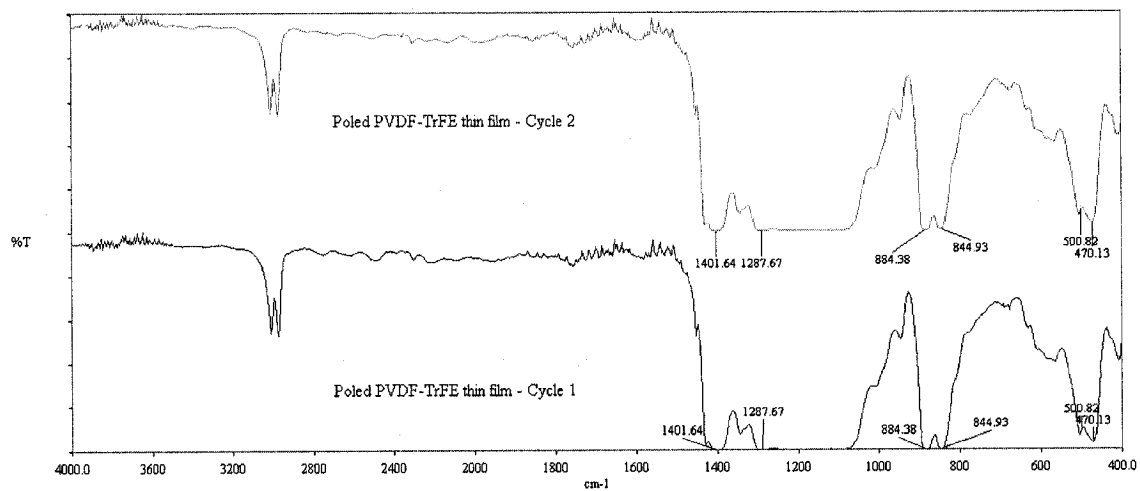


Figure 3.16: Comparison of transmission spectrum of poled sample (poled once) with respect to subsequent poled sample (poled twice).

3.3.5 Comparison of IR spectra with commercial PVDF thin films

In the present study, microfabricated PVDF copolymer thin films were analyzed by comparing with available commercial PVDF thin films. PVDF thin film samples were obtained from Good fellow Corporation & MSI Sensors. The thickness of the PVDF thin film is 28 microns the obtained PVDF thin films are double sided metallized with nickel-cadmium alloy. In order to obtain FTIR readings of the films, the metallized nickel-

cadmium alloy is etched out by using a suitable etchant. The etchant is heated at 60 °C in an ultrasonic bath for 15 minutes, the films are then dipped in the etchant to etch the metallized parts, The commercial PVDF thin films were then used to obtain absorption and transmission spectra from the Perkin Elmer FTIR instrument described above.

In the Figure 3.17. Transmission spectra of PVDF copolymer thin films is compared to commercially fabricated thin films It is obvious that in the PVDF-TrFE (65/35%) clearly shows many strong absorbance peaks at 1402, 1286, 1186, 1124, 1077, 883, 844 and 476 cm^{-1} and many weak absorbance peaks at 1430, 943, 678, 505 cm^{-1} compared with commercial PVDF thin film.

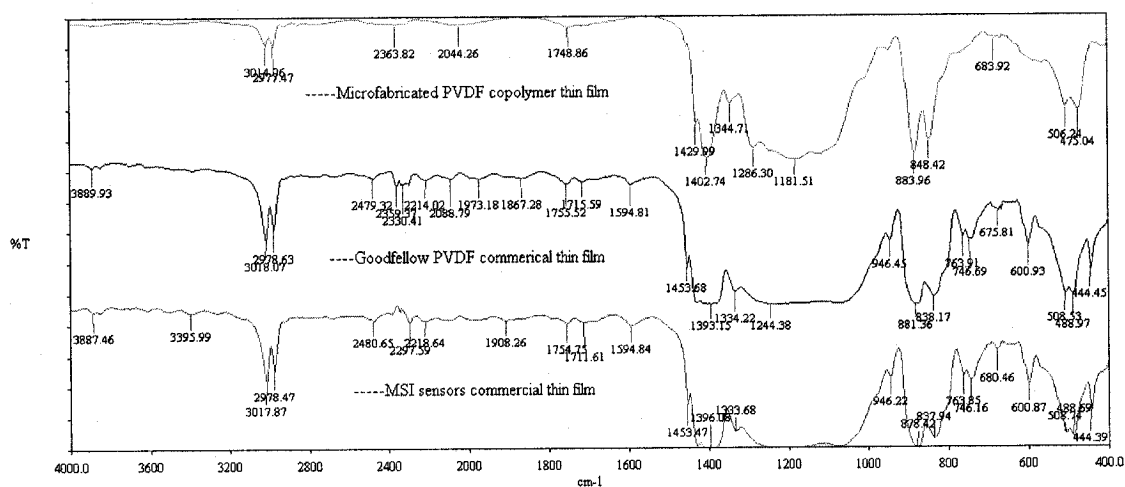


Figure 3.17: Comparison of transmission spectra of microfabricated PVDF copolymer thin film with commercial thin films.

In the PVDF-TrFE (65/35%) a strong absorbance peak at 1286 cm^{-1} is apparent which is characteristic of ferroelectric β phase. In the spectra of PVDF homopolymer the spectra clearly shows that the peaks at 1234 cm^{-1} and 768 cm^{-1} disappear and the peaks at 1077 cm^{-1} and 601 cm^{-1} become weaker. The peak at 812 cm^{-1} is characteristic of γ phase which is seen in PVDF but not in P (VDF-TrFE) copolymer (65/35%). It is reported by

lee that for a molar ratio of 65/35 % (VDF-TrFE) copolymer directly crystallizes into the ferroelectric phase from melting temperature [1]

From the Figures it is observed that the obtained spin coated, polarized sample is comparable to the standards of commercially fabricated PVDF thin film and a better piezoelectric phase can be realized by using the copolymer thin film as it crystallizes directly into piezoelectric beta phase at room temperature, which is not observed in the case of commercially fabricated homopolymer PVDF thin film.

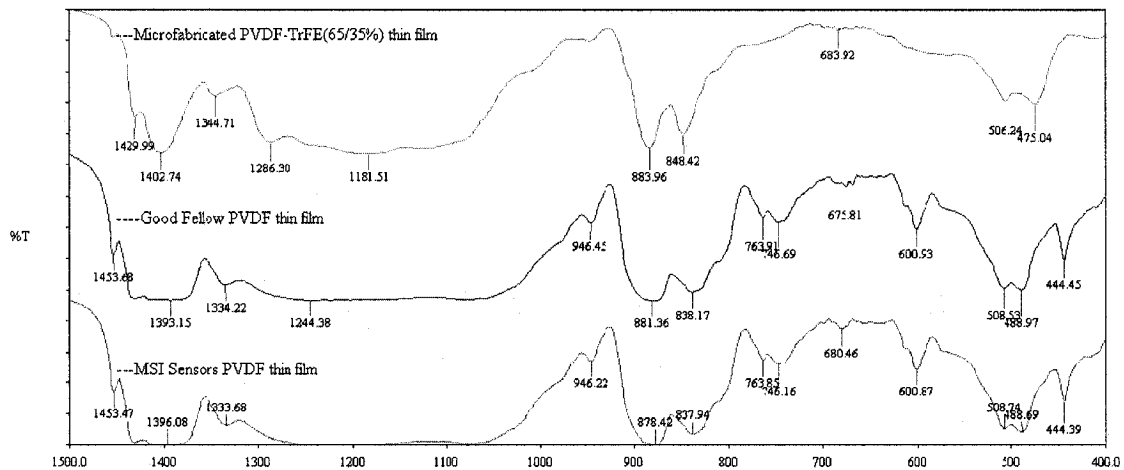


Figure 3.18: Comparison of Transmission spectra of PVDF copolymer thin films with commercial in the region 1500-400cm⁻¹

Hence through the comparison of FTIR characterization of PVDF copolymer thin films with commercially PVDF thin films, it is analyzed that a better piezoelectric PVDF copolymer thin film is observed for the application of thin films in the area of MEMS.

3.4 Summary

In this chapter FTIR characterization of the spin coated PVDF copolymer thin films is carried out and the spectra obtained at different annealing temperatures are analyzed, further the specimens subjected to subsequent annealing are also analyzed, the spectra of the poled spin coated specimens are compared to that of commercially available PVDF thin films. The significant polarized phase of the spin coated pvdf copolymer thin films is predicted at a particular wavenumber and it is analyzed that the obtained spin coated specimens show better piezoelectric properties than PVDF thin film.

Chapter 4

Characterization of microfabricated PVDF copolymer thin films

In the previous Chapter, we studied the fabrication and material characterization. It is important to characterize the piezoelectric performance of microfabricated PVDF copolymer thin films in relation with commercial films. This Chapter will present the testing method for piezoelectric characterization and comparison with test results of microfabricated thin films and commercial films.

4.1 Measurement of piezoelectric constant (d_{31}) of commercial PVDF thin film and microfabricated PVDF copolymer thin film.

A brief introduction, literature review on piezoelectric constants and review on experimental set up to quantify the mechanical properties of the PVDF thin film were presented in the objectives of Chapter 1.

In this Chapter, the characterization of PVDF copolymer thin films is performed through measurement of piezoelectric constants, which attribute to the piezo-mechanical properties of spin coated PVDF copolymer thin films. The predicted and experimental values of piezoelectric coefficient, d_{31} of the spin coated PVDF copolymer thin films are compared with those of commercially available PVDF thin films.

4.1.1 Piezoelectric constants

Piezoelectric materials are anisotropic in nature as their physical constants depend on the direction of the applied mechanical or electric force. Consequently, each constant generally has two subscripts that indicate the directions of the two related mechanical quantities, such as stress (force on the piezoelectric element / surface area of the element) and strain (change in length of element / original length of element) for elasticity.

The direction of positive polarization usually is made to coincide with the Z-axis of a rectangular system of x, y, and z axes direction x, y, or z is represented by the subscripts 1, 2, or 3, respectively and shear about one of these axes is represented by the subscript 4, 5, or 6, respectively. The piezoelectric charge constant, d , the piezoelectric voltage constant, g , and the permittivity, ϵ , are also dependent on temperature [29, 30, 54].

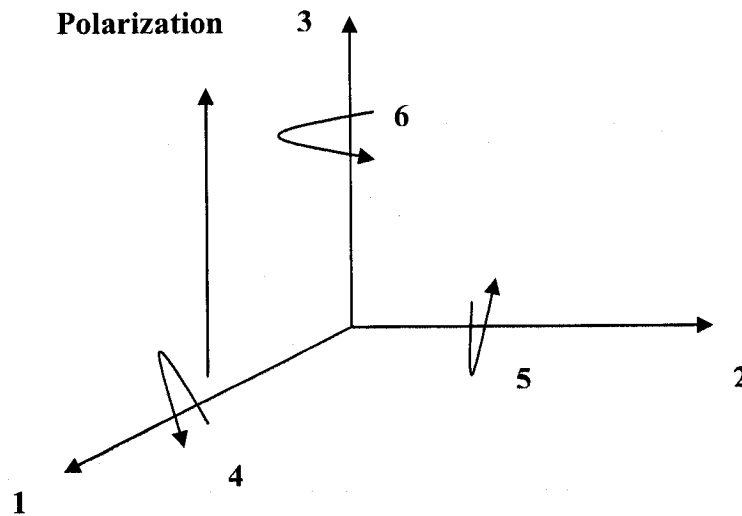


Figure 4.1 Polarization conventions.

4.1.2 Piezoelectric charge constant

The *piezoelectric charge constant*, d , is the polarization generated per unit of mechanical stress (T) applied to a piezoelectric material or, alternatively, is the mechanical strain (S) experienced by a piezoelectric material per unit of electric field applied. The first subscript to d_{ij} indicates the direction of polarization generated in the material when the electric field, E , is zero or, alternatively, is the direction of the applied field strength. The second subscript is the direction of the applied stress or the induced strain, respectively. The strain induced in a piezoelectric material by an applied electric field is the product of the value for the electric field and the value of d . The parameter d is an important indicator of a material's suitability for strain-dependent (actuator) applications. The constants are summarized and presented in Table 4.1 and sign conventions of the coordinate system is shown in Figure 4.1 [54, 55].

Table 4.1 Piezoelectric charge constants

d₃₃	induced polarization in direction 3 (per unit stress applied in direction 3 / induced strain in direction 3 per unit electric field applied in direction 3
d₃₁	induced polarization in direction 3 per unit stress applied in direction 1 / induced strain in direction 1 per unit electric field applied in direction 3
d₁₅	induced polarization in direction 1 per unit shear stress applied about direction 2 / induced shear strain about direction 2 per unit electric field applied in direction 1

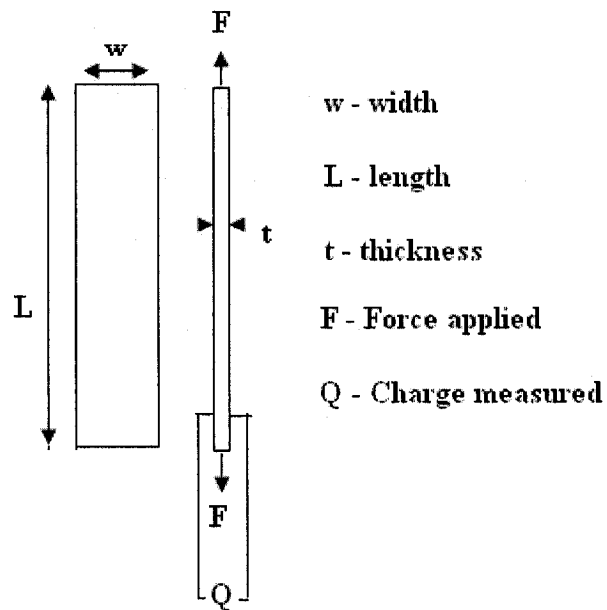


Figure 4.2 Geometry of PVDF thin film.

In the present work, measurement of piezoelectric constant d_{31} is carried out by applying force (F) along the plane of the film and the resulting charge output (Q) is measured

across the thickness of the PVDF thin film and eventually d_{31} is evaluated for the considered PVDF thin film as shown in Figure 4.2.

4.2 Experimental setup for measurement of piezoelectric constant, d_{31}

The experimental setup is illustrated in Figure 4.3. Commercially available PVDF thin film of thickness 28 microns from MSI sensors is taken for measuring the piezoelectric constant d_{31} . PVDF thin film of length 60 mm and width 6mm are cut from the available PVDF thin film sheets of size 5 inch x 5 inch, the obtained PVDF thin films are metallized with nickel-cadmium alloy as electrodes.

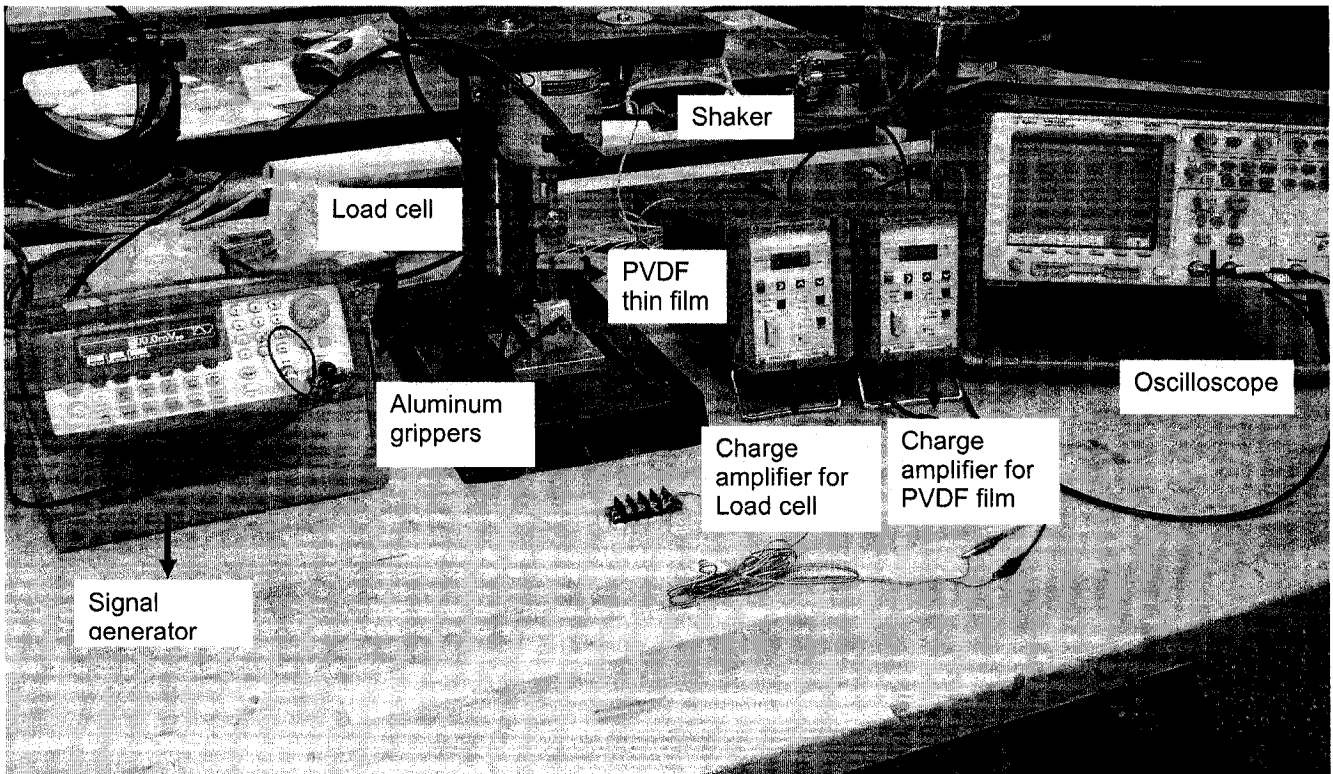


Figure 4.3 Experimental setup for the measurement of piezoelectric constant, d_{31}

A sinusoidal wave signal of specified frequency and amplitude is used to excite the shaker system which transmits force to the force sensor (load cell). PVDF thin film is

clamped by means of aluminum grippers which are connected to the load cell as illustrated in Figure 4.4. Hence a force along the plane of PVDF film is applied through a force sensor.

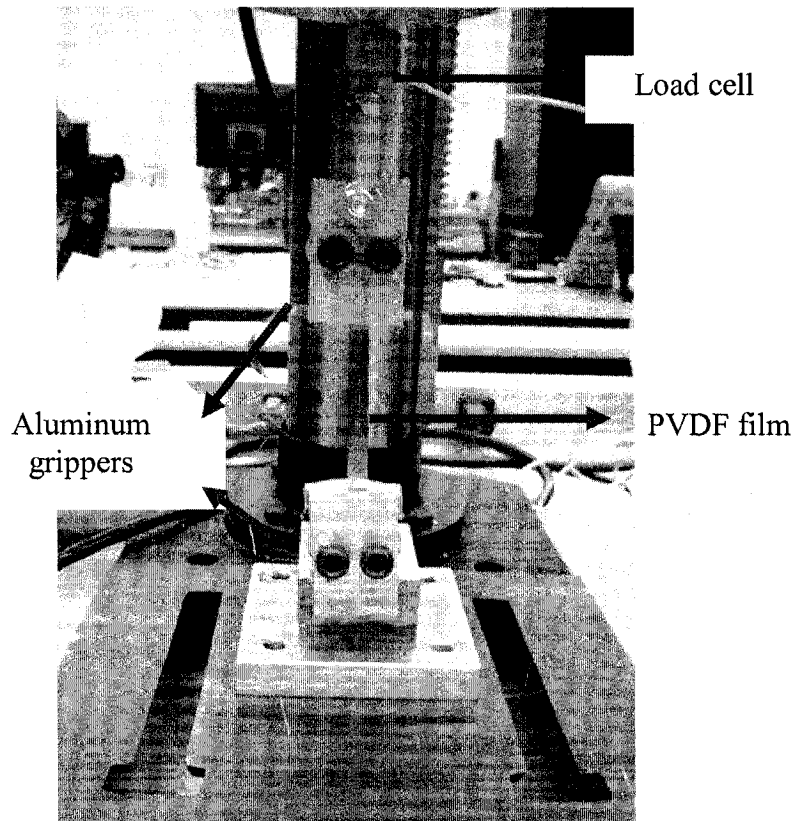


Figure 4.4 PVDF thin film clamped for testing.

Due to the application of force along the plane of the PVDF thin film a charge distribution is developed across the thickness of the PVDF thin film. The charge output is amplified by means of a charge amplifier which is connected across the thickness of the PVDF thin film.

Another charge amplifier is connected to the load cell to amplify the signal from the load cell. The sensitivity of the load cell is 12.26pC/N , the scale is 1N/Volt , and the gain of the load cell is 12.26pC/V .

4.2.1 Estimation of piezoelectric constant (d_{31}) of PVDF thin film.

The sensitivity of the PVDF film is estimated by setting the value for sensitivity as 23pC/N which is the piezoelectric constant d_{31} for the considered commercial PVDF thin film when a scale of 1000N/V is chosen, the gain of the PVDF film is 23000pC/V. The output from the charge amplifiers corresponding to the load cell and PVDF thin film are read on an oscilloscope in the form of sinusoidal signals. The voltage amplitude (peak-peak) of the signals are obtained. The voltage (peak to peak, channel 1) measured through the charge amplifier connected to the load cell corresponds to the “Force” applied along the PVDF thin film, and the voltage (peak to peak, channel 2) measured through the amplifier connected across the thickness of the PVDF thin film is noted down to evaluate the charge output. The charge output (Q_m) of the PVDF film is evaluated with the considered geometry of the film as follows:

$$\begin{aligned} \text{If} \quad \gamma & - \text{Gain of the PVDF thin film (pC/V)} \\ V & - \text{Voltage across the film (peak-peak)(Volts)} \\ \text{then} \quad Q_m & = \gamma V (\text{Coloumbs}) \end{aligned}$$

From the definition *charge density* is evaluated from the following equation

$$\rho = \sigma \cdot d_{31} \quad (4.1)$$

$$\text{Also} \quad \rho = \frac{Q}{A_q} \quad (4.2)$$

$$\sigma = \frac{F}{A_f} \quad (4.3)$$

From Eqns (4.1), (4.2) and (4.3)

$$\frac{Q}{A_q} = \frac{F}{A_f} \cdot d_{31} \quad (4.4)$$

Where	d_{31}	- piezoelectric charge constant	(pC/N)
	ρ	- charge density	(C/m ²)
	σ	- stress	(N/m ²)
	F	- force (Voltage peak to peak)	(N)
	Q_m	- charge measured	(C)
	A_q	- ($l \times w$) Cross sectional area across the length of the film.	(mm ²)
	A_f	- ($w \times t$) Cross sectional area across the thickness of the film.	(mm ²)
	l	- 60mm (length of the PVDF thin film)	(mm)
	w	- 6mm (width of PVDF thin film)	(mm)
	t	- 28 microns (thickness of PVDF thin film)	(μ m)

Hence from Eq 4 .4 piezoelectric constant is estimated as

$$d_{31} = \frac{Q_m t}{F l} \quad (4.5)$$

The testing of PVDF thin film is performed by varying the excitation frequency and amplitude of the signal using the function generator. Three sets of frequencies, namely, 10Hz, 15 Hz and 20 Hz with varied amplitudes of 1V to 10 V (peak to peak) are applied to excite the shaker system which transmits force to the PVDF film through a load cell. The Tables 4.2, 4.3 and 4.4 present the voltage (peak to peak) values obtained for the PVDF commercial thin film at different excitation frequencies of 10 Hz, 15Hz and 20 Hz. For each set of excitation frequency the average value of d_{31} for the PVDF commercial film is also presented.

V_{signal} (Volts)	V_{load} (Volts)	Load (Newtons)	$V_{\text{PVDF,c}}$ (Volts)	$Q_{\text{PVDF,c}}$ (Coulombs)	d_{31} (pC/N)
1	1.36E-01	1.36E-01	2.45E-01	5.64E-09	19.34
2	2.65E-01	2.65E-01	4.20E-01	9.66E-09	17.01
3	3.06E-01	3.06E-01	7.38E-01	1.70E-08	25.89
4	5.31E-01	5.31E-01	9.80E-01	2.25E-08	19.81
5	6.28E-01	6.28E-01	1.23	2.83E-08	21.02
6	8.13E-01	8.13E-01	1.47	3.38E-08	19.41
7	9.50E-01	9.50E-01	1.73	3.98E-08	19.55
8	1.08	1.08	1.92	4.42E-08	19.06
9	1.21	1.21	2.26	5.20E-08	20.05
10	1.33	1.33	2.45	5.64E-08	19.77
				Average	20.09

Table 4.2 Experimental test results of d_{31} for a commercial film at 10 Hz excitation

V_{signal} (Volts)	V_{load} (Volts)	Load (Newtons)	$V_{\text{PVDF,c}}$ (Volts)	$Q_{\text{PVDF,c}}$ (Coulombs)	d_{31} (pC/N)
1	1.40E-01	1.40E-01	2.50E-01	5.75E-09	19.17
2	2.60E-01	2.60E-01	5.12E-01	1.18E-08	21.14
3	4.00E-01	4.00E-01	7.50E-01	1.73E-08	20.13
4	4.75E-01	4.75E-01	9.30E-01	2.14E-08	21.01
5	6.44E-01	6.44E-01	1.25	2.88E-08	20.83
6	7.80E-01	7.80E-01	1.50	3.45E-08	20.64
7	9.10E-01	9.10E-01	1.73	3.98E-08	20.41
8	1.02	1.02	1.97	4.53E-08	20.73
9	1.14	1.14	2.22	5.11E-08	20.90
10	1.25	1.25	2.50	5.75E-08	21.47
				Average	20.64

Table 4.3 Experimental test results of d_{31} for a commercial film at 15 Hz excitation

V_{signal} (Volts)	V_{load} (Volts)	Load (Newtons)	$V_{\text{PVDF,c}}$ (Volts)	$Q_{\text{PVDF,c}}$ (Coulombs)	d_{31} (pC/N)
1	1.30E-01	1.30E-01	2.60E-01	5.98E-09	21.47
2	2.50E-01	2.50E-01	5.35E-01	1.23E-08	22.97
3	3.72E-01	3.72E-01	8.10E-01	1.86E-08	23.37
4	4.91E-01	4.91E-01	1.06	2.44E-08	23.17
5	6.25E-01	6.25E-01	1.30	2.99E-08	22.33
6	7.31E-01	7.31E-01	1.48	3.40E-08	21.73
7	8.40E-01	8.40E-01	1.70	3.91E-08	21.72
8	9.40E-01	9.40E-01	1.91	4.39E-08	21.81
9	1.02	1.02	2.10	4.83E-08	22.10
10	1.10	1.10	2.41	5.54E-08	23.52
				Average	22.42

Table 4.4 Experimental test results of d_{31} for a commercial film at 20 Hz excitation

The variation of $V_{\text{PVDF,C}}$ (voltage peak-peak) with respect to applied load for the commercial film at different excitation frequencies are presented in Figures 4.5, 4.6, 4.7, 4.8. The variation of $Q_{\text{PVDF,c}}$ and d_{31} against applied load are presented in the Figures 4.9, 4.10.

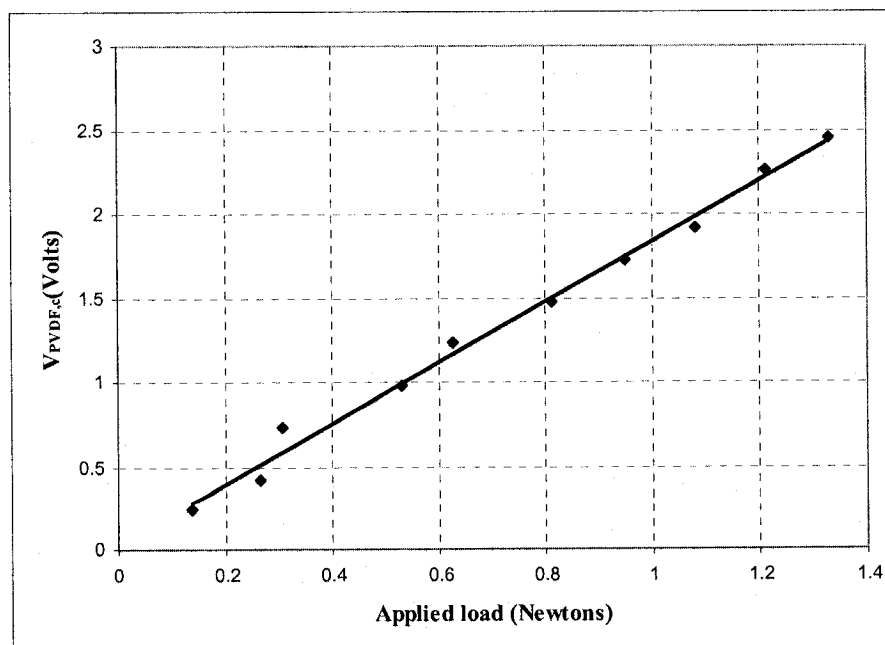


Figure 4.5 Variation of $V_{\text{PVDF,c}}$ with respect to applied load for the commercial PVDF thin film at 10 Hz excitation

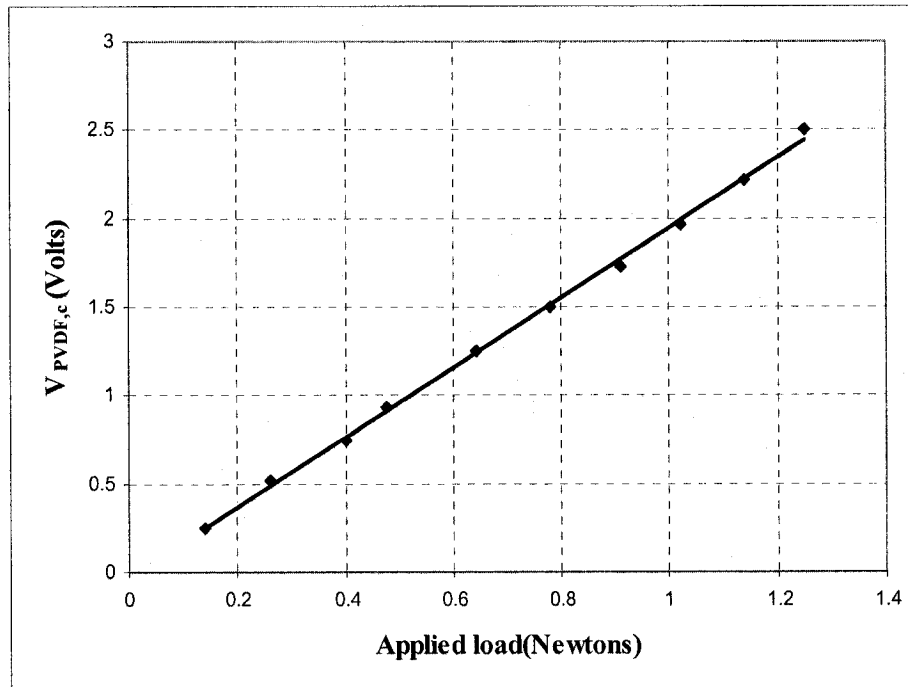


Figure 4.6 Variation of $V_{PVDF,C}$ with respect to V_{Load} for the commercial PVDF thin film at 15 Hz excitation.

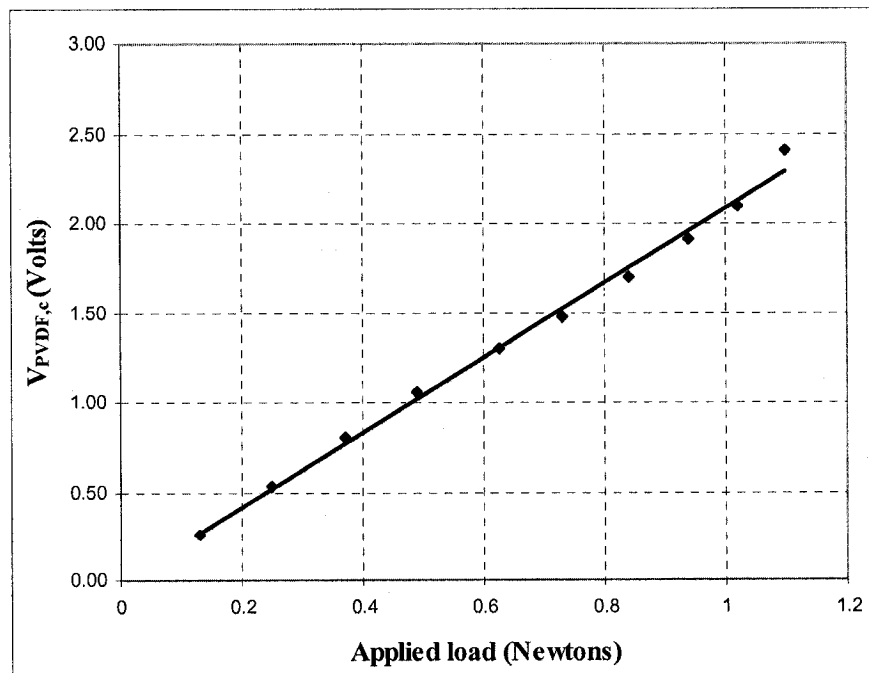


Figure 4.7 Variation of $V_{PVDF,C}$ with respect to V_{Load} for the commercial PVDF thin film at 20 Hz excitation

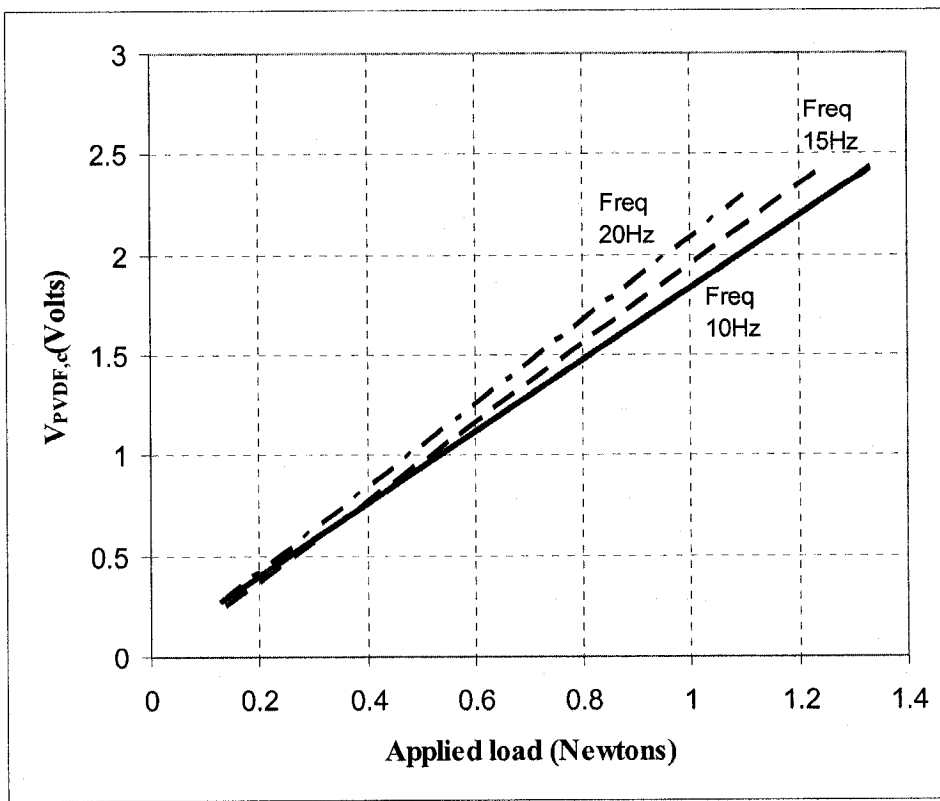


Figure 4.8 Variation of $V_{PVDF,C}$ against applied load for commercial PVDF thin film at different excitation frequencies

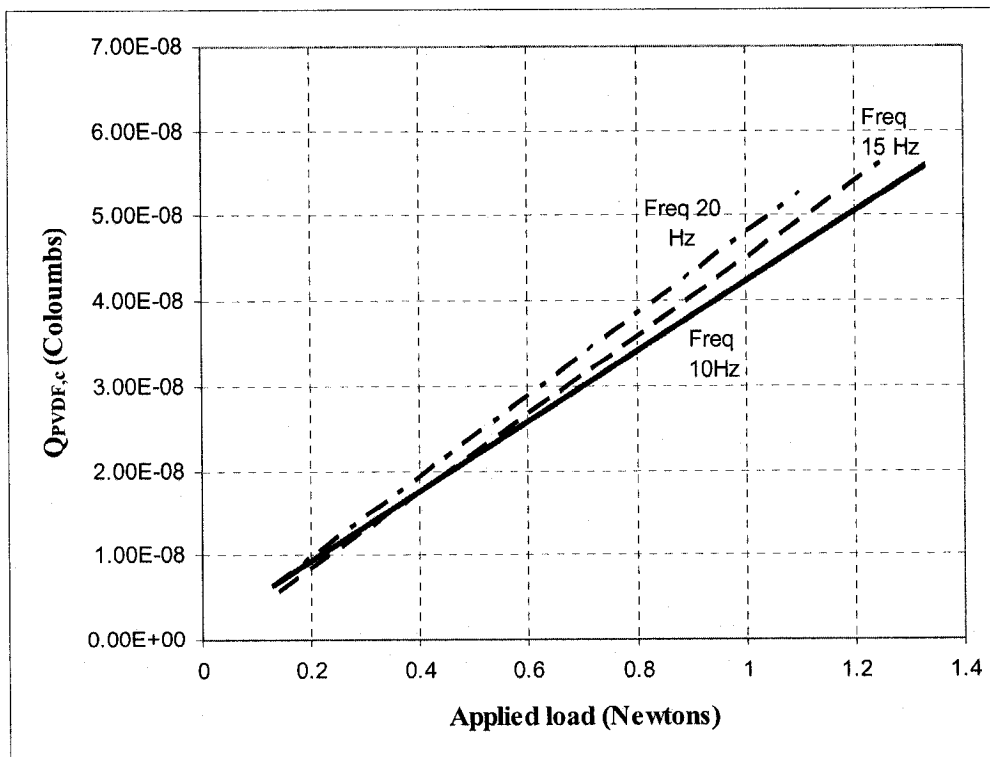


Figure 4.9 Variation of $Q_{PVDF,C}$ against applied load for commercial PVDF thin film at different excitation frequencies

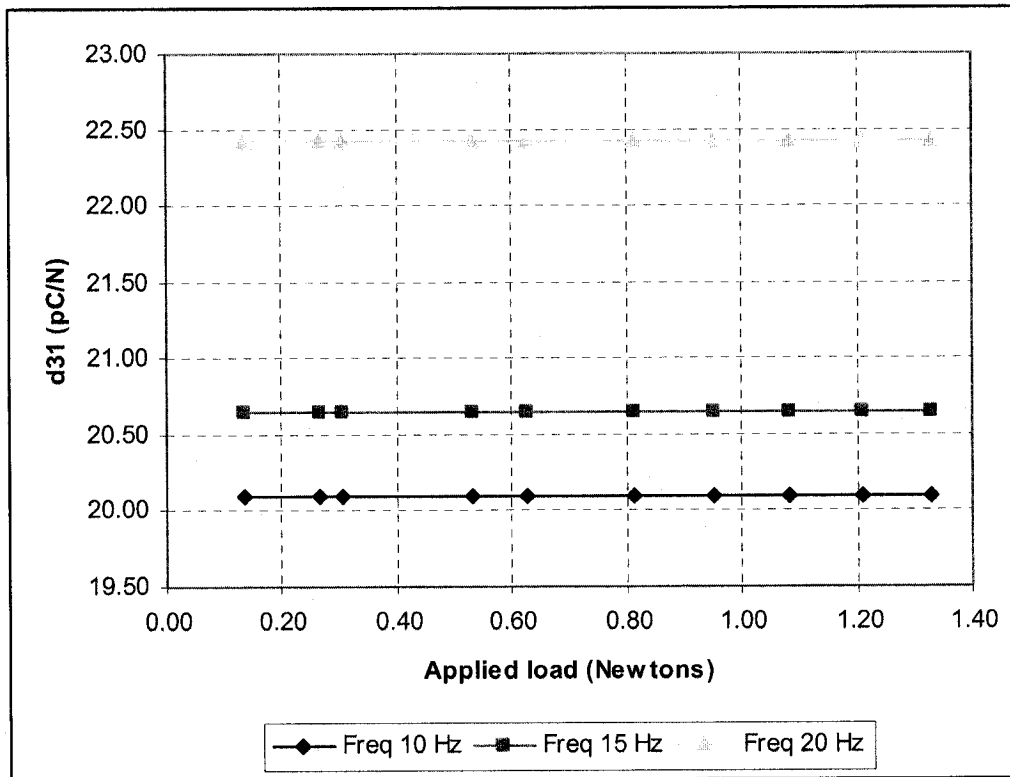


Figure 4.10 Variation of d_{31} (pC/N) against applied load for commercial PVDF thin film at different excitation frequencies

4.2.2 Estimation of piezoelectric constant (d_{31}) of microfabricated PVDF copolymer thin film.

In this chapter the mechanical properties of the microfabricated PVDF copolymer thin films are investigated. The spin coated PVDF copolymer thin films of approximately 28 microns thickness on silicon wafers are deposited with aluminum of around 0.7 microns on both sides of the film. Due to the non uniformity in the spin coating and aluminium deposition was observed that the film is curled due to the heating during the deposition. The spin coated PVDF copolymer thin films are peeled off from the wafer carefully and are cut into rectangular dimensions of 60mm x 6mm.

The charge output of the microfabricated PVDF copolymer thin film is measured according to the experimental procedure as explained above. The charge output of PVDF thin film of the specified geometry is obtained for varied forces applied along the plane of microfabricated PVDF copolymer thin film as shown in (Figure 4.11). The amplitudes (peak to peak) of the sinusoidal signals from load cell and PVDF thin film are obtained using the oscilloscopes. However, it is observed that the obtained sinusoidal signals in the case of PVDF copolymer thin film are not smooth as in the case of commercial PVDF thin film. This may be due to the curling of spin coated PVDF copolymer thin film which resulted due to the peeling of the film from the silicon wafer. In addition the electrode deposition on of PVDF copolymer thin film was not uniform as in the case of commercial PVDF thin films.

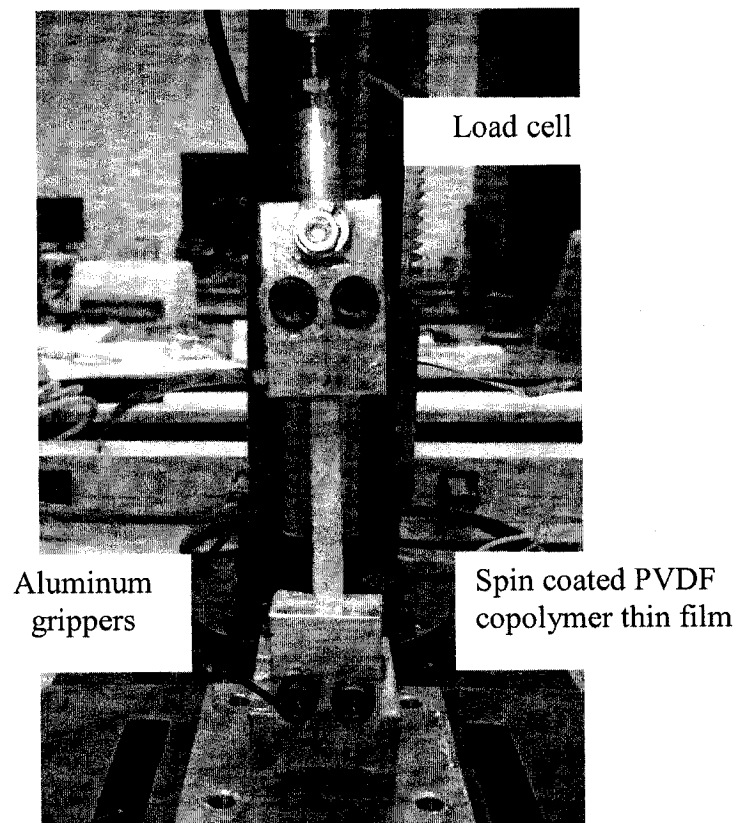


Figure 4.11 Microfabricated PVDF copolymer thin film clamped for testing

The sensitivity of the microfabricated PVDF copolymer thin film is estimated by setting the value for sensitivity as 23pC/N and a scale of 1000N/V. Hence the gain of the spin coated PVDF copolymer thin film is 23000pC/V. The output from the charge amplifiers corresponding to the load cell and PVDF copolymer thin film are read using an oscilloscope in the form of sinusoidal signals from which the voltage amplitude (peak-peak) are obtained. The voltage (peak to peak, channel 1) measured through the charge amplifier connected to the load cell corresponds to the “Force” applied along the PVDF copolymer thin film, and the voltage (peak to peak, channel 2) measured through the amplifier connected across the thickness of the PVDF copolymer thin film is noted down to evaluate the charge output. The charge output of the microfabricated PVDF copolymer film is evaluated with the considered geometry of the film as follows.

If γ^{sp} - Gain of the microfabricated PVDF copolymer thin film (pC/Volts)

V - Voltage across the film (peak-peak) (Volts)

then

$$Q_m = \gamma^{sp}V \quad (4.6)$$

From Equation 4.4

$$\frac{Q'_m}{A_q} = \frac{F}{A_f} d'_{31} \quad (4.7)$$

Where d'_{31} - Piezoelectric charge constant (pC/N)

F - Force (Voltage, peak to peak) (N)

Q'_m - Charge measured (C)

A_q - ($l w$) Cross sectional area across the length of the film. (mm²)

A_f - ($w t$) Cross sectional area across the thickness of the film. (mm²)

l	-	60mm (<i>length of the PVDF copolymer thin film</i>)	(mm)
w	-	6mm (<i>width of PVDF thin film</i>)	(mm)
t	-	28 microns (<i>thickness of PVDF thin film</i>)	(μm)

With the known geometry, applied force and charge measured, piezoelectric constant for PVDF copolymer thin film is estimated as follows.

$$d_{31} = \frac{Q'_m t}{F l} \quad (4.8)$$

Similar to the experimental procedure described for PVDF commercial thin film the testing of microfabricated PVDF copolymer thin film is performed by varying the excitation frequency and amplitude of the signal using the function generator. Three sets of frequencies namely 10Hz, 15 Hz and 20 Hz of signals with varied amplitudes of 1V to 10 V (peak to peak) are used to excite the shaker system that transmits force to the load cell. In this way force is applied along the plane of the PVDF copolymer thin film. The Tables 4.5, 4.6 and 4.7 present the voltage (peak to peak) values obtained for the microfabricated PVDF copolymer thin film at different excitation frequencies of 10 Hz, 15Hz and 20 Hz. For each set of excitation frequency the average value of d_{31} for the microfabricated PVDF copolymer film is also presented.

V_{signal} (Volts)	V_{load} (Volts)	Load (Newtons)	$V_{\text{PVDF/TiFE}}$ (Volts)	$Q_{\text{PVDF/TiFE}}$ (coloumbs)	d_{31} (pC/N)
1	1.36E-01	1.36E-01	2.72E-01	6.26E-09	21.50
2	2.65E-01	2.65E-01	5.11E-01	1.18E-08	20.70
3	3.06E-01	3.06E-01	8.05E-01	1.85E-08	28.20
4	5.31E-01	5.31E-01	1.09	2.50E-08	22.00
5	6.28E-01	6.28E-01	1.38	3.17E-08	23.60
6	8.13E-01	8.13E-01	1.64	3.77E-08	21.70
7	9.50E-01	9.50E-01	1.87	4.30E-08	21.10
8	1.08	1.08	2.16	4.97E-08	21.40
9	1.21	1.21	2.43	5.59E-08	21.60
10	1.33	1.33	2.65	6.10E-08	21.40
				Average	22.32

Table 4.5 Experimental test results of d_{31} for a PVDF copolymer thin film at 10 Hz excitation

V_{signal} (Volts)	V_{load} (Volts)	Load (Newtons)	$V_{\text{PVDF/TiFE}}$ (Volts)	$Q_{\text{PVDF/TiFE}}$ (coloumbs)	d_{31} (pC/N)
1	1.40E-01	1.40E-01	2.98E-01	6.85E-09	22.80
2	2.60E-01	2.60E-01	5.96E-01	1.37E-08	24.60
3	4.00E-01	4.00E-01	8.78E-01	2.02E-08	23.60
4	4.75E-01	4.75E-01	1.19	2.74E-08	26.90
5	6.44E-01	6.44E-01	1.42	3.27E-08	23.70
6	7.80E-01	7.80E-01	1.79	4.11E-08	24.60
7	9.10E-01	9.10E-01	2.09	4.80E-08	24.60
8	1.02	1.02	2.38	5.47E-08	25.00
9	1.14	1.14	2.66	6.12E-08	25.00
10	1.25	1.25	2.89	6.65E-08	24.80
				Average	24.60

Table 4.6 Experimental test results of d_{31} for a PVDF copolymer thin film at 15Hz excitation

V_{signal} (Volts)	V_{load} (Volts)	Load (Newtons)	$V_{\text{PVDF/TiFE}}$ (Volts)	$Q_{\text{PVDF/TiFE}}$ (Coulombs)	d_{31} (pC/N)
1	1.30E-01	1.30E-01	3.12E-01	7.18E-09	25.80
2	2.50E-01	2.50E-01	6.32E-01	1.45E-08	27.10
3	3.72E-01	3.72E-01	9.32E-01	2.14E-08	26.90
4	4.91E-01	4.91E-01	1.55	3.57E-08	33.90
5	6.25E-01	6.25E-01	1.87	4.29E-08	32.10
6	7.31E-01	7.31E-01	2.18	5.02E-08	32.10
7	8.40E-01	8.40E-01	2.49	5.72E-08	31.80
8	9.40E-01	9.40E-01	2.80	6.44E-08	31.90
9	1.02	1.02	3.00	6.90E-08	31.60
10	1.10	1.10	3.33	7.66E-08	32.50
				Average	30.60

Table 4.7 Experimental test results of d_{31} for a PVDF copolymer thin film at 20 Hz excitation

The variation of $V_{\text{PVDF/TiFE}}$ (voltage peak-peak) with respect to applied load for the commercial film at different excitation frequencies are presented in the Figures 4.12, 4.13, 4.14, 4.15. The variation of $V_{\text{PVDF/TiFE}}$ and $Q_{\text{PVDF/TiFE}}$ against applied load is presented in Figures 4.16, 4.17.

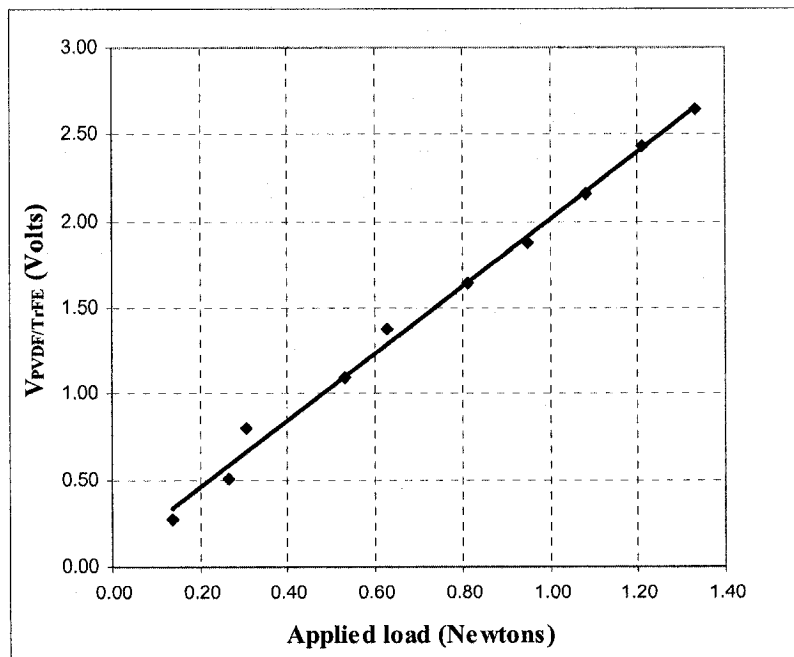


Figure 4.12 Variation of $V_{\text{PVDF/TiFE}}$ against applied load for the microfabricated PVDF copolymer thin film at 10 Hz excitation

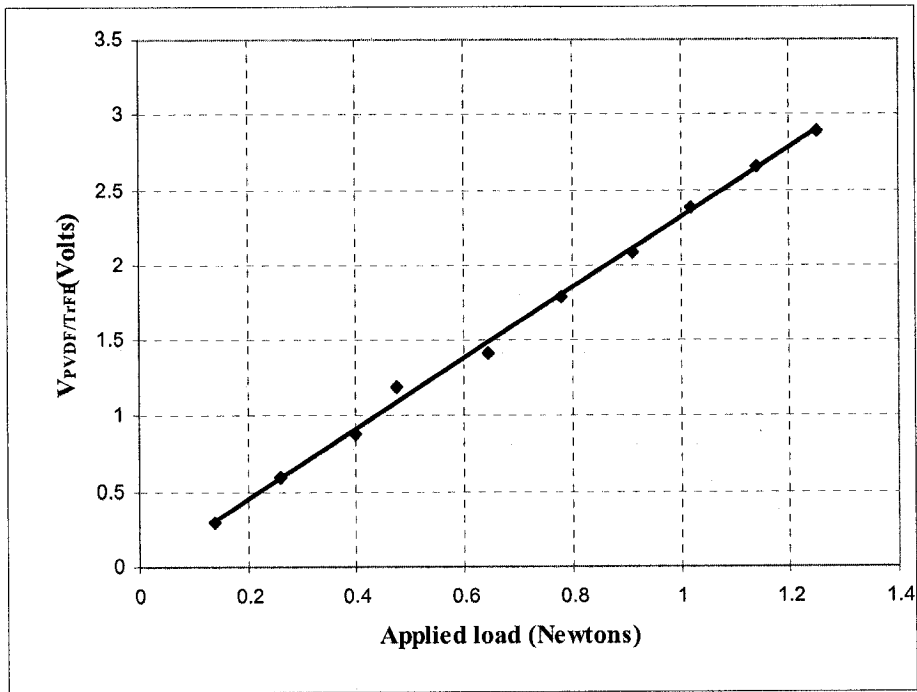


Figure 4.13 Variation of $V_{PVDF/TFE}$ against applied load for the microfabricated PVDF copolymer thin film at 15 Hz excitation

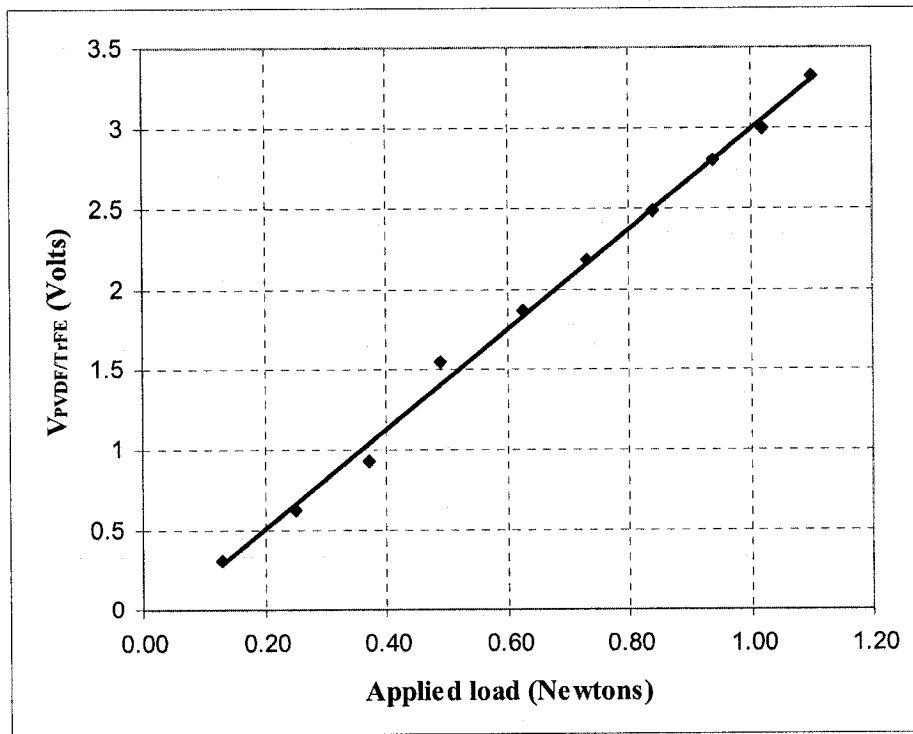


Figure 4.14 Variation of $V_{PVDF/TFE}$ against applied load for the microfabricated PVDF copolymer thin film at 20 Hz excitation

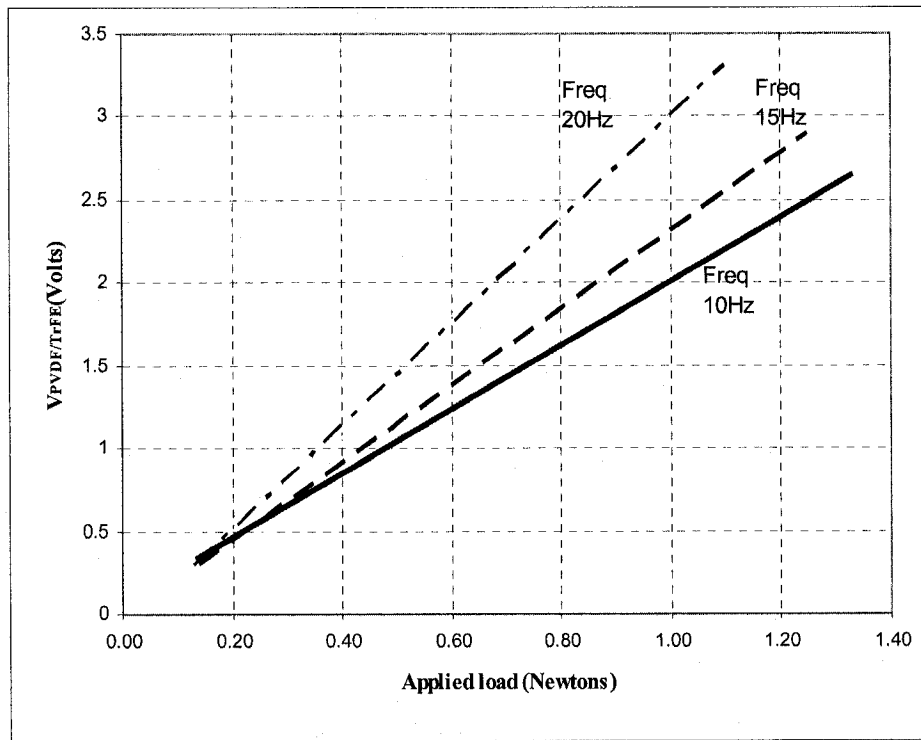


Figure 4.15 Variation of $V_{PVDF/TiFE}$ against applied load for PVDF copolymer thin film at different excitation frequencies

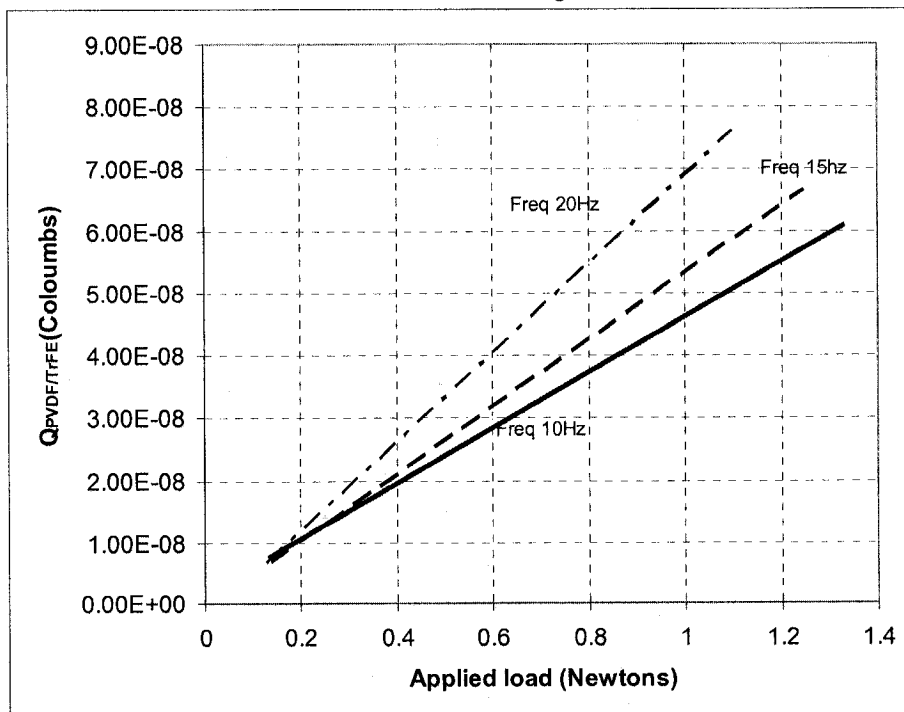


Figure 4.16 Variation of $Q_{PVDF/TiFE}$ against applied load for PVDF copolymer thin film at different excitation frequencies

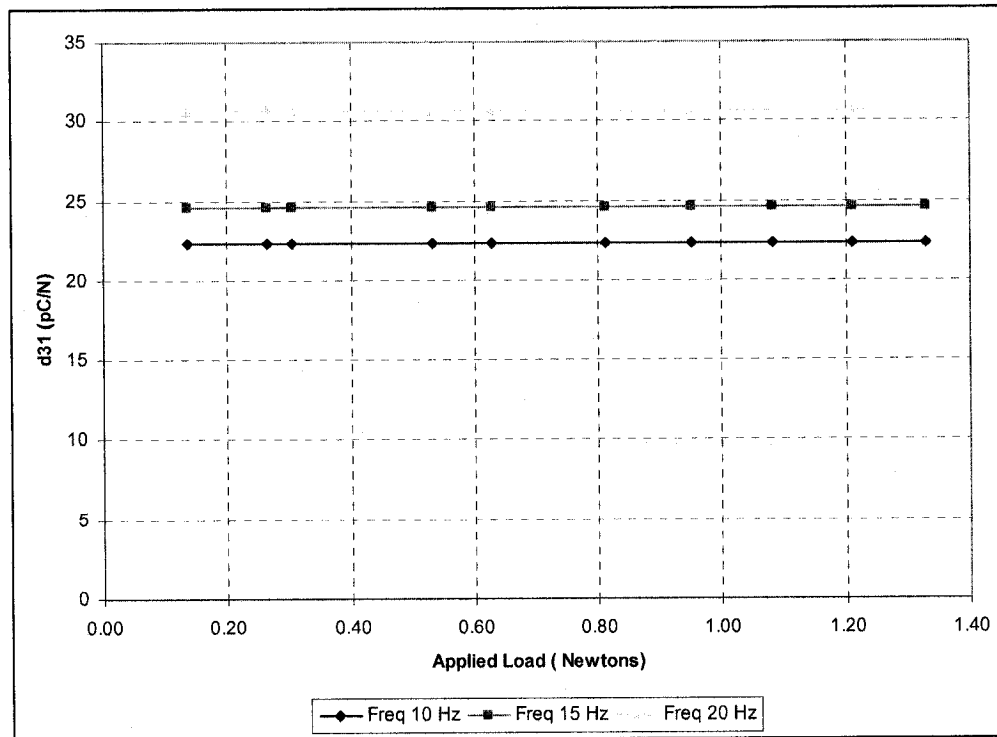


Figure 4.17 Variation of d_{31} against applied load for PVDF copolymer thin film at different excitation frequencies

4.3 Results and conclusions

In the above presented results (Table 4.3 to Table 4.6) it is observed that the piezoelectric constant (d_{31}) is relatively higher at higher excitation frequencies for commercial PVDF thin film and microfabricated PVDF copolymer thin film.

In comparison with the PVDF commercial thin film, the piezoelectric constant d_{31} of microfabricated PVDF copolymer film is slightly higher at excitation frequency of 10Hz and 15 Hz and relatively much higher at excitation frequency of 20 Hz. Hence it is observed that the microfabricated PVDF copolymer thin film possesses relatively better mechanical properties than the commercial PVDF thin film.

However, the charge output obtained in the case of PVDF commercial thin film is much uniform and smooth than in the case of microfabricated PVDF copolymer thin film. This

may be attributed to the non uniform electrode deposition on the PVDF copolymer thin film and also due to the curling of the film which is caused while peeling from the silicon wafer.

4.4 Summary

A basic experimental setup was proposed and presented to measure the piezoelectric constant (d_{31}) of the PVDF thin films. Initially the experimental setup is calibrated with the available commercial PVDF thin films and further the piezoelectric constant (d_{31}) of the spin coated PVDF copolymer thin film is estimated for the considered geometry. The values of d_{31} for the commercial and microfabricated thin films are presented and a comparison of the results are presented and discussed.

Chapter 5

Modeling and simulation of PVDF copolymer thin film actuated optical attenuator

A brief introduction and literature review on the various types of optical attenuators are presented and discussed and further in the literature review the advantages of using PVDF copolymer thin films over PVDF homopolymer thin films is emphasized. In this chapter a simple and novel approach of attenuation is presented. The chapter includes modeling and simulation of a Variable optical attenuator (VOA) with cylindrical waveguide which incorporates piezoelectric actuation mechanism. The attenuation can be controlled by varying the applied voltage across the PVDF thin films which is adhered to the optical fiber.

5.1 Introduction

Modeling of the cylindrical waveguide is performed using finite element model tool ANSYS 9.0. Three different geometrical configurations of the cylindrical waveguide are considered by varying the length of the optical fiber. The deflection of the optical fiber can be varied by varying the applied voltages across the PVDF thin film adhered to the optical fiber. The results of the finite element model are applied to evaluate the attenuation characteristics such as “Coupling Efficiency and “Insertion Loss” for the considered geometrical configurations. The Proposed optical fiber is adhered with a PVDF thin film of standard material properties, the modeling is further extended by the application of PVDF copolymer thin films. While modeling the device in ANSYS, the

values of the piezoelectric constant (d_{31}) which were experimentally estimated for the commercial PVDF thin film and microfabricated PVDF copolymer thin films in Chapter 4 are considered.

5.2 VOA (Variable optical attenuator)

Possible solutions for actuation would be mainly the piezoelectric, electrostatic and metal bimorph. In this work piezoelectric actuation simulation is retained. This solution proposes deposition of thin layer on optical fibers based on piezoelectric polymers such as PVDF (Poly Vinylidene Fluoride) material. The PVDF material is interesting for its low cost and simplicity for microfabrication. The complete system is actuated with some external voltage creating a certain deformation and inducing some attenuation depending on the deflection. Basically, the system can be considered as a cantilever that is deflected from its original position to create a desired attenuation in the optical path. The application of the piezoelectric material needs to be well controlled, specifically for the thickness and overall length, in order to obtain appropriate control voltages with respect to acceptable deformations.

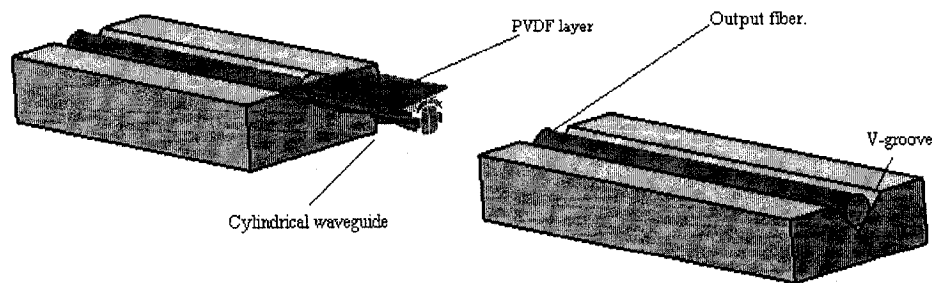


Figure 5.1: Schematic diagram of cylindrical waveguide with PVDF layer.

When the two fibers are used for measurement, they need to be initially spaced apart. The existing initial gap creates an initial coupling loss that is not desirable, but unavoidable. The desired deflection of the moving fiber will dictate the initial gap between the two fibers. A compromise shall be set between the initial coupling loss and the desired maximum attenuation loss. The PVDF covered cylindrical waveguide is positioned in a V-groove as shown in Figure 5.1 and over hanged at the end to act as a cantilever. The distance from the free end and the fixed end is another aspect that has to be well controlled for repeatability of the attenuation. Variation of film geometry in length and thickness is also an important design factor for consideration.

5.3 Modeling and simulation of the VOA (Variable optical attenuator)

A 3-D modeling and piezoelectric analysis is performed using FEA tool ANSYS as shown in Figure 5.2. The dimensions of the cylindrical wave guide are considered to be the standard dimensions of optical fibers with buffer jacket as the outer layer. Following are the geometrical parameters used for the model.

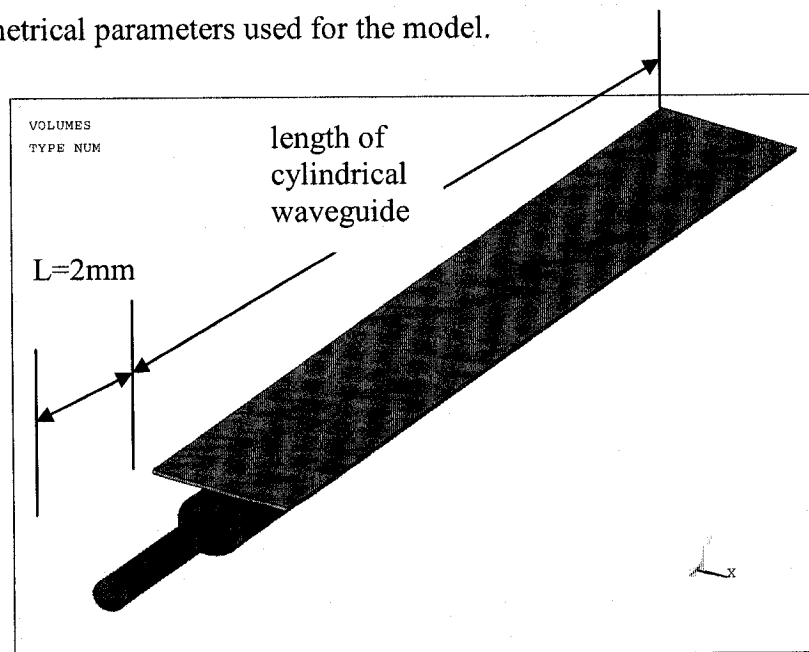


Figure 5.2 3-D Model of Variable Optical Attenuator VOA

- Diameter of the cylindrical waveguide is $250\mu\text{m}$.
- Diameter of the buffer jacket is $500\mu\text{m}$
- Lengths for the cylindrical waveguide considered are 5mm, 7.5mm, and 10mm.

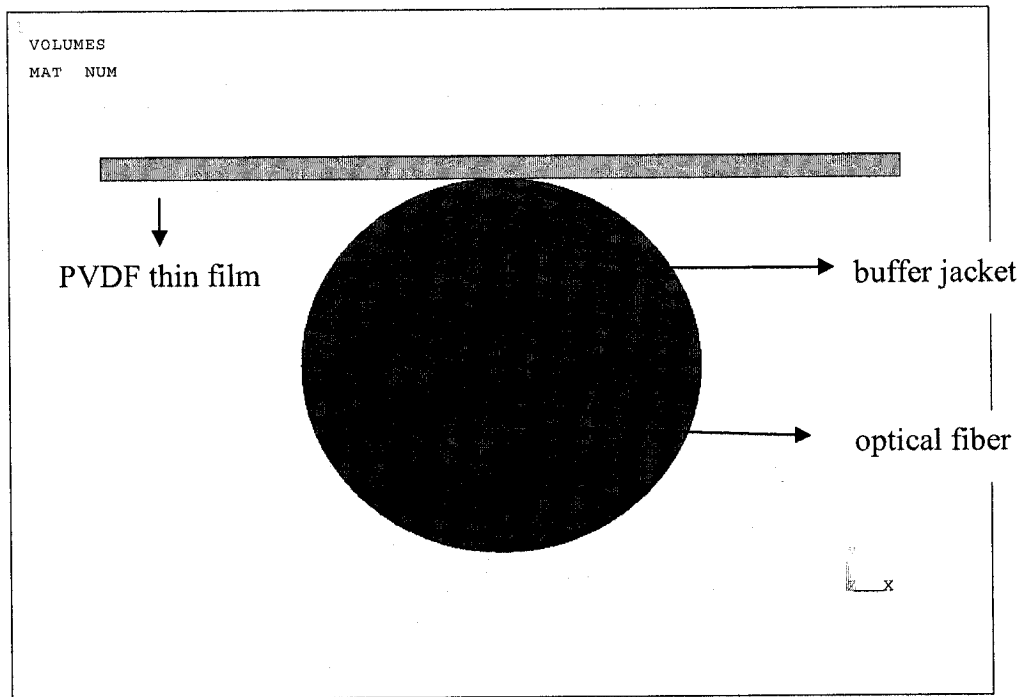


Figure 5.3: Cross sectional view of cylindrical waveguide.

Standard geometrical and material properties of PVDF are considered. The thickness of the commercial PVDF film considered is $28\mu\text{m}$ [56]. Cross sectional view (not to be scaled) of geometry of cylindrical waveguide with PVDF thin film adhered is shown in Figure 5.3. Linear structural analysis is carried out using elements SOLID 98 (coupled field element) for PVDF layer and SOLID 45 for optical fiber. The degrees of freedom for SOLID 98 are u_x , u_y , u_z and voltage and for SOLID 45 are u_x , u_y , and u_z . In the modeling, cylindrical waveguide is placed in a V-groove is equivalently considered as a cantilever and hence the boundary conditions for the model are assumed of a cantilever.

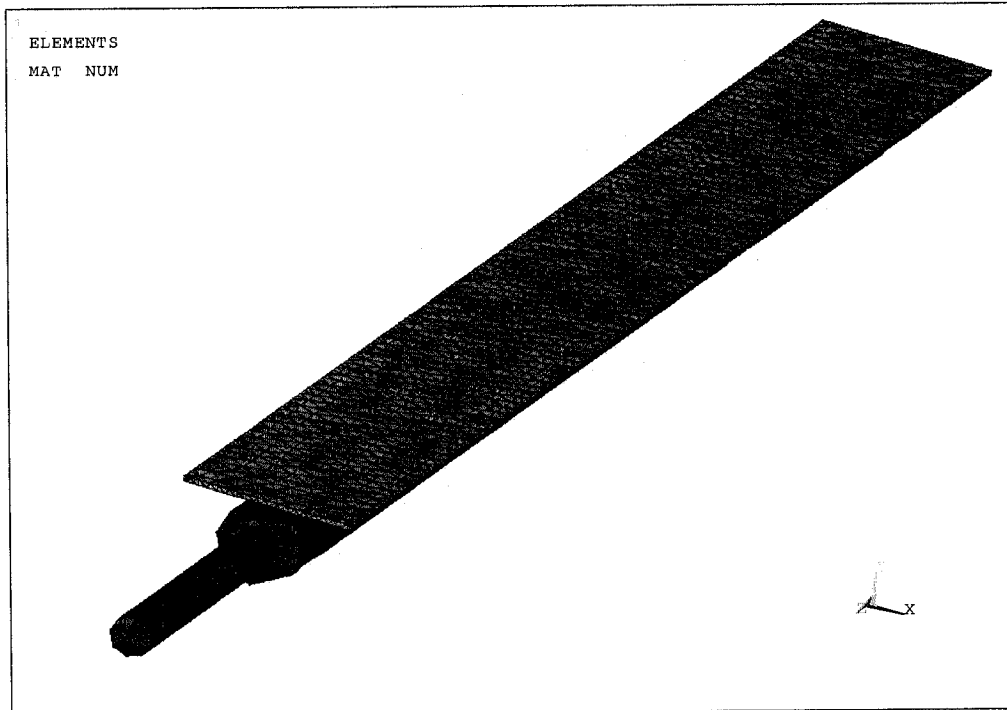


Figure 5.4: Finite element model of cylindrical waveguide.

Structural analysis was performed by varying the length of the cylindrical waveguide. The tip deflection in Figure 5.4 of the optical micro system is calculated by static analysis and the desired deflections are obtained by varying the applied voltages on the PVDF thin film layer. The distribution of the induced deflection through out the cylindrical waveguide is shown in Figure 5.5 and 5.6. For larger lengths of 7.5mm and 10mm of cylindrical waveguide the deflections observed are higher.

5.4 Piezoelectric actuation using commercial PVDF thin film

While designing the model of the cylindrical wave guide using commercial PVDF thin film the piezoelectric constant (d_{31}) of the commercial PVDF thin film is taken from the estimated experimental values obtained in Chapter 4. In this case the d_{31} value is considered to be equivalent to the value obtained at excitation frequency of 20 Hz. Hence the piezoelectric constant d_{31} is equal to 22.4 pC/N. Figures 5.5 -5.7 represents deflection of the cylindrical waveguide for three different geometrical lengths 5mm, 7.5mm and 10 mm at different applied voltages.

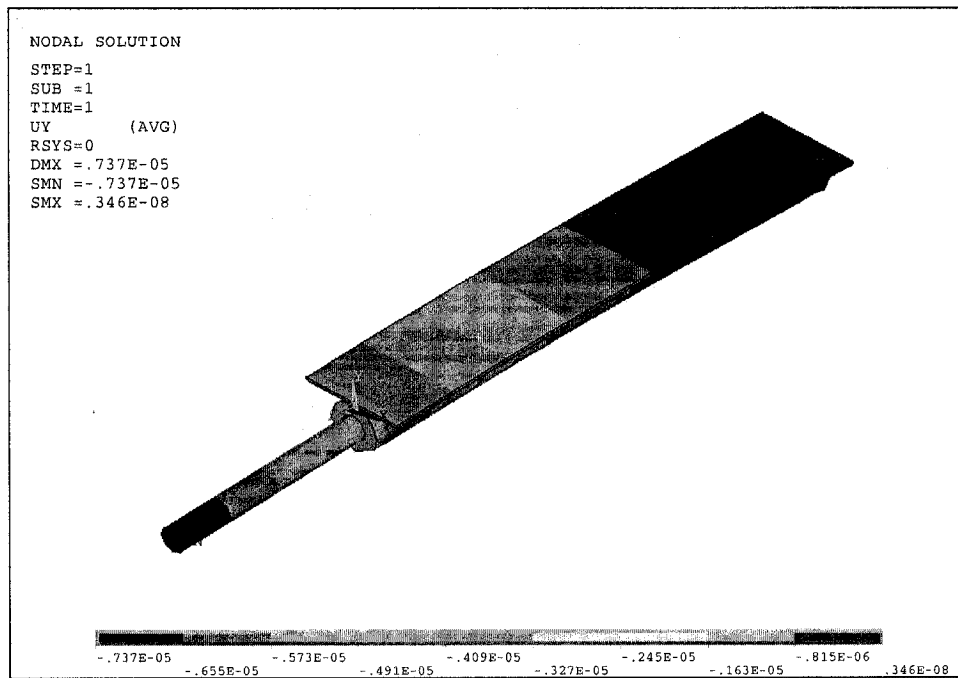


Figure 5.5 Distribution of the static deflection of the optical fiber (length 5mm) at 100V

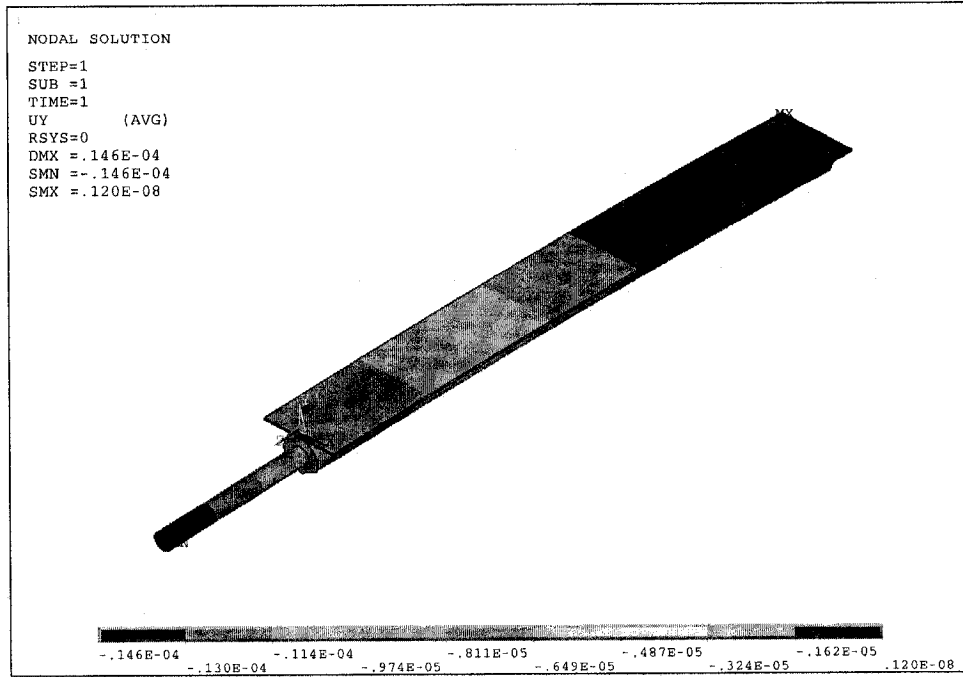


Figure 5.6 Distribution of the static deflection of the optical fiber (length 7.5mm) at 100V

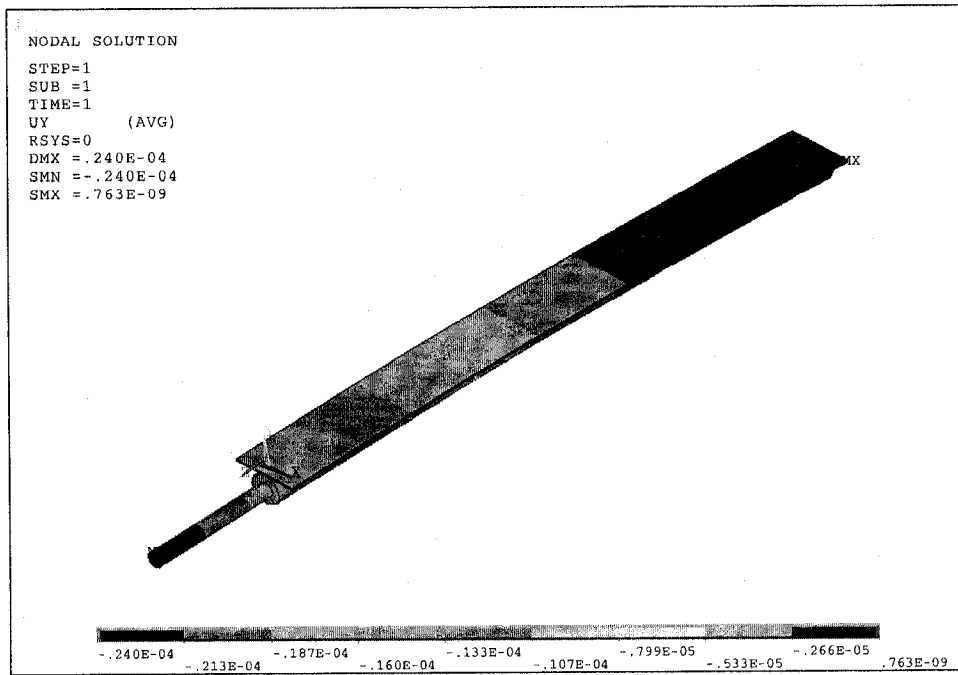


Figure 5.7 Distribution of the static deflection of the optical fiber (length 10mm) at 100V

It is observed that relatively higher deflections are obtained for optical fiber length of 10mm at higher applied voltages. Hence in the proposed model piezoelectric actuation is achieved through which optical attenuation can be achieved by the virtue of the deflection of the waveguide.

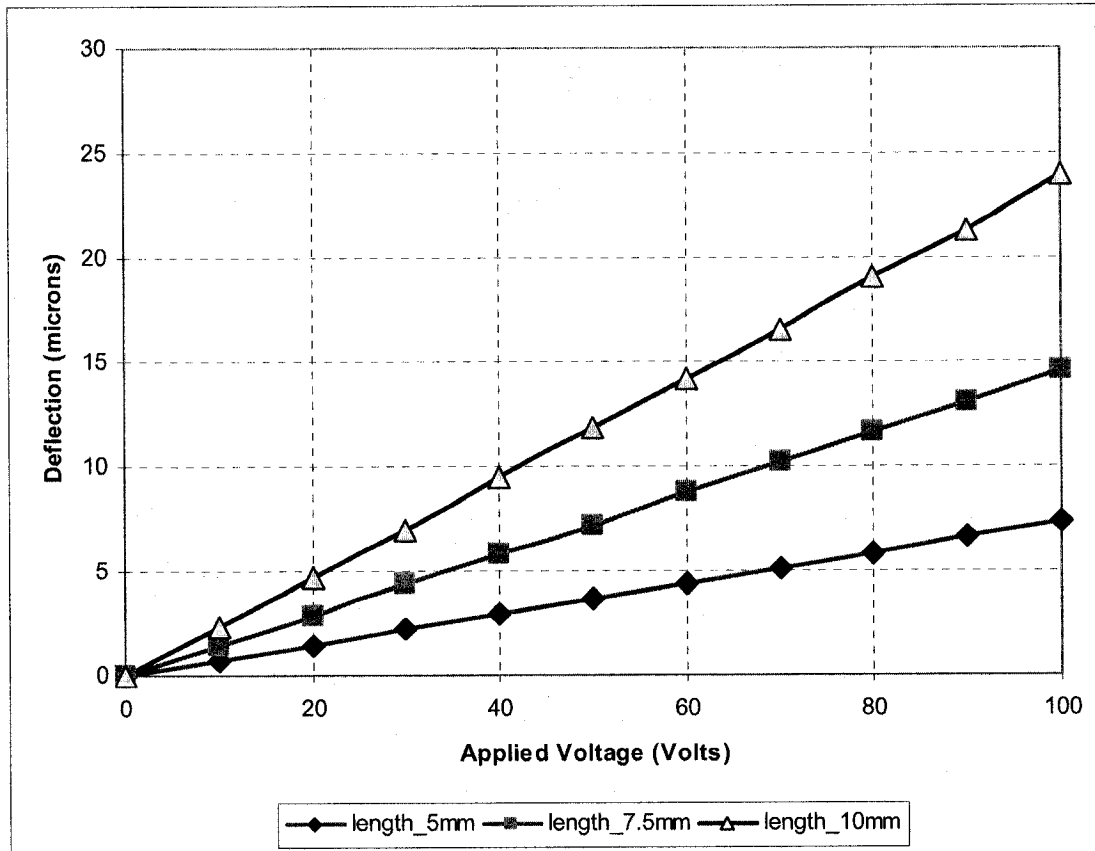


Figure 5.8: Deflection of optical attenuator using commercial PVDF thin film for different lengths at different applied voltages

5.5 Piezoelectric actuation using PVDF copolymer thin film

The modeling and simulation is further extended by the application of PVDF copolymer thin films. The piezoelectric constant (d_{31}) of the PVDF copolymer thin film is taken from the experimental values obtained in Chapter 4. In this case the d_{31} value is considered to be equivalent to the value obtained at an excitation frequency of 20 Hz.

which is equal to 30.6 pC/N. Figures 5.6- 5.11 represents the deflection of the cylindrical waveguide for three different geometrical lengths 5mm, 7.5mm and 10 mm at different applied voltages. It is observed that relatively higher deflections are obtained for optical fiber length of 10mm at higher applied voltages.

In comparison with commercial PVDF thin film, the deflection achieved through copolymer thin film is relatively much higher and therefore it can deliver better optical attenuation characteristics. Figures 5.9, 5.10 and 5.11 represents deflection of optical fiber for lengths of 5mm, 7.5 mm and 10mm respectively at different applied voltages.

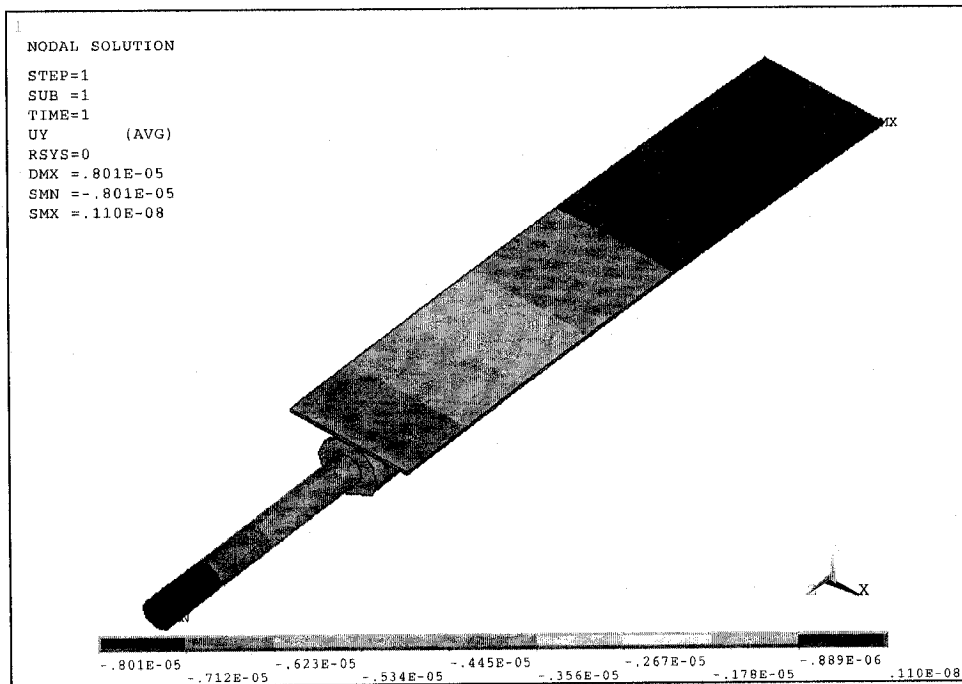


Figure 5.9 Distribution of the static deflection of the Optical Fiber (length 5mm) at 100V

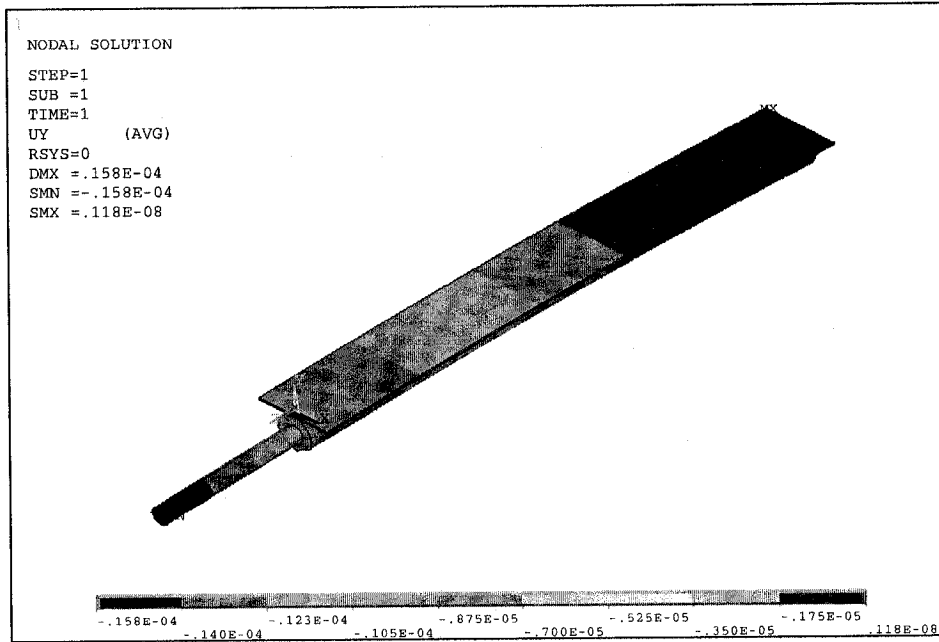


Figure 5.10: Distribution of the static deflection of the optical fiber (length 7.5mm) at 100V

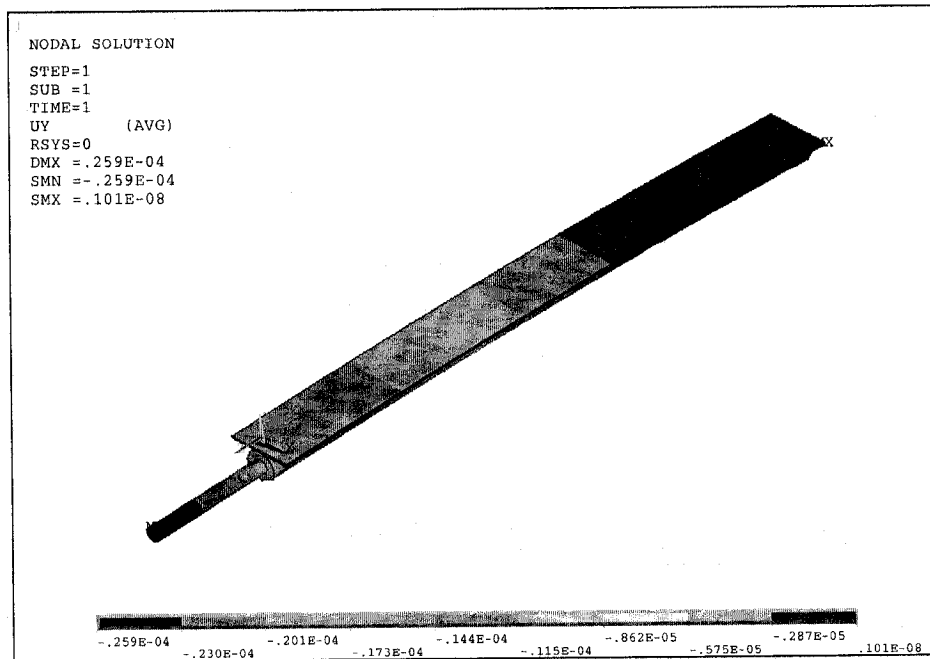


Figure 5.11: Distribution of the static deflection of the Optical Fiber (length 10 mm) at 100V

Deflection of the cylindrical waveguide using PVDF copolymer thin films for three different geometrical lengths 5mm, 7.5mm and 10 mm at different applied voltages is shown in Figure 5.12

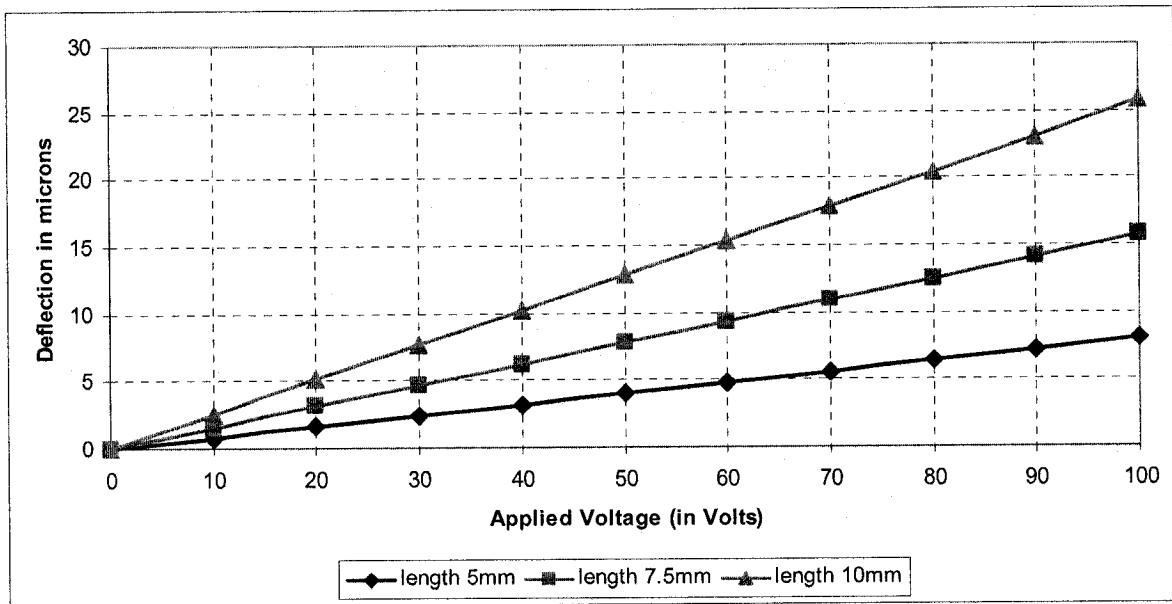


Figure 5.12: Deflection of optical attenuator using PVDF copolymer thin film for different lengths at different applied voltages

At higher lengths of optical fibers a relatively larger deflections of optical fiber is achieved and moreover it is observed that the piezoelectric actuation is higher using PVDF copolymer thin films than using PVDF commercial thin films.

5.6 Application of piezoelectric actuator as an optical attenuator using commercial PVDF thin films and PVDF copolymer thin films.

Piezoelectric actuation is a promising type of actuation because of its quick response time and its low range displacement which is required in the micro system. Several piezoelectric actuators were proposed for optical applications [2]. A possible optical attenuation is proposed by deflecting the cylindrical waveguide through the actuation of

piezoelectric material, which is adhered to the cylindrical waveguide. In the presented model a variable optical attenuation is obtained by varying the applied voltages on the PVDF film, there by achieving desired deflections for the cylindrical waveguide. The input optical fiber is positioned in a V-groove and is actuated to a desired deflection in order to attenuate the transmitted signal. V-groove dimensions are considered such that the cylindrical waveguide is positioned accurately. The coupling efficiency due to lateral, angular mismatch and separation between the fibers has been evaluated using the Equations for Gaussian distribution as shown below [9-10]:

$$\eta_{lateral} = e^{-U^2} \quad (6.1)$$

$$\eta_{angular} = e^{-T^2} \quad (6.2)$$

$$\eta_{separation} = e^{-M^2} \quad (6.3)$$

Where $U = \frac{\delta}{w_o}$, δ is the lateral displacement, w_o is the mode field radius equal to

$5\mu\text{m}$ and $T = \frac{\sin \theta}{\lambda / n_o \pi w_o}$, θ is the angular misalignment between the fibers, which is the

slope of the cantilever at the tip, λ is the wavelength of the free space equal to $1.55\mu\text{m}$, n_o is the refractive index of the medium equal to 1 for air, $M^2 = \log_e(Z^2 + 1)$ [57], where

$Z = \frac{z\lambda}{2\pi n_o w_o^2}$, z is the separation distance between the fibers. The net coupling efficiency

for the optical microsystem can be calculated by Equation 6.4.

$$\eta_{net} = e^{-(U^2+T^2+M^2)} \quad (6.4)$$

In the evaluation of insertion loss of the optical fibers, the total coupling losses considered for the optical fibers are loss due to lateral displacement, loss due to angular misalignment and loss due to separation between the optical fibers. A distance of 30 microns between the optical fibers is considered in the evaluation of the optical coupling efficiency and insertion loss. The total insertion losses in dB of the optical microsystem can be calculated using the formula given below.

$$L = -10 \log_{10}(\eta_{net}), dB \quad (6.5)$$

The obtained loss due to separation between the fibers is very less compared to the loss due to lateral displacement. This novel concept proposed in this work facilitates the attenuation of the optical signal by giving small displacements to the optical fiber without any additional component such as blades [57], shutters [58] and reflectors [59].

The optical attenuation characteristics for the cylindrical waveguide using commercial PVDF thin films and microfabricated PVDF copolymer thin films are evaluated. The Figures 5.13, 5.14 represents the variation of coupling efficiency and insertion loss with respect to variation of applied voltage for optical attenuation achieved using commercial PVDF thin films and the Figures 5.15, 5.16 represent the variation of coupling efficiency and insertion loss with respect to variation of applied voltages for optical attenuation achieved using PVDF copolymer thin films.

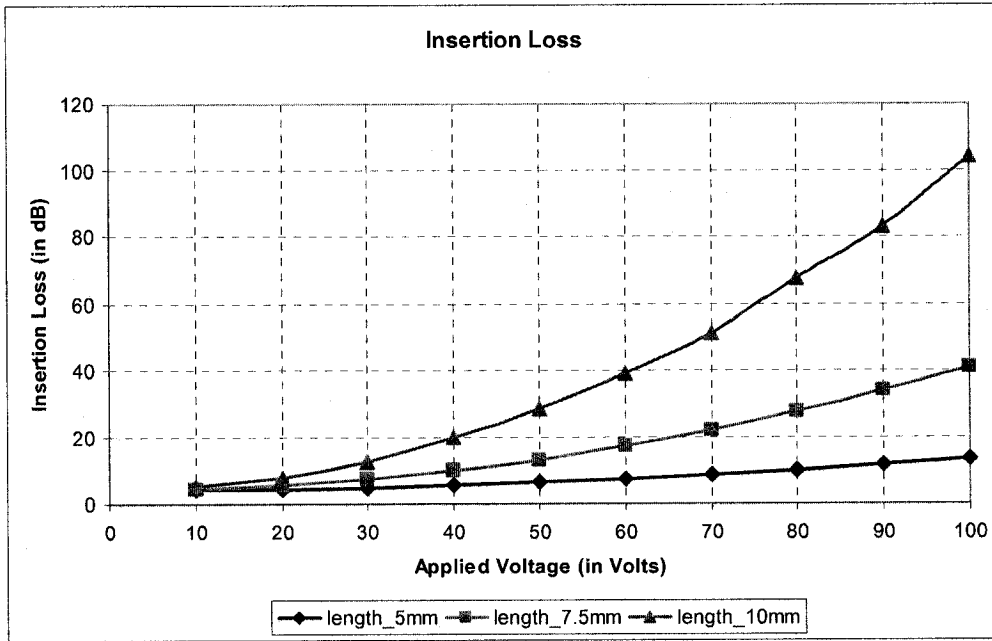


Figure 5.13.: Insertion loss of optical attenuator using commercial PVDF thin film for different lengths at different applied voltages.

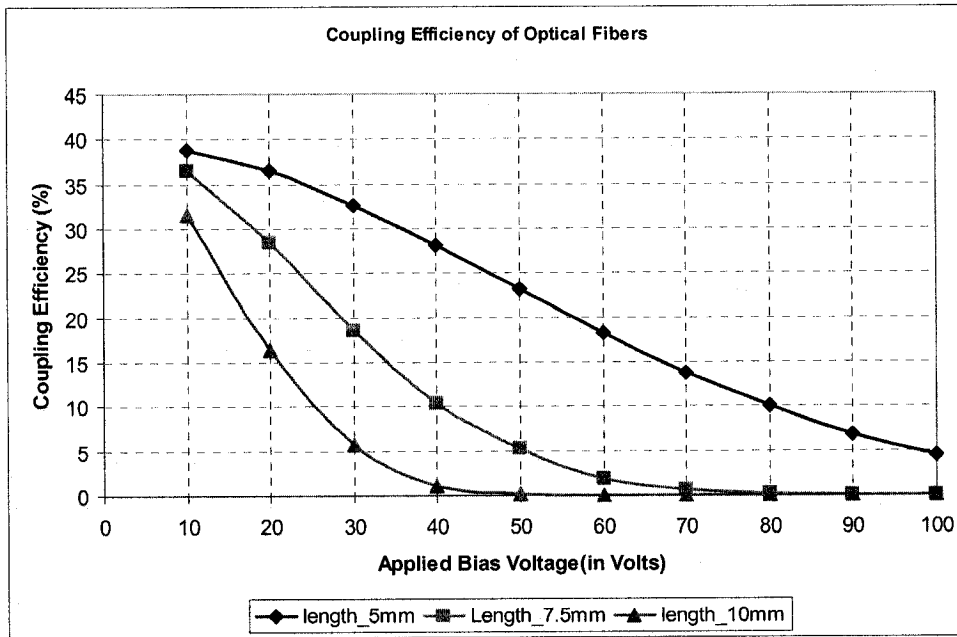


Figure 5.14: Coupling efficiency of optical attenuator using commercial PVDF thin film for different lengths at different applied voltages.

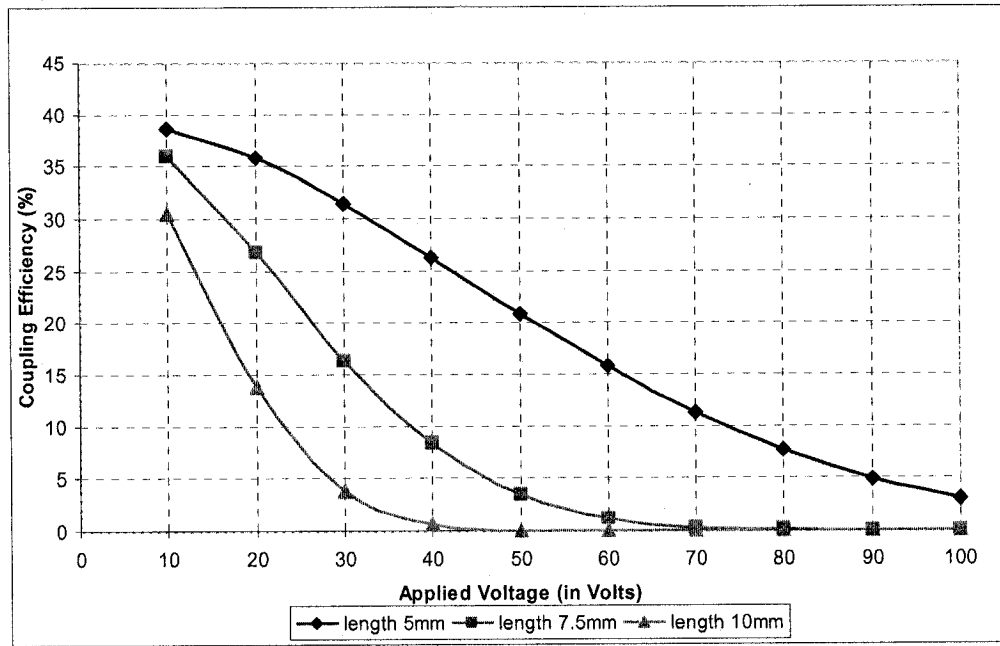


Figure 5.15: Coupling efficiency of optical attenuator using PVDF copolymer thin film for different lengths at different applied voltages

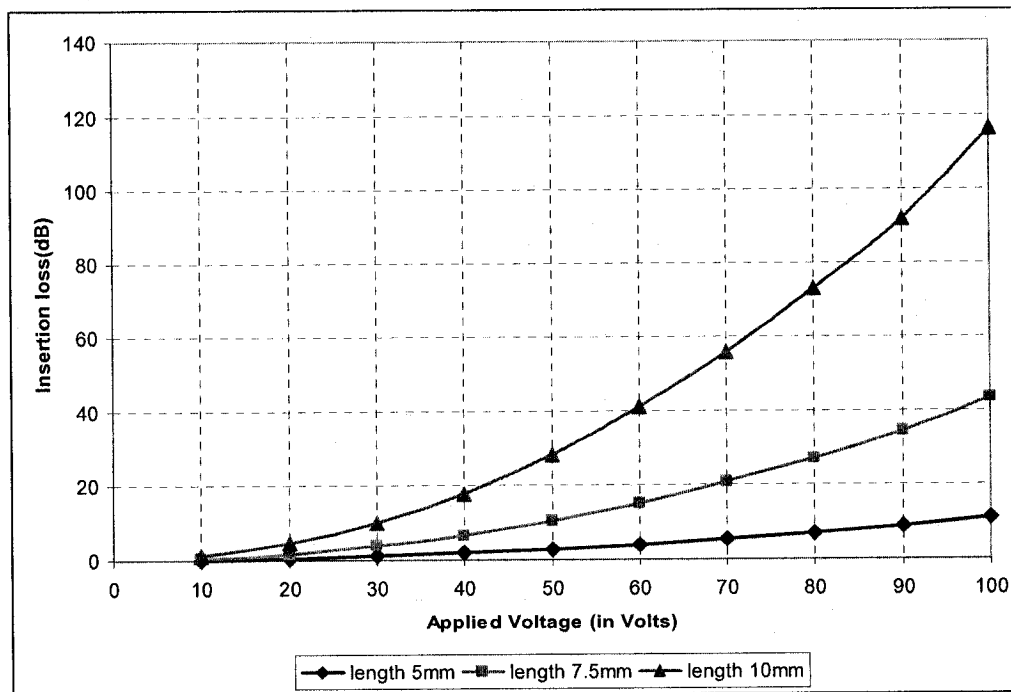


Figure 5.16: Insertion loss of optical attenuator using PVDF copolymer thin film for different lengths at different applied voltages

5.7 Modeling and simulation of the VOA (Variable Optical Attenuator) using PVDF thin film deposition.

In the present work another aspect of designing VOA using PVDF thin films is presented in this approach instead of using readily available commercial PVDF thin films, PVDF thin film deposition onto the cylindrical waveguide is presented. The deflection of the optical fiber using this methodology is presented and later on the optical attenuation characteristics are evaluated.

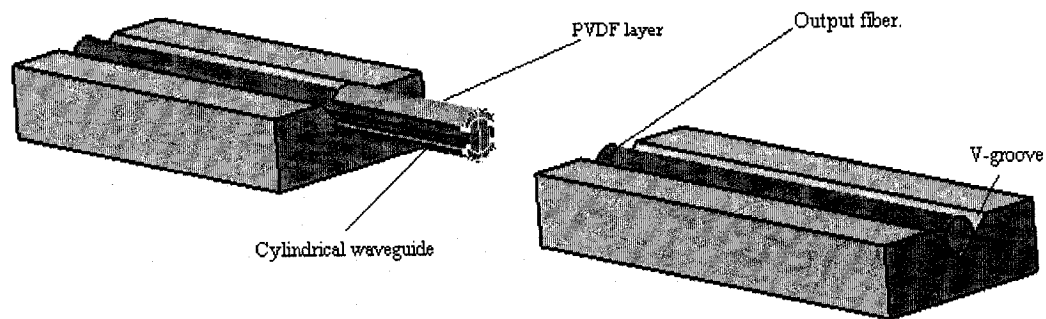


Figure 5.17: Schematic diagram of cylindrical waveguide with PVDF thin film deposition layer.

A 3-D modeling and piezoelectric analysis is performed using FEA tool ANSYS. The dimensions of the cylindrical wave guide are considered to be the standard dimensions of optical fibers. Following are the geometrical parameters used for the model.

- Diameter of the cylindrical waveguide is $125\mu\text{m}$.
- Lengths for the cylindrical waveguide considered are 10mm, 15mm, and 20mm.

Standard geometrical and material properties of PVDF are considered. Thickness of the PVDF film considered is $28\mu\text{m}$.

The coverage angle made by the piezoelectric film considered is 135° .

Cross sectional view (not to be scaled) of cylindrical waveguide with PVDF deposited film is shown in Figure 5.18. Two design aspects of the cylindrical waveguide are considered while modeling.

- Model-1: A quarter model (Figure 5.19) is considered for larger lengths of 15mm and 20mm.
- Model-2: Full model with one PVDF layer deposited (shown in Figure 5.20) length of 10mm.

As the optical micro system is symmetrical in geometry and due to memory constraints in the FEA software a quarter model shown in Figure 5.18 is considered for analysis of the cylindrical waveguide. Therefore, the results obtained from the quarter model represent the entire cylindrical waveguide model. Linear structural analysis is carried out using elements SOLID 98 (coupled field element) for PVDF layer and SOLID 45 for optical fiber. The degrees of freedom for SOLID 98 are u_x , u_y , u_z and voltage and for SOLID 45 are u_x , u_y , and u_z . In the modeling, cylindrical waveguide is placed in a V-groove is equivalently considered as a cantilever and hence the boundary conditions for the model are that of a cantilever. To validate the complete model symmetric boundary conditions are given to the quarter model.

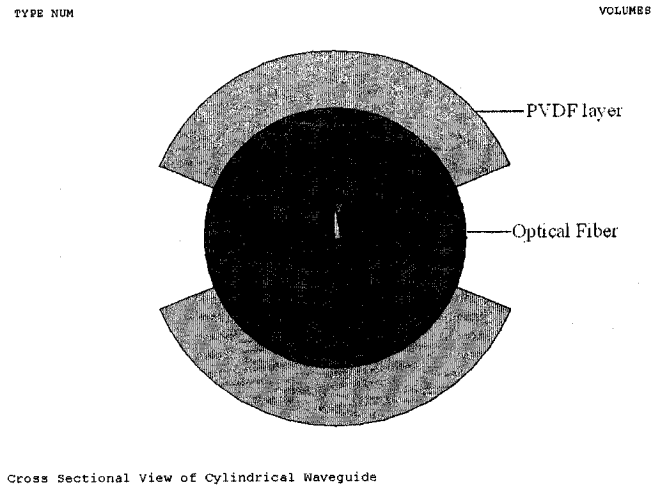


Figure 5.18: Cross sectional view of cylindrical waveguide

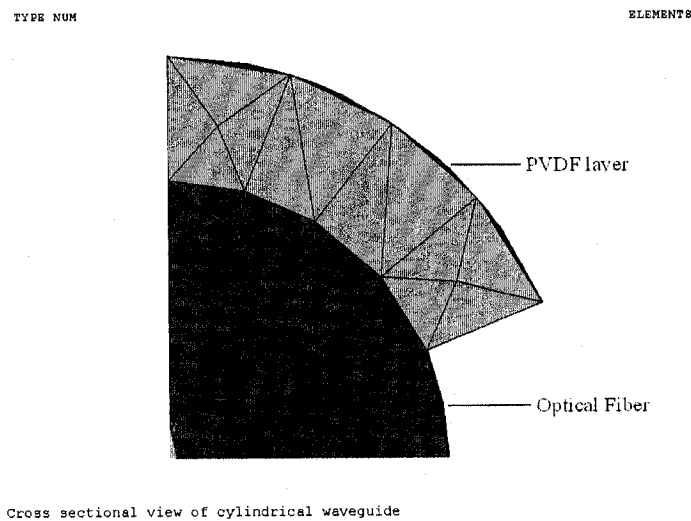


Figure 5.19: Cross section of the quarter model of cylindrical waveguide (model-1)

Structural analysis was performed by varying the length of the cylindrical waveguide. The tip deflection in Figure 5.20 of the optical micro system is calculated by static analysis and the desired deflections are obtained by varying the applied voltages on the PVDF layer.

For length of 10mm, the deformed results shown in the Figure 5.20 are only for one PVDF layer and hence the net deflection for the optical micro system with two deposited layers (top and bottom) would be twice the deflection (Y) obtained. The distribution of the induced

deflection throughout the cylindrical waveguide is shown in Figure 5.21. For larger lengths of 15mm and 20mm the deflections observed are higher than that of length 10mm.

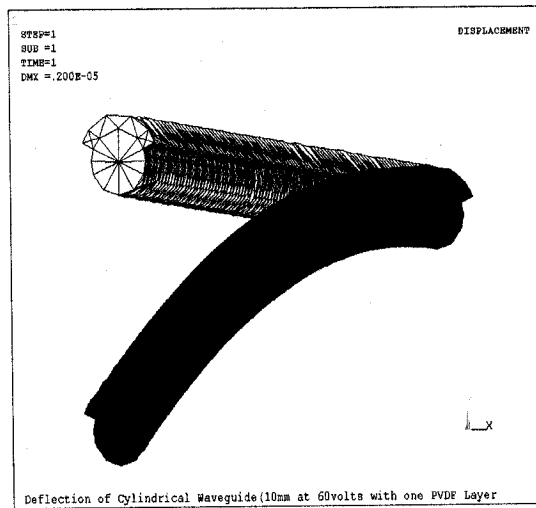


Figure 5.20: Deformation of the cylindrical waveguide (model-2)

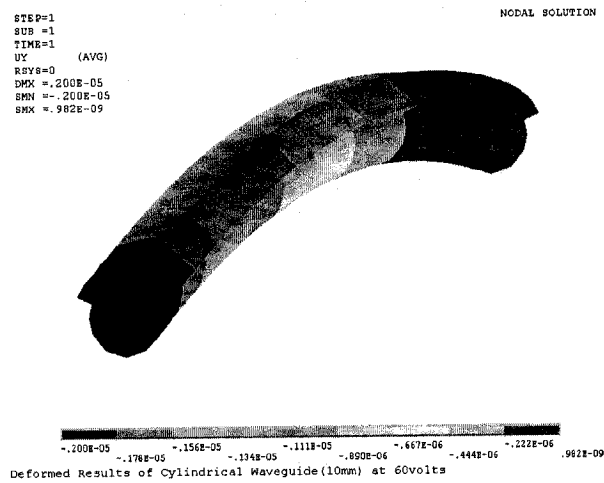


Figure 5.21: Deformation results of the cylindrical waveguide-model-2

5.8. Results and discussions

The geometrical length of PVDF film deposited on top and bottom of optical fiber is varied and the variation of deflection is observed for three different lengths and voltages as shown in Figure 5.22. The variation of the coupling efficiencies and the insertion losses for various voltages are shown in Figures 5.23 and 5.24, respectively. For a fixed length, the deflection observed is varying linearly with the voltage due to the linear relationship between the piezoelectric force and the voltage. For a fixed voltage, the coupling efficiency is lower and the insertion loss is higher for the longer cylindrical waveguide. Depending upon the optical microsystem requirements cylindrical waveguides of different length can be selected. Attenuation in the range of 30 dB is achievable for low voltages of approximately 50 Volts.

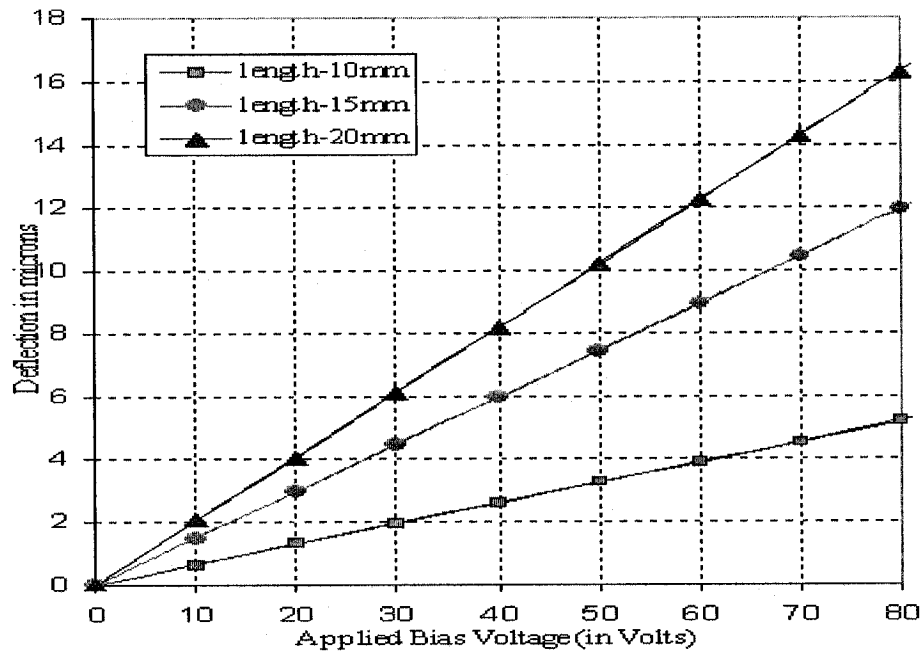


Figure 5.22: Variation of deflection for different voltages

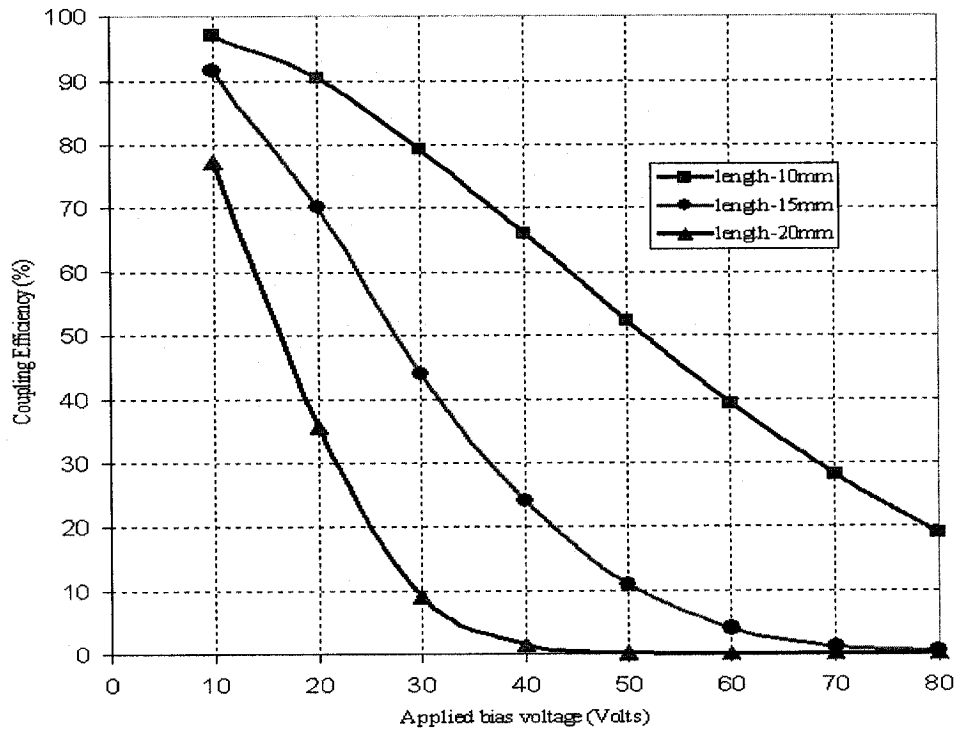


Figure 5.23: Variation of coupling efficiencies for different voltages.

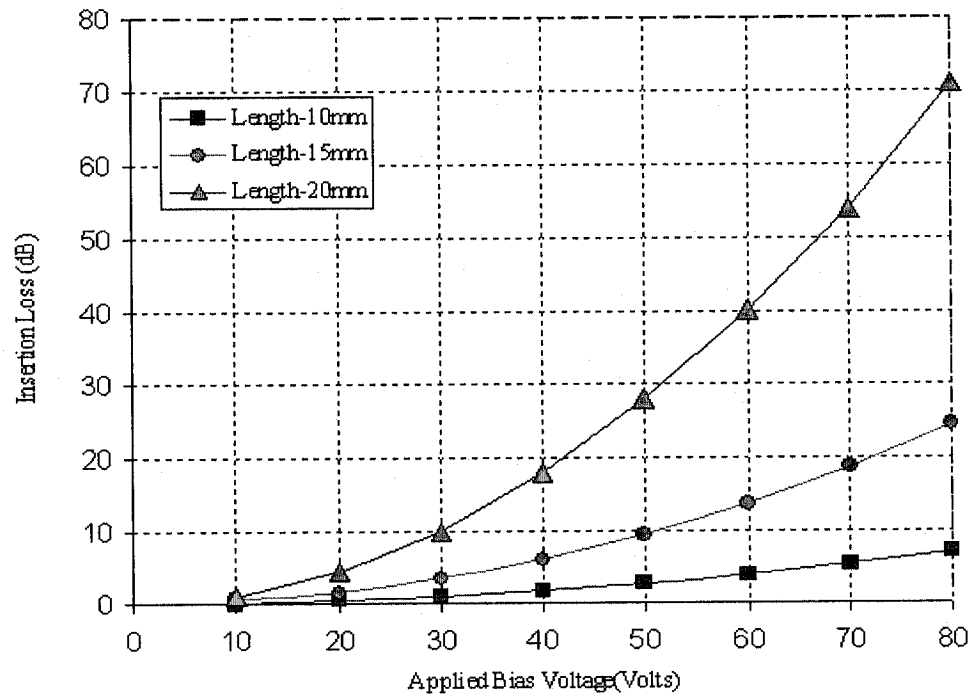


Figure 5.24: Insertion loss of optical fibers for different Voltages.

5.9 Summary

The work carried out in this chapter presented a simple and novel application of PVDF thin films for optical attenuation. Simulation of attenuating the optical signal is presented by using piezoelectric actuation mechanism. Variable optical attenuation can be achieved using piezoelectric actuation by varying the voltage along the PVDF thin film deposited/adhered on the optical fiber. An attenuation of 30 dB can be achieved at low voltages for larger lengths of cylindrical waveguide. The present work demonstrates a new way of attenuation through PVDF actuated cylindrical waveguides. This work also emphasizes the application and advantages of using PVDF copolymer thin films which are promising to be more capable of achieving relatively higher attenuation than commercial PVDF thin films. For length of 7.5 mm and 10mm a considerable attenuation of around 30dB to 50 dB can be obtained at low voltages. In comparison with commercial PVDF thin films, attenuation achieved through the usage of PVDF copolymer thin films is more significant and hence a better output optical attenuation characteristics is predicted.

In the second approach of using PVDF thin film deposition. Variable optical attenuation can be achieved using piezoelectric actuation, by varying the voltage along the PVDF layer deposited on the optical fiber. A significant attenuation of 30 dB can be achieved at low voltages for larger lengths of cylindrical waveguide. The present work demonstrates a new way of attenuation through PVDF actuated cylindrical waveguides.

Chapter 6

Conclusions and future work

6.1 Conclusions

An introduction to the piezoelectric materials and a brief discussion on thin film technology in PVDF MEMS was carried out. The work also discusses about the advantages of PVDF copolymer thin films over PVDF homopolymer films. A brief literature review on the commercially available optical attenuators is also presented. A short description of the experimental setup on the measurement of piezoelectric constant (d_{31}) is also presented.

In the present work the literature review on various available deposition techniques in thin film technology is presented. The microfabrication of PVDF thin films using “*spin coating*” method is adopted. The basic stages involved in the spin coating process and basic mathematical model of spin coating method are also discussed. Further, microfabrication of PVDF copolymer thin films using spin-coating and spinning characterizations of microfabricated PVDF copolymer thin films for various spin parameters. The optimum spin parameters for consistent and uniformly coated PVDF copolymer thin films are figured out; A brief description of the stepwise poling method adopted for the obtained PVDF copolymer thin films is included.

Further, the work also emphasizes Infrared spectroscopic studies on PVDF copolymer thin films. FTIR characterization of the spin coated PVDF copolymer thin films is carried

out and the spectra obtained at different annealing temperatures are analyzed. The specimens subjected to subsequent annealing are also analyzed and the spectra of the poled spin coated specimens are compared to that of commercially available PVDF thin films. The significant polarized phase of the spin coated PVDF copolymer thin films is predicted at a particular wavenumber. It is noted that the spin coated specimens show better piezoelectric properties than commercial PVDF thin film.

The work extends to evaluate the mechanical properties of the spin coated PVDF copolymer thin films. A simple experimental set up is presented to estimate the piezoelectric constant (d_{31}) of the spin coated PVDF thin film. To benchmark the output characteristics of the spin coated PVDF copolymer thin films, a comparative study is carried out by evaluating and estimating the piezoelectric (d_{31}) constant with respect to the available commercial PVDF thin films. The piezoelectric constants of the spin coated PVDF copolymer thin film and commercial PVDF thin films are estimated by measuring the charge output across the thickness of the PVDF thin film for a specific geometry of PVDF thin film. Later, the piezoelectric constant (d_{31}) is evaluated for the considered geometry of the PVDF thin films. PVDF thin films are excited along the length of the film and charge output is measured across the thickness of the PVDF thin film. Films are excited at frequencies of 10Hz, 15 Hz and 20Hz for various amplitudes of signals.

It is observed that the output characteristics of the PVDF copolymer thin films exhibit as better than the available commercial PVDF thin films. At higher excitation frequencies of 15Hz and 20Hz the spin coated PVDF copolymer thin films exhibit a relatively higher

charge output and hence the piezoelectric constant for the considered geometry of PVDF copolymer thin film found to be slightly higher than that of commercial PVDF thin films.

Also in the present work a simple and novel application of PVDF copolymer thin films is proposed for optical microsystems. A novel and a feasible design of VOA is proposed. Piezoelectric actuation of the optical fibers between the input and output fibers deviates the input signal and hence causes an attenuation of the input signal. The optical fiber is adhered/deposited with a PVDF thin film. When a voltage is applied across the PVDF thin film, it creates a movement, deflecting the input optical fiber and thereby achieving optical attenuation. Variable optical attenuation is achieved by varying the applied voltage across the PVDF thin film.

The presented simulation of the optical attenuator proposes the application of PVDF thin films by adhering onto the optical fiber. However direct PVDF thin film deposition onto the optical fiber can be much more promising in attaining a better optical attenuation characteristics as it involves a proper contact between the piezoelectric material and the device thereby a higher piezoelectric force can be transferred. The presented simulation is performed in ANSYS and it initiates a new conceptual design of applying PVDF thin films for optical microsystems.

The conclusions that can be inferred from the work done in this thesis are presented as follows:

- 1) The main aspect of this work is to propose a unique approach for optical microsystems and to eventually realize a VOA using PVDF copolymer thin films. To obtain a better output, a better piezoelectric material is required. The presented PVDF copolymer thin films exhibit better piezoelectric properties.
- 2) Among different available deposition techniques, “Spin coating” technique for deposition of PVDF copolymer thin films is proposed. Further, spinning characterization of the PVDF copolymer thin films is carried out for various spinning conditions. The variation in thickness of films is achieved by varying the concentration of the solute (PVDF) in the solution. Eventually an ideal set of spin coating parameters such as spin speed and spin time are figured out for a particular concentration of solution.
- 3) In this work step-wise poling method is adopted to polarize the PVDF thin films. Significantly, high voltages are applied across the thickness of the PVDF thin film to polarize the thin film. Polarization of the spin coated PVDF thin films is achieved through this method .
- 4) To monitor the polarization phase in PVDF copolymer thin films, Fourier Transform Infrared spectroscopy study is chosen to evaluate both absorbance and transmittance characteristics of the spin coated PVDF thin films. Further an in-depth analysis for finding the exact annealing temperature and number of cycles of annealing for spin coated PVDF thin films is carried out. The variation in absorbance and transmittance spectra for the samples annealed at different temperatures is studied. Also the number

of cycles of annealing is figured out by studying the comparison of the obtained absorbance and transmittance spectra through FTIR. Sample annealed at 140°C shows better piezoelectric properties. Samples annealed for 3 cycles exhibits better piezoelectric properties.

- 5) Further characterization of the “Poled” and “Unpoled “samples are conducted through infrared spectroscopy. Increase in the absorbance peaks for the poled samples are observed indicating that a significant polarized phase is observed and hence polarization of the spin coated thin films is achieved. The effect of number of cycles of poling is studied and it is discovered that there isn’t any significant change of piezoelectric phase in absorbance and transmittance spectra of the PVDF copolymer thin films. In FTIR analysis, to benchmark the piezoelectric phase of the spin coated PVDF copolymer thin films a comparative analysis of transmission spectra and absorbance spectra are done with the commercially available PVDF thin films, the obtained spin coated PVDF thin films. The obtained spin coated PVDF thin films exhibit relatively better piezoelectric properties.
- 6) Characterization of the spin coated PVDF copolymer thin films is extended by estimating the mechanical properties of the PVDF thin films. It is observed that a relatively higher d_{31} value is estimated for the PVDF copolymer thin films at an excitation frequency of 20Hz for the considered geometry of the PVDF thin film.
- 7) A novel approach in designing VOA is realized through the application of PVDF copolymer thin films, in which a significant attenuation is achieved at low voltages.

6.2 Future work

The present work initiates a new view of applying thin film technology into optical microsystems. The present work mainly aims to have a device out of piezoelectric thin films. Infrared spectroscopic analysis can be further investigated for different samples varying in thickness, composition and annealing conditions. The design of the variable optical attenuator can be further enhanced by deposition of PVDF layer onto the optical fiber rather than using PVDF copolymer thin films. A suitable and feasible method of depositing PVDF thin films on to the optical fiber should be realized.

References

- [1] A. Lee et al, "Design and fabrication of a silicon P(VDF-TrFE) piezoelectric sensor", *Thin Solid Films*, Vol.181,1989, pp. 245-250.
- [2] Helene Debeda et al, "Development of miniaturized piezoelectric actuators for optical applications realized using LIGA technology", *IEEE Journal of Microelectromechanical Systems*, Vol.8, No. 3, 1999, pp. 258-263.
- [3] Cady, W.G., "Piezoelectricity", McGraw-Hill, 1946.
- [4] Seymour, R.B et al, "Piezoelectric Polymers", *Products of Chemistry* Vol.67.9, 1990, pp. 763-765.
- [5] Haertling, G.H. "Ferroelectric Ceramics: History and Technology." *Journal of the American Society* Vol.82.4, 1999, pp.797-818.
- [6] Kawai, H, "The Piezoelectricity of Poly(vinylidene Fluoride)", *Japanese Journal of Applied Physics* Vol. 8, 1969, pp. 975-976.
- [7] P. Sajkiewicz et al, "Phase transitions during stretching of poly (vinylidene fluoride)", *European Polym. J*, Vol.35, 1999 pp.423-426.
- [8] Tamura, M. et al, "Piezoelectric Polymer Properties and Potential Applications", *Ultrasonic Symposium Proceedings* 1987, pp. 344-346
- [9] M.G. Broahurst et al, "Piezoelectricity and Pyroelectricity in Poly (vinylidene fluoride)", *Journal of Applied. Physics*, Vol.49 No.10, 1978, pp. 4992-4996
- [10]. A.J. Lovinger, "Annealing of poly (vinylidene fluoride) and formation of a fifth phase", *Macromolecules* Vol.15, 1982, pp. 40.
- [11] E. Giannetti, "Semi-crystalline fluorinated polymers", *Polym. Int*, Vol.50, 2001 pp. 10-14

- [12]. B.-E. El Mohajir et al, "Changes in structural and mechanical behavior of PVDF with processing and thermomechanical treatments", *Polymer Science* Vol.42, 2001 pp.5661-5668
- [13]. P. Sajkiewicz et al, "Phase transitions during stretching of poly (vinylidene fluoride)", *European Polym. Journal*, Vol. 35, 1999 pp. 423-426
- [14]. R. Gregorio Jr et al, "Effect of crystalline phase, orientation and temperature on the dielectric properties of poly (vinylidene fluoride)", *Journal of Material. Science* Vol.34 1999, pp.4489-4493.
- [15]. E. Yamaka, "Pyroelectric Devices in the Application of Ferroelectric Polymers", Chapman and Hall, 1988.
- [16]. I. Seo and D. Zou, "Electromechanical Applications in Ferroelectric Polymers: Chemistry, Physics and Applications, Ed. H. S. Nalwa, Marcel Dekker, Inc, 1995, pp. 699-734.
- [17] Fukada.E, "New Piezoelectric Polymers", *Japanese Journal of Applied Physics* Vol.37, 1998, pp. 2775-2780.
- [18] Broadhurst, M,"Polymer Physics." *Physics Today*, 1994, pp.51-52.
- [19] Weiping Li et al, "Structural Changes of 80/20 Poly(vinylidene fluoride-trifluoroethylene) Copolymer Induced by Electron Irradiation", *Journal of Applied Polymer Science*, Vol. 91, 2004, pp. 2903–2907
- [20] Xu, H. S et al, *Macromolecules*, Vol.33, 2000, pp. 4125
- [21] Tahiro et al, *H Macromolecules* Vol.14, 1981, pp.1757.
- [22] Lovinger et al, *Journal of Polymer Science*, Vol. 28, 1987, pp. 619-625
- [23] Hector. A et al, *K. Polym Degrad Stab*, Vol.61, 1998, pp.265.

- [24] MI Akcan et al "Pyroelectric and dielectric properties of spin coated thin films of vinylidene fluoride-trifluoroethylene copolymers", Society of chemical industry, Polym Int Vol.0959-8103, 2001.
- [25] Gregario R Jr, F Master Sci, 31 1996, pp.2925-2930
- [26] Victor Sencadas et al,"Poling of β -poly (vinylidene fluoride): dielectric and IR spectroscopy studies", e-Polymers No. 002, 2005.
- [27] B. Hilczer, "The Method of Matching Resonance Frequencies in Coupled Transmitter PVDF/TRFE Diaphragms", IEEE Transactions on Dielectrics and Electrical Insulation, Vol. 7, No.4, 2000, pp.498-502.
- [28] Philips et al, "The Design, Processing, Evaluation and Characterization of Pyroelectric PVDF Copolymer/Silicon Mosfet Detector Arrays", Applications of Ferroelectrics, Proceedings of the Ninth IEEE International Symposium on, 1991, pp.725-728.
- [29] G. Kovacs, "Micromachined Transducers Sourcebook", McGraw-Hill, 1998.
- [30] M. Madou, "Fundamentals of Microfabrication", CRC Press, 1997.
- [31] A F Armitage, et al,"Infrared sensing using pyroelectric polymers", Napier University Publications", Napier University, Electrical & Electronic Engineering Dept, 1998
- [32] Bernd Bloss et al,"Poling of Polymer films with Ferroelectric Electrodes", Institut fur angewandte Physik, Universitat Karlsruhe, 1996.
- [33] S. N. Fedosov, et al,"Corona Poling of Ferroelectric and Nonlinear Optical Polymers", Moldavian Journal of the Physical Sciences, N2, 2002

- [34] Jose A. Giacometti, "Corona Charging of Polymers: Recent Advances on Constant Current Charging", *Brazilian Journal of Physics*, Vol. 29, No. 2, 1999, pp.269-279
- [35] Doris Schilling et al,"Electron-Beam Poling of very thin PVDF and PVDF-TrFE copolymer films", *Electrets*, (ISE 6) Proceedings 6th International Symposium, 1988, pp.80-86.
- [36] Dadi Setiadi et al," Poling of VDF/TrFE Copolymers Using a Step-Wise Method", *IEEE, Electrets*, 1996. (ISE 9), 9th International Symposium, 1996, pp.831-835.
- [37] D.Setiadi et al,"A 3×1 integrated pyroelectric sensor based on VDF/TrFE copolymer" *Sensors and Actuators*, Vol.52, 1996, pp. 103-109.
- [38] D.Setiadi et al,"Realization of an integrated VDF/TrFE copolymer-on-silicon pyroelectric sensor", *Journal of Microelectronic Engineering*, Vol.29, 1995, pp.85-88.
- [39] D.Setiadi and P.P.L Regtlen,"Application of VDF/TrFE copolymer for pyroelectric image sensors" *Sensors and Actuators A*, Vol. 41-42, 1994, pp.585-592.
- [40] M.Gallagher et al,"The Role of Micro engineering in Pedabarography", Department of Applied Physics and Electronics and Mechanical Engineering, University of Dundee.
- [41] Su-Hong Park, et al "The Dielectric Properties of Functional PVDF thin films by Physical Vapor Deposition Method" 1997, pp. 2651-2654
- [42] Akiyoshi "Preparation and piezoelectricity of beta form poly (vinylidene fluoride) thin film by vapor deposition", *Thin Films*, 1991, pp.189-191.
- [43] Jiro Sakata et al "Crystal forms and their orientation in poly (vinylidene fluoride) films prepared by an ionized vapor deposition method", *Thin Solid Films*, Vol. 188, No. 1, 1990, pp. 123-132.

- [44] Sergei Fedosov et al, "Electret properties of polymer films deposited by vacuum evaporation" Electrets, (ISE 7) Proceedings, 7th International Symposium, 1991, pp.272-274.
- [45] M.Grant Norton, et al "Pulsed laser ablation and deposition of fluorocarbon polymers", Applied surface science, 1995, pp.617-620.
- [46] K.L. Choy et al, "Preparation of oriented Poly (vinylidene fluoride) thin films by a cost-effective electrostatic spray-assisted vapor deposition-based method", Thin solid films, 1999, pp.6-9.
- [47] Jonathan et al, "Electrophoretic deposition of the piezoelectric polymer P(VDF-TrFE)" Berkeley Sensor & Actuator Center , 2002
- [48] Emslie et al,"Flow of a viscous fluid on a rotating disc"Journal of Applied Physics, Vol.29, 1958, pp.858-862.
- [49] Meyerhofer D, "Characteristics of resist films produced by spinning", Journal of applied Physics, Vol.47, 1978, pp.3993-3997.
- [50] "Spin coat theory", Brewer science, Inc, 1997
- [51] Jack, "Infrared and Raman Spectroscopy of Polymers", Rapra Technology, 2001.
- [52] Michael C. Martin,"A compilation of extra information about FTIR spectroscopy and IR materials", 1997.
- [53] A.Salimi, "FTIR studies of beta-phase crystal formation in stretched PVDF films", Polymer Testing Vol.22, 2003, pp. 699–704.
- [54]. V.V.Vardan, "Measurement of All the Elastic and Dielectric Constants of Poled PVDF Films", Ultrasonic Symposium, 1989, pp.727-730.
- [55] H Zhang,"An investigation of thin PVDF films as fluctuating-strain-measuring and

Damage-monitoring devices” Smart Materials . Vol. 2, 1993, pp. 208-216.

[56] Piezo Sensors, “Measurement specialities Inc”.

[57] R. R. A Syms et al, “Sliding Blade MEMS iris and variable Optical Attenuator,”
Journal of Microelectromechanical Systems, Vol.14, 2004, pp 1700-1710.

[58] Chengkuo et al , “3-V Driven Pop-Up Micromirror for Reflecting Light Toward
Out-of-Plane Direction for VOA Application”, IEEE Photonics Technology Letters, Vol.
16, No. 4, 2004, pp 1042-1044,

[59] Robert Wood et al, ”A MEMS Variable Optical Attenuator”, Optical MEMS, 2000,
pp. 21-24

[60] C. Marxer et al “Comparison of MEMS variable optical attenuator designs,” Optical
MEMS, Conference Digest. IEEE/LEOS International Conference, 2002, pp.189-190

[61] Lijie Li, et al”Integrated Self-Assembling and Holding Technique Applied to a 3-D
MEMS Variable Optical Attenuator”, Journal of microelectromechanical systems, Vol
13, No.1, 2004, pp.83-90